If you have discovered material in AURA which is unlawful e.g. breaches copyright, (either yours or that of a third party) or any other law, including but not limited to those relating to patent, trademark, confidentiality, data protection, obscenity, defamation, libel, then please read our Takedown Policy and contact the service immediately

A THREE DIMENSIONAL SURFACE MEASUREMENT AND RECONSTRUCTION SYSTEM FOR RESPIRATORY FUNCTION ANALYSIS

TIMOTHY EARTHROWL

Doctor of Philosophy

UNIVERSITY OF ASTON IN BIRMINGHAM

October 2002

Summary

Respiration is a complex activity. If the relationship between all neurological and skeletomuscular interactions was perfectly understood, an accurate dynamic model of the respiratory system could be developed and the interaction between different inputs and outputs could be investigated in a straightforward fashion. Unfortunately, this is not the case and does not appear to be viable at this time. In addition, the provision of appropriate sensor signals for such a model would be a considerable invasive task.

Useful quantitative information with respect to respiratory performance can be gained from non-invasive monitoring of chest and abdomen motion. Currently available devices are not well suited in application for spirometric measurement for ambulatory monitoring.

A sensor matrix measurement technique is investigated to identify suitable sensing elements with which to base an upper body surface measurement device that monitors respiration.

This thesis is divided into two main areas of investigation; model based and geometrical based surface plethysmography. In the first instance, chapter 2 deals with an array of tactile sensors that are used as progression of existing and previously investigated volumetric measurement schemes based on models of respiration. Chapter 3 details a non-model based geometrical approach to surface (and hence volumetric) profile measurement. Later sections of the thesis concentrate upon the development of a functioning prototype sensor array. To broaden the application area the study has been conducted as it would be for a generically configured sensor array.

In experimental form the system performance on group estimation compares favourably with existing system on volumetric performance. In addition provides continuous transient measurement of respiratory motion within an acceptable accuracy using approximately 20 sensing elements. Because of the potential size and complexity of the system it is possible to deploy it as a fully mobile ambulatory monitoring device, which may be used outside of the laboratory. It provides a means by which to isolate coupled physiological functions and thus allows individual contributions to be analysed separately. Thus facilitating greater understanding of respiratory physiology and diagnostic capabilities.

The outcome of the study is the basis for a three-dimensional surface contour sensing system that is suitable for respiratory function monitoring and has the prospect with future development to be incorporated into a garment based clinical tool.

Acknowledgements

I would like to give thanks primarily to Dr. Tom Allsop who has given much guidance, assistance and has taught me literally all I know about photonic sensing. I would also like to acknowledge the encouragement and support given to me by Professor Barrie Jones.

Contents

Table of figures

List of Tables

1 Introduction

This thesis investigates methods for respiratory function measurement that allows subjects to move freely without constraint. Continuous measurement of both tidal breathing and determination of spatio-temporal relationships of breathing manoeuvres will contribute to further studies of respiratory physiology and pathophysiology. Extending the technique to include ambulatory and exercising subjects yields information hitherto unobtainable.

Such a device offers considerable benefits over available products. In the role of respiratory monitoring it will provide an entirely non-invasive indication of respiratory function that can take into account a subject's posture especially during motion in exercise. It will also provide hitherto unavailable diagnostic functionality that can be used in a range of working environments rather than being available only within a specialised laboratory. This would bring respiratory monitoring inline with the diagnostic capabilities employed in cardiology with routine 24 hour monitoring of heart rhythm for the diagnosis of cardiac dysrhythmias.

The objectives of this study are to investigate the benefits / practicality of employing new technology to measure respiration and to develop sensor technology suitable for this application. This will involve consideration of the overall construction of a sensing system that will form the basis for a new device from a systems perspective.

The potential impacts of this study will provide the basis of a new respiratory function monitoring device for clinicians with which to study physiology and diagnose disease by new information.

1.1 Respiratory physiology

Breathing is the product of chemical and neural influences on a network of neurones, motor nerves and muscles, of which the result is dependent upon the mechanical properties of chest, lung and airways. Breathing is caused by rhythmic contractions of skeletal muscle that are entirely dependent upon intact nervous connections from the medulla through the spinal cord and the phrenic and intercostal nerves. Networks of neurones in the medulla bring about the origin of the phasic impulses, which are controlled and coordinated with related motor acts such as swallowing and speech. The medullary centre is influenced by chemical factors, PO_2 and PCO_2 and pH in arterial blood and brain extracellular fluid, and also by a multitude of neural factors. Breathing may also be affected at the spinal cord level by segmental and intersegmental reflexes, whilst voluntary changes are probably mediated by corticospinal pathways that bypass the respiratory centres.

Skeletomuscular influences on respiration primarily involve the contraction of the diaphragm causing it to flatten from its normally domed shape. This increases the vertical dimension of the thoracic cavity and accounts for approximately 75% of the air that enters the lungs during inspiration. During normal quiet breathing the diaphragm descends about 1cm, which produces a pressure difference of 1-3 mm Hg and inhalation of about 0.5 litres. In strenuous breathing, the diaphragm may descend 10cm, which produces 100mm Hg pressure difference an inhalation of 2-3 litres [Balfour et al, 1981].

At the same time as diaphragmatic contractions the intercostals muscles between ribs also contract. This produces both an expansion in both anterior-posterior and superior-inferior dimensions of the thoracic cavity, referred to as the pump and bucket handle displacements by Wilson et al [1987].

Whilst a great deal is known about the chemical and neurological influences on ventilation, there is relatively little knowledge about the balance between diaphragmatic and thoracic contributions to ventilation and how each is recruited under varying circumstances.

1.2 Spirometry

Clinical measurement of lung function is predominantly based upon the use of spirometric devices that either measure the volume of gases expired (or inspired) at the mouth, or the corresponding flow rate. The measured output requires that an individual blow forcibly in a mouthpiece attached to a recording system.

The generated output is in the form of a transient waveform and this is interpreted on the basis of defined parameters, such as forced vital capacity (FVC) and a number of instantaneous flow rates throughout the cycle. Breathing metrics include the total minute volume of ventilation (V), also its components tidal volume (V_T) and frequency (f), the duration of inspiration and expiration (T_i, T_E), the flow patterns, and the end expiratory lung volume (the functional residual capacity, FRC). The American Thoracic Society [1979] has put forward a performance standard for such devices these are reproduced in Table 1.

The examination of such metrics provides the medic with quantitative information with which to identify and diagnose a variety of respiratory conditions, asthma as well as obstructive diseases. However the standard metrics themselves provide no more than an averaged representation of lung function behaviour and the condition of the respiratory system as a whole. As such the current method has limitations, namely:

- Detailed information is not provided that reflects the contributions from different parts of the chest. Therefore a method that establishes the relationship

between changes in regional motion and ventilatory function may be useful in contributing to further studies of respiratory physiology and pathophysiology. Extending the technique to include ambulatory and exercising subjects yields information hitherto unobtainable.

- The measured output requires that an individual blows forcibly in a mouthpiece attached to a recording system. For continuous monitoring it is not possible to breathe comfortably with a mouthpiece in situ for a prolonged period. It is also suggested [Block et al, 1995] that the mouthpiece itself perturbs measurements obtained this way. The technique is therefore unsuitable for ambulatory monitoring of individuals, or continuous monitoring of patients in hospital.

Increasing the understanding of these regional respiratory mechanisms alongside continuous real-time monitoring of breathing would provide a tool with which to study and ultimately diagnose a much broader range of respiratory conditions than is possible at the present time.

Test	*Range/Accuracy BTPS (litre)*	*Flow Range (litre / sec)*	*Time (sec)*	*Start Point*	*Resistance and Back Pressure*	*Test Signals*
VC	7 litre / ±3% of reading or 50ml, whichever is greater	0 → 12	30	-		Calibrated Syringe
FVC	7 litre / ±3% of reading or 50ml, whichever is greater	0 → 12	10.0	-		2 simulated FVC signals in range (1) FVC = 5 τ = 0.4 sec (2) FVC = litre τ = 0.4 sec
FEV_t	7 litre / ±3% of reading	0 → 12	T	Back extrapollate or equivalent	Less than 1.5 cm H_2O litre / sec at 12.0 litre / sec flow	Same as FVC
FEV_1			1.0	-		
FEF 25-75%	7 litre / ±5% of reading or 0.1 litre/sec, whichever is greater	0 → 12	10.0	-	Same as FEV_t	Same as FVC
$\dot{V}_E$	12 litre /sec / ±5% of reading or 0.2 litre/sec, whichever is greater	0 → 12	10.0	-	Same as FEV_t	Manufacturer proof
MVV	Sine wave 250 litre / min @2 litre to ± 5 % of reading	0 → 12 ± 5 %	12 - 15 ± 3 %	-	Pressure less than ±10 cm H_2O @ 2 litre TV 2.0 Hz	Sine wave pump 0 - 4 Hz ± 10 % @ 12 litre / sec

Table 1 Spirometry performance standards as prescribed by the American Thoracic Society

1.3 Spirometric measurement from surface motion

A number of less-invasive alternatives have been adopted that circumvent this type of closed circuit spirometry in order to tackle the problem areas of this application identified in the preceding section. Here these are collectively termed surface plethysmography.

1.3.1 Two degree of freedom surface plethysmography

Konno & Mead [1967] demonstrate the possibilities of non-invasive estimation of tidal volume from chest wall and abdomen motion measurements. With this device the changes in anterio-posterior diameters of the rib cage, measured by linear differential

transducers are used to compose a near linear two-degree of freedom model of ventilation. It is based on a two-degree of freedom (DOF), the chest and abdomen contributions being separate and additive in a similar ratio in all breathing patterns and irrespective of body attitude. The model for this approach is formulated as follows:

$$\Delta V_T = K_1\left[K_2 \Delta V_{RC} + \Delta V_{AB}\right]$$

Equation 1

Where: ΔV_{RC}, ΔV_{AB} are changes in ribcage and abdomen respectively and parameters K_1, K_2 are constants found empirically during calibration, K_2 representing the ratio of compartmental contributions.

This model is the foundation for many spirometry solutions for measuring ventilation directly from the thoacoabdominal surface. Predominantly changes in volume ΔV_{RC} and ΔV_{AB} are approximated from measurements of the perimeter of chest and abdomen with various forms of elastic strain transducer.

A number of devices composed of two transducer bands encircling the rib cage and abdomen have been offered, each respond to the inflationary state of each respective breathing compartment. Such devices include Respiratory inductance plethysmograph (RIP) [Watson et al, 1980] which measure the inductance change in coiled wire bands. Changes in the cross-sectional area of each breathing compartment alters the self inductance of wire coils and the frequency of their oscillations can reflect the magnitude and rate of gas inspired / expired. This method was also used to quantify the effects of nose-clip and mouthpiece on breathing patterns during spirometric measurements by Paek and McCool [1992]. RIP has been employed in a widely adopted clinical tool (Respitrace ™), however in a clinical environment it is rarely used for quantitative

measurement, being most widely used to detect breathing frequency and the onset of apnoea as well as an indication of the relative depth of respiration.

A number of other devices which operate on a similar principle to that of RIP have been indicated in technical literature, however there is little evidence that any have been adopted for use in a clinical environment. Morel et al [1983] introduce the bellows pneumograph, an air filled pocket as part of a band, in which changes in pressure are measurable as it is strained. Brinacombe [1993] offers another variation that reacts to changes of capacitance in coiled wire bands. Lafortuna et al [1995] describe a similarly composed instrument in which they measure the delay in ultrasound emission and reception inside rubber tubes.

An improved magnetic transducer system comprising a pair of magnetometer coils was proposed by Mead et al [1967] allow the 3-dimensional positional change of selected anatomical locations to be used in the model (Equation 1). In this case ΔV_{RC}, ΔV_{AB} are substituted by the changes in anterior-posterior and / or lateral dimensions of each compartment and allow another term ΔX_i to be employed in equation(1) that represents the vertical separation of the area approximations, in generalised form:

$$\Delta V_T = \alpha \Delta_{RC} + \beta \Delta V_{AB} + \gamma \Delta X_i$$

Equation 2

However not until 1975 was this method of instrumentation reported [Sharp et al 1975] in their study of breathing patterns and subsequently refined by Stagg et al [1978] with the addition of computer-based automation. More recently Robertson et al [1980] have reappraised the methodology and concluded that improvements could be made with the addition of more sensors placed laterally along the chest wall.

Devices that measure respiration on these principles determine the changes in chest and abdomen volumes as being equivalent to changes in a singular cross-sectional area of

each compartment. This technique ignores distortions which occur in the rib cage which occur with an increasing volume range of ventilation and relies on additional parameters which compensate for geometrical factors in cross-section cumulatively lumping them as part of the K_1,K_2 coefficients in Equation 1 and Equation 2 as part of a calibration procedure.

A number of calibration procedures have been adopted to estimate the parameters in the above models. The most prevalent include:

- The two-position method, in which the ratio of thoracic to abdominal contribution is determined from data collected from a subject, in most cases upright and recumbent body positions. The ratio K_2 or α / β is determined as constant in both attitudes where the mode of breathing differs.

- An alternative is to perform a closed system manoeuvre, where inspired gas is exchanged between chest and abdomen against a closed glottis. Setting $\Delta V_T = 1$, ratio K_2 or α / β can be calculated from collected data.

In either case parameters can be estimated by regression, least squares or simultaneous equations, however alternative graphical and numerical methods are also reported [Warren et al, 1988][Loveridge et al, 1983][Banzett et al, 1995][Robbertson et al, 1980][Chadda et al, 1982].

Evaluation studies of the RIP technique [Tobin et al, 1987][Zimmerman et al, 1983][Guyatt et al, 1983] have identified that limitations exist particularly with respect to changes in posture after calibration. It follows that the technique is not suitable for monitoring ambulating individuals. Accuracy has also brought into question when this method is used over wide variations in tidal volumes with the suggestion that the data are qualitative rather than quantitative [Banzett et al, 1995].

Simple 2 or 3 DOF can provide accurate approximation (±5% error in V_T) for a limited range breathing conditions, accuracy is degraded with changes in posture as well as breathing pattern and magnitude. In those validation studies reported using these techniques, errors of as much as ±30% in V_T are not uncommon in a significant number of samples (up to 20% of the sample population as shown in Table 2. Such devices must be re-calibrated frequently if the results produced are to be regarded as more than qualitative over an extended period.

An alternative approach [Earthrowl-Gould et al, 2001] is studied in chapter 2 . The concept is based upon the use of an array of strain / displacement sensors at specific anatomical locations similar to the methods used in 2 DOF systems. The sensor is integrated into a fabric structure in an array so that the sensors will mechanically coupled in both vertical and horizontal directions. For all intents and purposes a coupled array of one or two-dimensional sensors can be used to produce a 3-D surface map in conjunction with a geometric model of respiration. Alternatively a statistical model can be applied to reconstruct sensory data. Measurements normal or parallel to the chest and abdomen surface can be used to divide the overall surface area, which by application of a generalised model of ventilatory surface mechanics can be used to describe a finite volume element. The sum total of changes in these small volume elements captures the total change in respiratory volume. This is similar to the topological model used in optical reflectance systems. The simplest form of the model is as follows:

$$\Delta V_T = \sum_{i=1}^{N} \alpha_i \Delta Vs_i$$

Equation 3

Where N represents the number of sensors, $[\alpha_1\ \alpha_2 \ldots \alpha_N]$ a parameter vector and ΔVs the local surface motion.

Source	No. of observations	% No. Values P<20% Vt(sp)	% No. Values P<30% Vt(sp)	Mean absolute deviation Vsp/Vm ± SD	Mean error ± SD (litres)	Mean Correlation coefficient	Notes
Sackner et al,1989 Method: RIP	76	90	97	10 ± 8.3	N/A	N/A	Results for 6 normal non-smoking men, obtained in supine position with varied breath amplitude.
Hudgel et al, 1984 Method: RIP	50 Breaths	67	N/A	7.6	0.12 ± 0.16	N/A	5 patients with COPD in supine position, 18-22 breaths per minute
Cantineau et al [24]	1,009 Breaths	100			0.019 0.013	±0.95	13 patients with obstructive sleep apnea, during wakefulness. 11/13 supine, 2/13 lateral decubitus. Results here have been modified by central limit theorum to obtain overall performance.
McCool et al, 1986	6 Subjects						6 normal male subjects in standing position. Tested during calibration * procedures using models (1) & (2) for RIP and magnetometers. 30 breaths total; 10 emphasising RC, 10 emphasising AB and 10 emphasising extension of spine.
RIP							
model (eqn. 1)		83	83	N/A	N/A	0.929	
model (eqn. 2)		100	100			0.992	
Magnetometers							
model (eqn. 1)		30	50			0.707	
model (eqn. 2)		100	100			0.993	
Earthrowl-Gould et al, 2001							
Array	14 breaths	(p<0.025)	(p<0.005)	5.8±6.8	0.077±0.072	0.9681	
Row	"	87	99	10.5±8.1	0.156±0.127	0.9627#	
Pair	"	56	85	17.6±14.8	0.255±0.210	0.9665#	

* Higher performance shown due to results obtained on calibration data.

R2 based on high instantaneous volume estimation of highest performing combination. P values based on Students t-test.

Table 2. Performance Comparison of different methods of surface respiratory measurements.

1.3.2 Multiple degree of freedom surface plethysmography

In search of performance gains attention has been made to those physiological components of respiration overlooked in the 2 DOF approximation. Wilson et al [1987] favoured image processed x-ray tomography as instrumentation for their study and offered a picture of rib cage mechanics of a more complicated nature, emphasising the

change in shape of the chest compartment during breathing. With an absence of similar mechanical model for the abdomen a number authors have made efforts to obtain a more complete appreciation of thoracoabdominal motions. One such model is depicted in the block diagram in Figure 1 as reproduced from Kenyon et al [1997]. The most notable modifications are a coupling effect between thoracic and abdominal contributions as well as dividing the thoracic contribution in to two components Pulmonary (or lung) opposed rib cage (RC_p) and Abdominal (or diaphragm) opposed ribcage (RC_a). The total body pressure (P_{bs}) and hence volume being dependent on three compartment contributions.

To validate this model the authors employ an optical reflectance system (ELITE) developed by Cala et al [1996] and studied by De Groote et al [1997] and Sanna et al [1999], which operates from a purely geometrical standpoint. This method of instrumentation employs reflective markers, which are attached to the skin of a subject at predetermined locations. The apparent relative positions of these markers when recorded from multiple camera angles are then used to describe the geometry of the chest wall and abdomen over time. The markers divide the surface area into a number of geometrical areas the boundaries of which are tracked with cameras in three dimensions and used to provide a sum volume motion from individual elements.

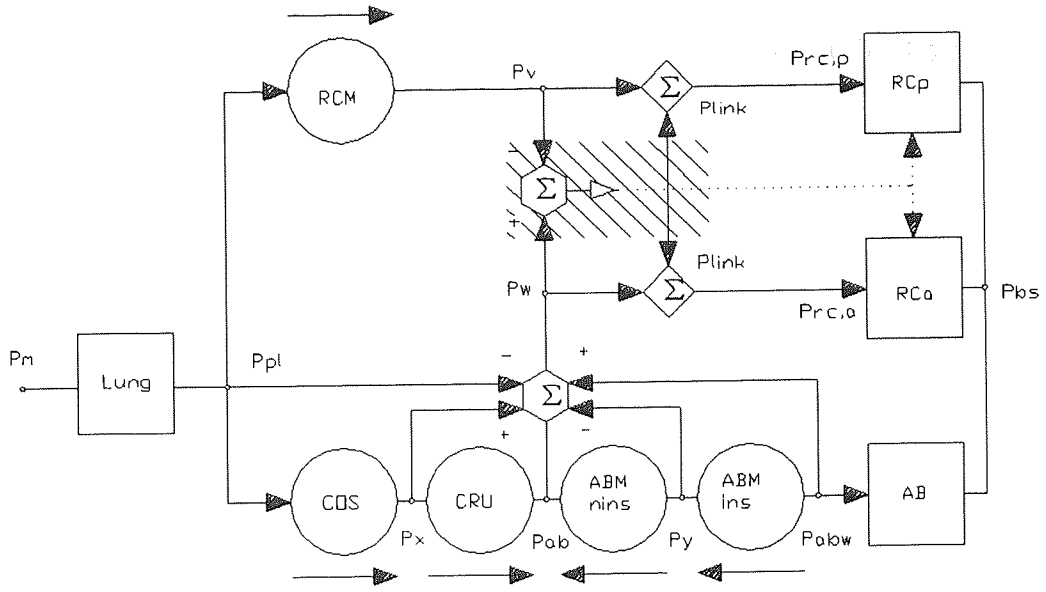

Figure 1. Block Diagram of Kenyon , Cala et al[15] Two-compartment Rib cage [pulmonary (RCp) and abdominal (RCa)] and abdomen (AB) model of respiration. Circles represent pressure generators, which increase pressure in direction indicated by arrows above each generator. Hexagons and diamonds represent summing junctions. Inputs to summing junction are signed to indicate effect on junction of pressure increases from each of inputs. Summing junction in shaded area determines the net difference in pressure acting on RCp and RCa, which produces rib cage distortion. Output of this junction (open arrowhead) is restoring force represented by a pressure (Plink) that acts in opposite directions on RCp and RCa. Dotted line to RCp and Rca indicated that distortion of rib cage affects compliance of rib cage compartments. Pv, imaginary pressure on RCp before effect of rib cage distortion is taken into account; Pw, analogous pressure for Rca; Px and Py imaginary pressures between parts of muscles with different action sas indicated by mode; Pm, mouth pressure; Pbs pressure at body surface; Pabw, pressure from passive stretching of abdominal; wall; RCM, rib cage muscles; Plink, restoring pressure; Prc,p, elastic recoil pressure of RCp; Prc,a, elastic recoil pressure of Rca; Ppl, plural pressure COS, costal part of diaphragm; CRU, crual part of diaphragm; Pab, abdominal pressure; ABM, nins, abdominal muscles with no action on Rca; ABM, ins, abdominal muscles acting to deflate Rca.

Another optical solution originating from a group at the Brompton Hospital, London [Peacock et al, 1984][Gourlay et al, 1984][Morgan et al, 1984] involves the projecting a coded pattern of light over the subject. These fringes are then used to produce a contour map when recorded on video. Surface motion can then be analysed using computer based image processing.

Optical approaches such as this approach neutralises to a greater extent many of the drawbacks associated with posture and dynamic range associated with other techniques and allow a more detailed appreciation of respiratory mechanics. Solutions of this type utilise an off body reference point for measurement and as such are not suited to free ambulatory monitoring of respiration. Limited data collection because of processing limitations (currently 20s of data, as of report dated 1997). The accuracy reported claims to be within 4% V_T but still relies on a calibration factor to account for discrepancies. During exercise errors are introduced with the interpretation of marker positions with skin movement in increased ventilation have been estimated as 10%Vrc and 2.5% Vab [Cala et al, 1996], these are generally overlooked. Because of the nature of the ELITE systems operation the subject must hold or have his arms suspended at or above shoulder height. It is accepted that this in itself limits validity of the observations made to the exercise or breathing manoeuvre under investigation, as this posture will have an effect on the pattern of breathing.

1.4 Requirements

In order to meet the diagnostic aims such devices requires measurement of individual respiratory contributions. The primary need is to establish sensing technology for use as the basis of the device. This is the primary objective of the study.

An alternative multiple degree of freedom approach studied in chapter 3 is based on an array of geometrical shape sensors that react to local chest and abdominal movement and provide signals that represent the thoracic surface profile can be related algorithmically to volumetric generated by conventional spirometric devices. The concept is based upon the use of an array of optical fibre bend sensors. For all intents and purposes a coupled array of one or two-dimensional sensors can be used to produce

a 3-D map of the surface profile. This negates the need for a model based relationship between respiratory motion and surface geometry.

1.5 Sensor selection

It is envisaged that regardless of the sensing scheme employed that an array of sensors will be incorporated in a flexible structure, most likely the solution will be constructed into some form of garment. As such the mechanism to be measured will be the state of stress in the structure, either in flexion as with the measurement of geometry or the interaction between the surface of the chest and abdomen and the tension in the structure or just tension alone for the model based approach.

In the case of model based plethysmography the sensing principle will be deformation (strain). This may be accomplished form either direct or indirect measurement of strain in the garment whether the measurement be from changes in electrical characteristics, capacitance, inductance, charge or resistance, in sensor elements or for that matter the characteristics of any other medium. There is also a multitude of configurations and materials by which to construct such elements. This too applies to sensors applicable for geometric sensing, however in this case the measurement comparison would be made against the deformation of a substrate with known flexural characteristics.

A survey of commercially available sensors did not produce any suitable sensor candidates for either approach. A decision was made to investigate the benefits of using an array of sensors constructed from generic sensing methodology. Owing to limited fabrication facilities the simple resistive sensor array detailed in chapter 2 was adopted because of low cost and ease of manufacture.

1.6 Summary

During the preceding discussion it has been identified that useful quantitative information with respect to respiratory performance can be gained from non-invasive monitoring of chest and abdomen motion. Currently available devices are not well suited for application for spirometric measurement for ambulatory monitoring. two degree of freedom devices, such as RIP are sensitive to changes in posture, movement and are subject to frequent calibration, as such they generally find application as monitors for recumbent patients, for example monitoring of sleep and postoperative apnoeas.

Three-dimensional systems geometrically based systems exhibit a higher fidelity, however at the cost of added complexity of equipment and operational methods as too with the loss of portability available with existing products. They are not suited to ambulatory monitoring because they must be used with a specific clinical environment and are limited in data throughput. Therefore, in order to diagnose accurately various respiratory conditions from readily available sensor readings, an alternative solution must be developed that will concur with the established standards associated with existing spirometric devices and be robust to a wide range of operational conditions.

Irrespective of whether a physiological model base or a geometrical approach is employed there are a number of considerations:

- Non-respiratory motion artefacts - Signals are strongly influenced by perturbations resulting from the measured subjects posture (walking, arm movements etc.) this has an influence on both the pattern of breathing as well as the shape of the thoraco-abdominal volume. As a consequence the system must provide a sophisticated adaptive process that can either identify or filter out signal elements, which are not part of respiration.

- Breathing patterns - Different individuals exhibit different breathing patterns and this needs to be investigated to decide to what extent this is taken into account by the calibration system and the overall medical implications on the measurements made. The recognition of speech and how this alters the pattern of breathing is also required.

- Factors governing respiratory performance - The system provides the facilities to observe the regional contributions made by the different muscle actions of the chest. Again each action will contribute towards the total volumetric flow delivered from the system. The extent of which these actions can (or should) be related need to be investigated and defined. This requires the creation of a data library to include subjects with a full range respiratory conditions.

- Validation - The sensor signal outputs need to be related to those generated by conventional spirometric devices and standards, which provide information in terms of volume and flow rate. However with no such equivalent mechanism being available for the comparison of regional contributions an objective method of verification needs to be resolved.

1.7 Objectives

The objectives of this study are therefore:

- To investigate the benefits / practicality of employing an array of sensors to measure respiratory motion on the chest and abdomen surface in both model based and geometrical plethysmography.

- To develop sensor technology suitable for application in a surface plethysmography device.

- To consider the overall construction of a sensing system that will form the basis for a surface plethysmography device from a systems perspective.
- To discover a method by which to validate the integrity of such a system.

2 Model based surface plethysmography

The purpose of this chapter is to investigate an array based approach to surface plethysmography, extending existing model based methods (RIP etc.) to provide a full three-dimensional / regional appreciation of respiratory motion.

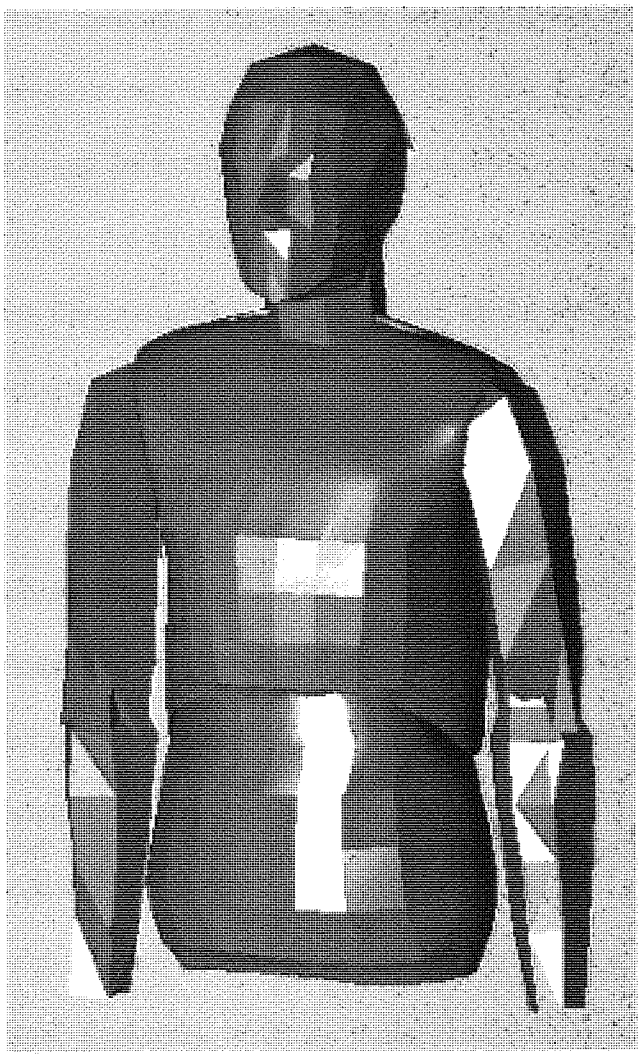

Figure 2 Rendered wire-frame model of male torso. Head, neck and arms are included for image clarity.

Promayon et al [1997] has put forward a surface motion model for volumetric respiration. This is based on a collection of patch objects each of which have associated properties of compliance, preferred trajectory during motion and linking properties to it

neighbours. This approach allows a wire-frame model of the chest and abdomen to be realised for a given volume and boundary conditions. Whilst most of these boundary conditions are difficult to effect in a real world variety of subjects it provides a tractable explanation for the physiological processes that occur during respiration. Modification of this modelling rationale to predict surface motion in response to sensing array signals is a straightforward task assuming that boundary conditions can be estimated from at mouth spirometric measurements and geometric dimensions. However the diversity of physical statures that might be encountered would necessitate a considerable library of model parameters. Initially the arbitrary wire-frame surface model of Figure 2 was used to estimate a base-line the mid-tidal volume position of the simulation with which to superimpose sensory signals.

2.1 Sensor array architecture

As an initial approach sensors were constructed from a sandwich of two stiff copper coated boards and conductive foam packaging 25mm square and 9mm deep (Figure 3). When electrically energised an ohmic relationship exists between the contact pressure of the foam copper interface and by virtue of the elasticity of the foam, its compressed dimension. The electrical characteristics (Figure 4) have been established as a in response to a sinusoidal displacement of the top sensor surface at a frequency of 0.5Hz over 50% of the foam thickness, with an initial 1mm deflection pre-load. These parameters have been chosen to represent the range of expected respiratory signal magnitudes, according to the foam stiffness and comfort when the sensors are restrained on the chest / abdomen surface.

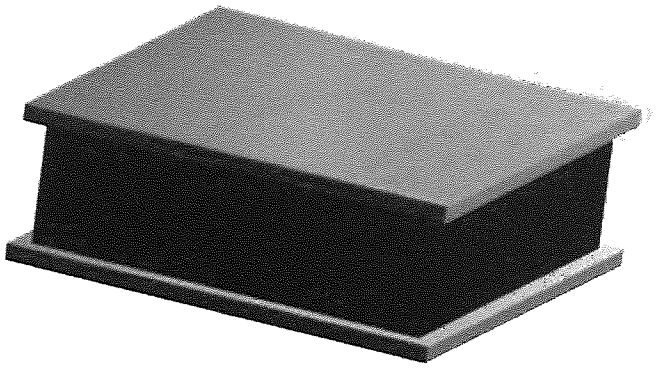

Figure 3 - Sensor construction. The sensors have been fabricated from copper coated resin board and 7mm thick carbon filled anti-static foam. Overall dimensions are 25x25x9 mm.

Experimentation has also shown this type of sensor element exhibits an amount of zero drift as well as other non-stationary behaviour. This has been attributed to temperature and mechanical wear within the foam. Subsequent experiments have been confined to shorter periods in order to minimise these effects.

Whilst the repeatability performance of this sensor is low, it is proposed that future development and miniaturisation will improve reliability and function. It should be noted that this kind of sensor was adopted for its low cost and ease of manufacture.

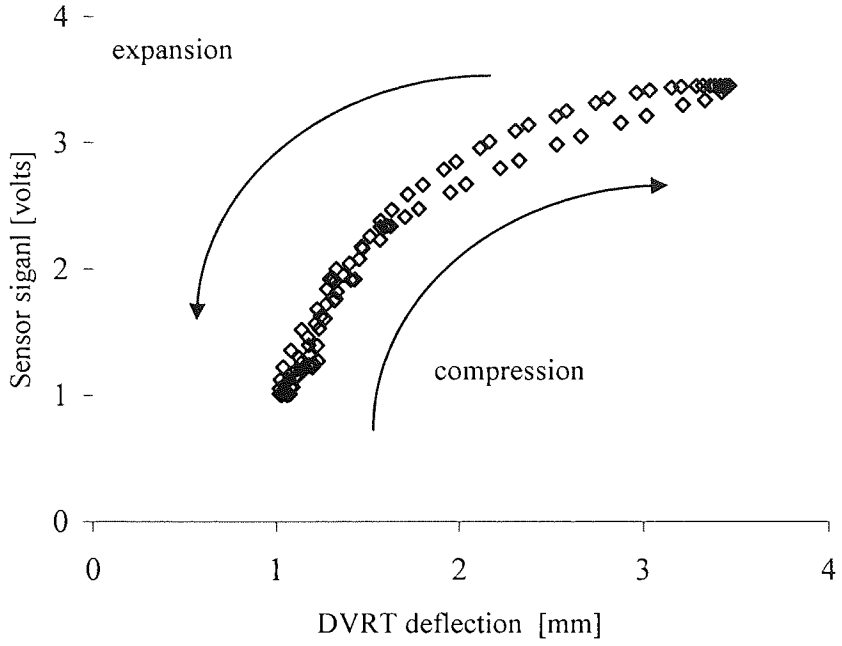

Figure 4. Sensor electrical characteristics, response to sinusoidal displacement over 50% foam thickness after a 1mm pre-load. Displacement was measured synchronously with a differential variable reluctance transducer (DVRT).

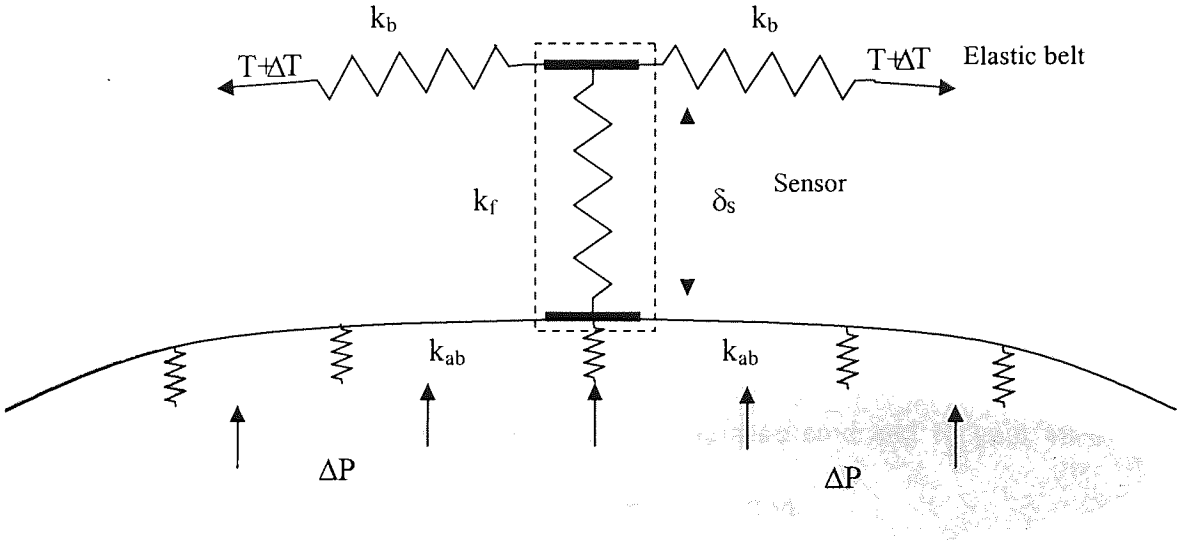

Figure 5 - Sensor operational schematic diagram. Where symbols represent, belt tension (T), intra-abdominal pressure (P), abdominal wall compliance (kab), Sensor displacement (δ), sensor and elastic belt stiffness (kf) and (kb) respectively.

The sensors are to be positioned over the skin surface, restrained by an elastic belt or vest. Figure 5 shows a schematic of the sensors operation. Fifty-six such sensing

elements were arranged on two elastic support belts. Providing an 8 by 7 array at approximately 5cm vertical and lateral intervals. The support belts are elastic in the lateral direction only and thus confine each sensor measurements to 1 DOF lateral expansion measurements. The terminals of each sensor were connected in the lattice configuration of Figure 6, providing 15 terminals. Switching the electrical supply between pairs of row and column terminals systematically energises each sensor individually and in turn. This was controlled by an auxiliary circuit comprising a bi-stable clock for timing both switching and triggering data conversion, two 8-bit binary counters and two 8-bit multiplexors, in DIL IC packages, which control array switching on every second clock pulse. Data was acquired to the PC via a Computer Boards PCM-DAS16S, 16-bit analogue to digital conversion card each sample triggered at the clock speed of 132 Hz, however only every second conversion was FIFO buffered to reduce transient noise in the system. Data is in effect collected from each sensor at a constant frequency of 66Hz.

The overall performance of the system is low, noise being the primary limitation of this preliminary approach. This is evident in a noise component on each sensor channel with an average signal to noise ratio of approximately 9dB. It can easily be concluded that this approach is far from optimum. It should be emphasised that these experiments have been devised in order to validate the modelling scheme and to gain an insight into requirements of sensor performance and configuration.

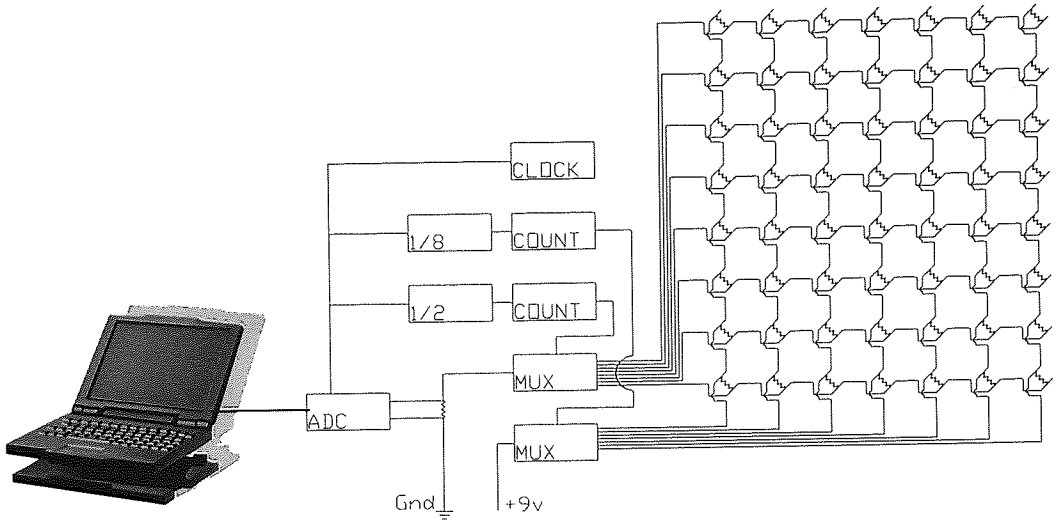

Figure 6- Construction of the sensor array.

Figure 7- Sensor array belts.

2.2 *Performance evaluation*

Four experiments were conducted on a standing male subject. Each belt was positioned so as to cover the upper thorax from the 4th intercostal space to the lower rib margin with one belt, the other extending down to the umbilicus. Three validation data sets were collected at steady incremental tidal volumes: low, mid-range and high, the fourth at an increasing tidal volume used to obtain the models parameters. Simultaneous measurements were also made at the mouth of volume flow with a pneumotachograph. The data used for parametric modelling is shown in Figure 8. The comparatively high sampling rate compensates for the small number of breath samples examined.

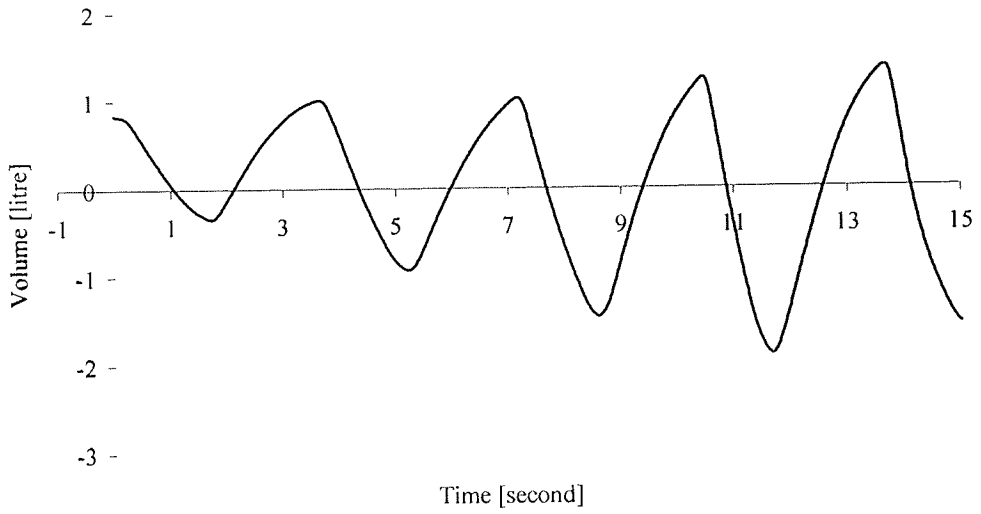

Figure 8. Calibration data set

The support belts are elastic in the lateral direction only and thus confine each sensor measurements to 1 DOF lateral expansion measurements. Isolating signals from one chest and one abdomen elevation / row in the array provide an appreciation of a duel-

compartment measurement system with a similar performance. Performance gains in increasing the DOF in the calculation of total volume change can then be compared.

A minimum least squares method of parameter estimation was adopted in keeping with accepted methods used in previous publications. Performance was based on a mean square error metric and was obtained for:

(a) **Two-sensor performance**, the best performing combination of two sensors one from the thoracic belt and one from the abdomen. This being the simplest representation of the model described in Equation 1.

(b) **Row-sum performances,** here the signals from all sensors on each elevation of the array were combined and the best performing pair combination one from the thoracic belt and one from the abdomen. This was chosen to be more representative of the performance of perimeter measurement devices based on model (Equation 1).

(c) **All sensors,** parameters were calculated for each individual sensor as in equation (Equation 3).

The result in Figure 9 plots the performance of each of the above model performances. Unexpectedly two-sensor performance exceeds that of row-sums. This may however be a result of the cumulative contribution of noise components in the summation. The poor responses to larger peak and trough tidal volumes evident in all models can be attributed to signal attenuation due to saturation of the sensors signals.

The sensor array performance in volumetric terms gives a mean absolute error for all sensors in each of the four increasing tidal periods in the evaluation data set as 200ml. Assuming that the system noise is a simple additive process the noise free system performance can be estimated:

$$\mu_{NF} = \mu_{SA}, \sigma_{NF} = \sigma_{SA} - \sigma_n \sum_{i=1}^{N} \alpha_i$$

Equation 4

where μ represents mean, σ is standard deviation and subscripts NF, SA, n refer to a noise free system, sensor array and noise respectively. This then relates to a standard deviation 134ml. For a Gaussian distribution, within the confidence limits 2σ, errors are within 7.4, 7.5, 8.4 and 11.4 % of the spirometer measurements for each of the four tidal displacements respectively. Figure 10 shows the identity plot of measured values, indicating absolute ratio performance margins. Figure 11shows the Altman-Bland difference performance of each data. It is assumed here that poorer performances at lower tidal volumes are a symptom of non-linear sensor artefacts. The performance has reasonable agreement in comparison to those published in earlier work. A variety of performance metrics have been calculated for the performance data in Table 2 (chapter 1) in order to aid the comparison. While a direct relationship cannot be formulated due to the diversity of test conditions of the table data, the system under test performs acceptably well with consideration to its rudimentary construction.

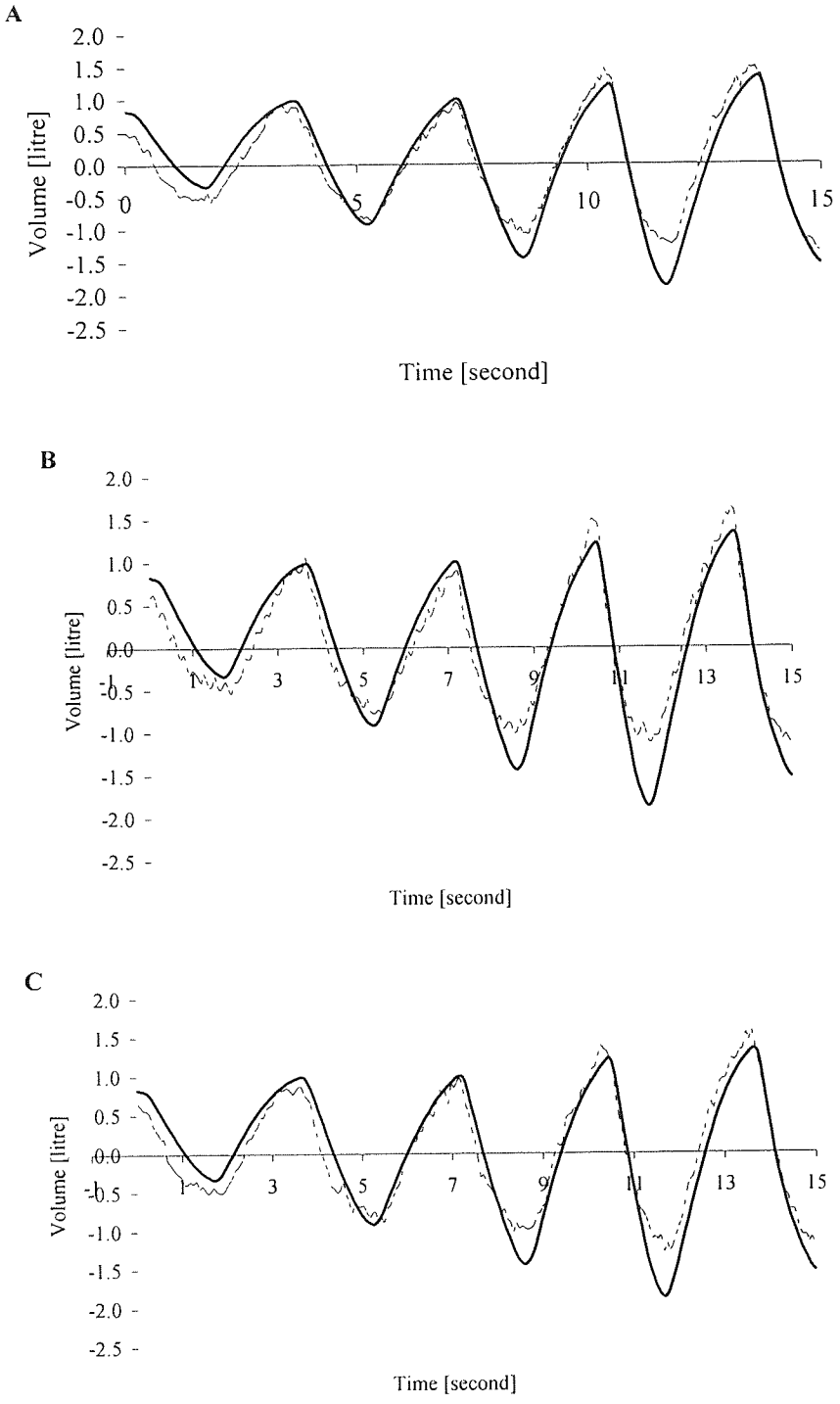

Figure 9. Performance curves, solid lines are gas flow measured at mouth and broken lines minimum least square model response for each configuration. (A) array performance with mean square error 0.05, (B) best performing row sum performance (rows 2 and 6, MSE 0.07) and (C) best two sensor performance (elements (2,7) and (5,2), MSE=0.06).

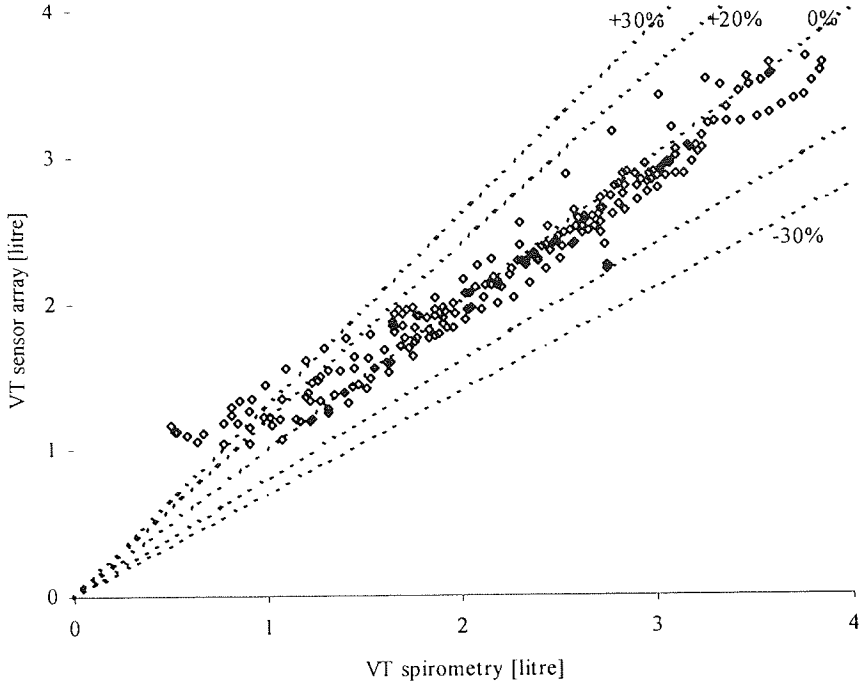

Figure 10. Identity plot V_T(sensor array) vs. V_T(spirometry)

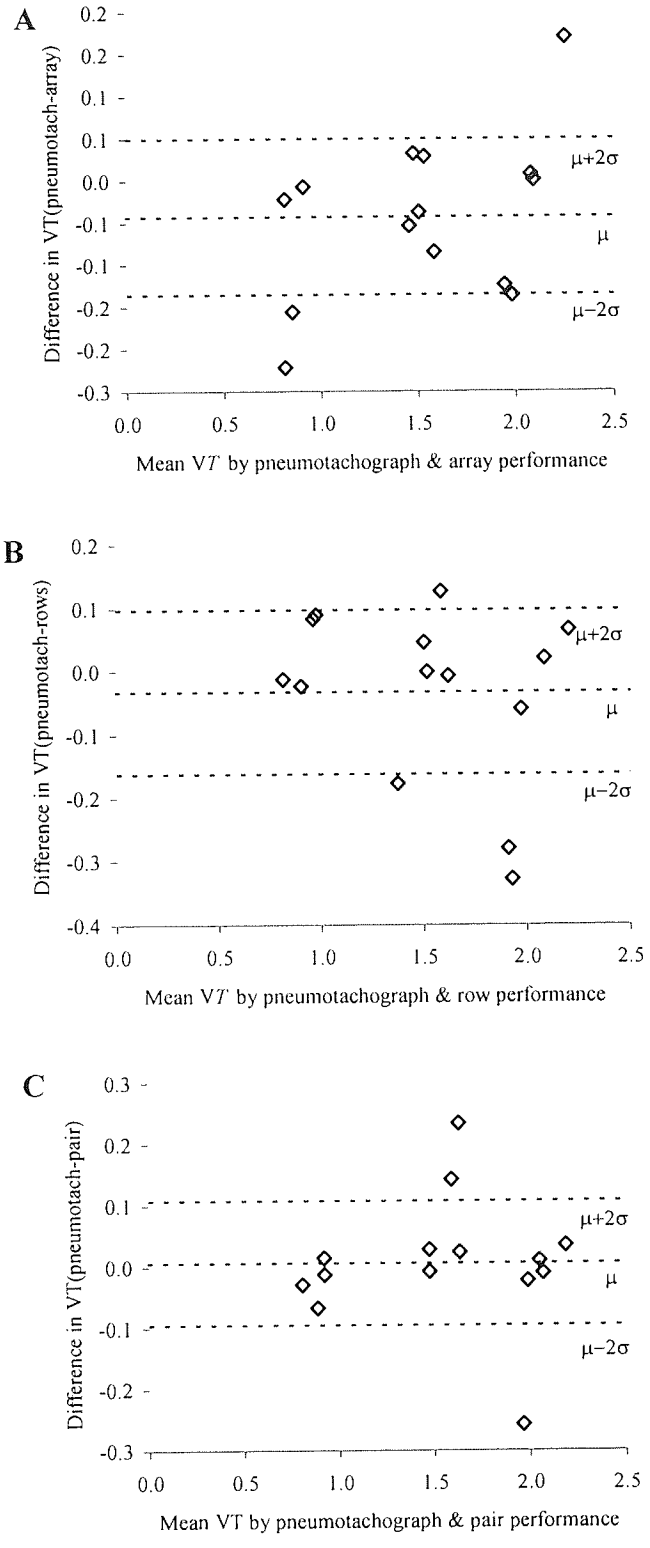

Figure 11. Altman-Bland plot of bias performance for the three sensor configurations investigated.

2.3 Sensor density

In order to appreciate the number and resolution of sensors that might be required to reproduce the whole thoracoabdominal volume the chest surface is considered in terms of a number points interconnected by patches of area. Within a patch, the surface can be described using a geometric model as:

$$S(u,v)=\begin{bmatrix} N_{0,4}(u) & N_{1,4}(u) & N_{2,4}(u) & N_{3,4}(u) \end{bmatrix}\begin{bmatrix} P_{00} & P_{01} & P_{02} & P_{03} \\ P_{10} & P_{11} & P_{12} & P_{13} \\ P_{20} & P_{21} & P_{22} & P_{23} \\ P_{30} & P_{31} & P_{32} & P_{33} \end{bmatrix}\begin{bmatrix} N_{0,4}(v) \\ N_{1,4}(v) \\ N_{2,4}(v) \\ N_{3,4}(v) \end{bmatrix}$$

Equation 5

where $N_{ij}(u)$ represents a Cubic B-spline equation [Woodward, 1988] and P_{ij} represents a matrix of control points.

In Eq. (2), the control point matrix is to be determined using a number of sensors on the chest surface. For each patch, as there are 16 elements to be determined in total, 16 sensors will be required to sample the data of an arbitrary chest upper surface (Figure 12). Once the matrix **P** is determined, the surface will be reconstructed using the model as in Equation 5 (Figure 13).

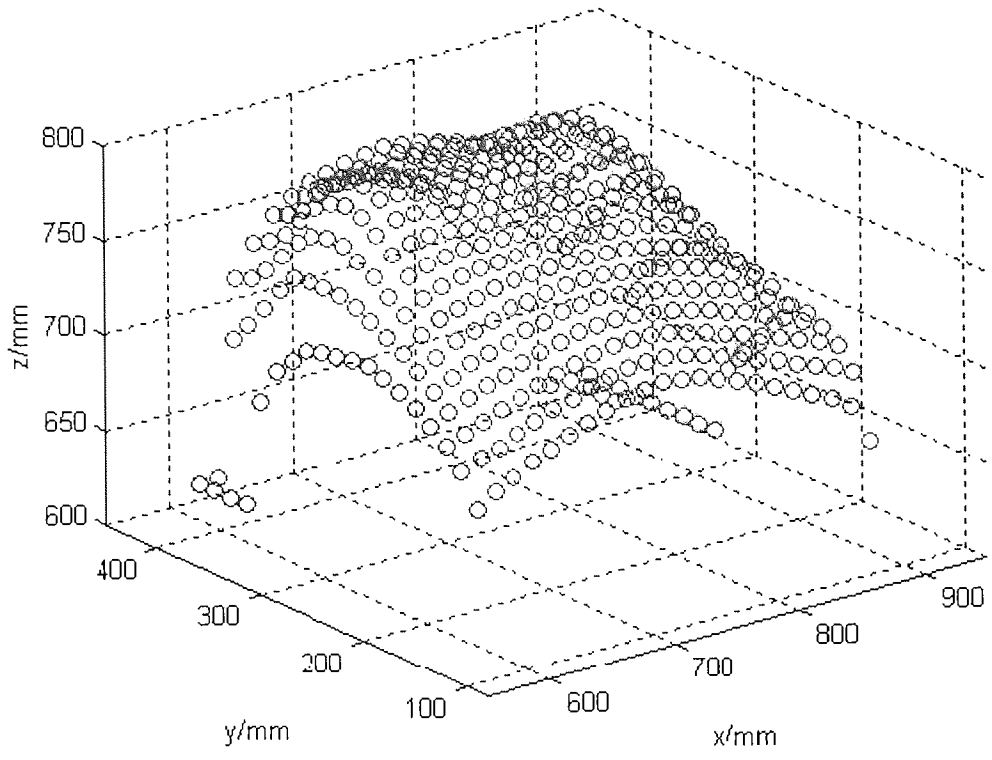

Figure 12 Data points obtained using multiple sensors on the chest surface

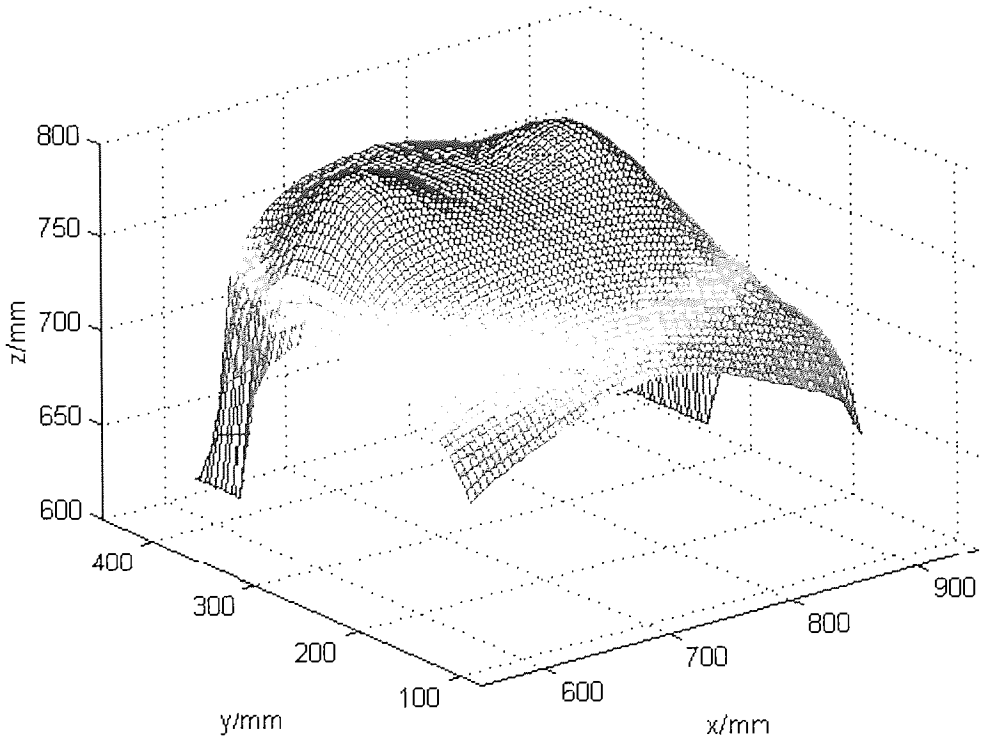

Figure 13. Surface generated from the geometric model

Errors between the surface generated from the geometric model and the actual chest surface can be quite small if more data points are taken to determine the control point matrix (Figure 14). This means the chest surface has to be sub-divided into a large number of patches and the number of sensors required will increase.

Figure 15 shows the relationship between the maximum error in the model and the number of patches. The relationship of the model error with the patch size is also illustrated (Figure 15).

It is noted that a smaller patch size means that the distance between the sensors on the chest surface will be smaller, and as such, a denser distribution of sensors.

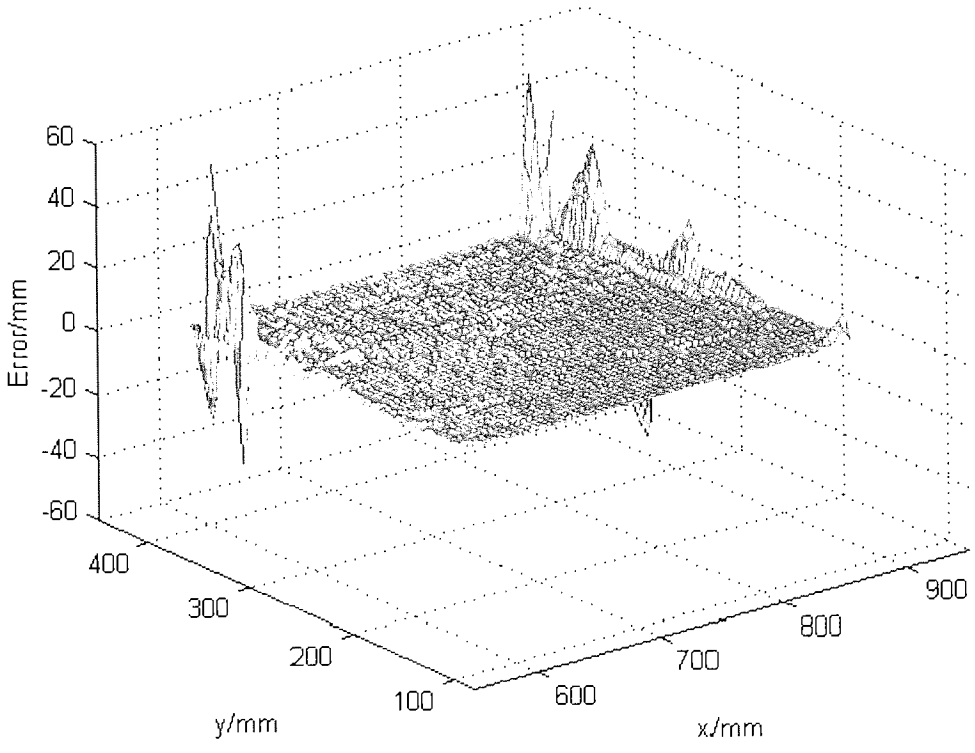

Figure 14. Errors between the model and the actual surface

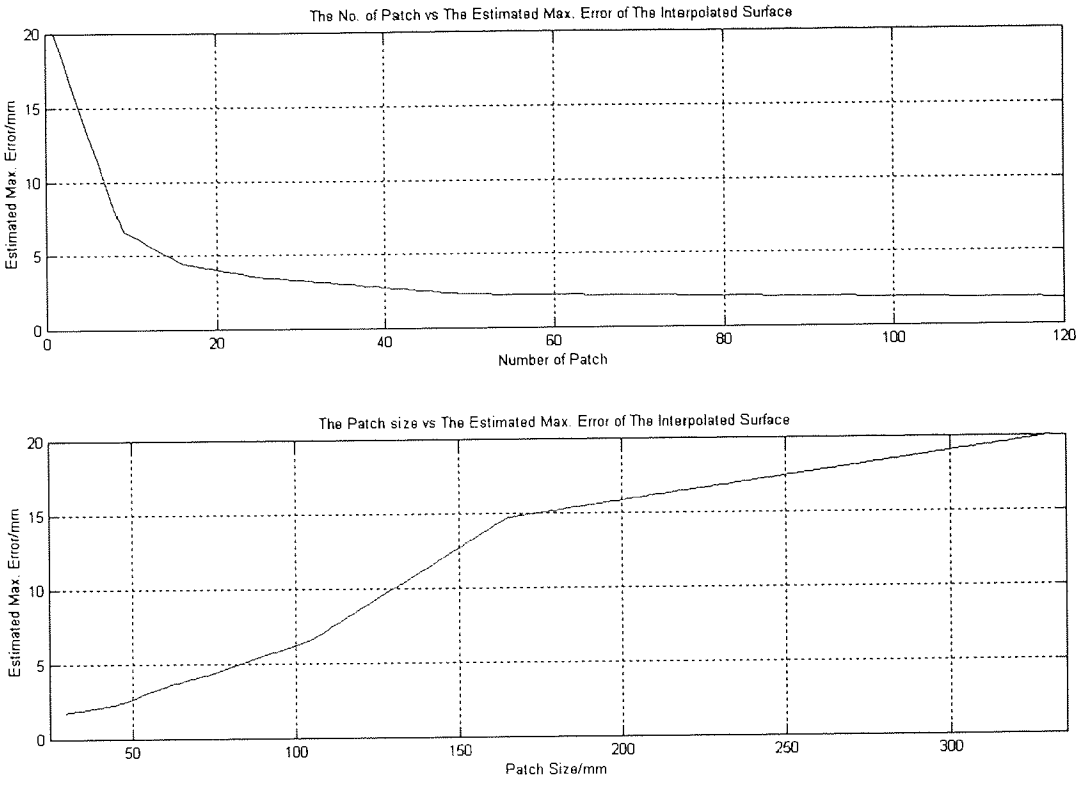

Figure 15. Maximum model error vs patch number and size

2.4 Respiratory signal extraction in motion peturbation

For the purpose of respiratory monitoring over extended periods and in ambulation it is important to be able to distinguish between chest and abdomen surface motion caused by body respiration from that of other body movements. The complex notion of how surface motion of the chest occurs during breathing establishes the underlying physiological impetus for the respiratory component of surface motion. When this is put into practice and extended to include the abdomen in a computer-simulated model [Promayon, 1997] it is recognised that the near-linear relationship between thoracic and abdominal compartment contributions as in 2 degree of freedom approximation methods applies to some extent also to spatially separated sites on the same compartment. Therefore respiratory surface motion will follow a deterministic pattern

for a particular set of boundary conditions (e.g., physical stature, pulmonary rate) and over a time period where conditions are stationary. This being so, it is necessary only to recognise the signal components that do not fit this pattern. It is not anticipated that signal components caused by walking, running etc., will produce spatially symmetrical displacements on the array, nor at the respiration frequency. The problem is to find a method by which to recognise and filter out consistent respiratory signals.

In order to judge the sensor array's ability to discriminate between respiratory and other motion the following experiment was devised.

Initially the three constant respiration data were used to obtain the parameters for a simple linear model using a recursive least squares algorithm. Thus providing a baseline reconstruction for volume estimation. This approach has been demonstrated to provide adequate performance with this type of system in the absence of body motion [Earthrowl-Gould et al, 2001]. Figure 16 shows the estimated instantaneous volume response for the respiration / arm movement composite signal alongside that of the target data obtained from the pneumotachograph. This shows a high level of corruption.

The more complex notion of how surface motion of the chest occurs during breathing [Wilson et al, 1987][Grimby et al,1968][Sharp et al, 1975][Paek & McCool, 1992][Delgado et al, 1982] establishes the underlying physiological impetus for the respiratory component of surface motion. When this is put into practice and extended to include the abdomen in a computer-simulated model [Promayon et al, 1997] it is recognised that the near-linear relationship between thoracic and abdominal compartment contributions as in 2 degree of freedom approximation methods applies also to spatially separated sites on the same compartment. Therefore respiratory surface

motion will follow a deterministic pattern for a particular set of boundary conditions (e.g., physical stature, pulmonary rate) and over a time period where conditions are stationary. This being so, it is necessary only to recognise the signal components that do not fit this pattern. It is not anticipated that signal components caused by walking, running etc., will produce spatially symmetrical displacements on the array, nor at the respiration frequency. The problem is to find a method by which to recognise and filter out consistent respiratory signals. To test his theory an artificial neural network was constructed and trained in order to recognise and cancel the arm motion signal in the configuration of Figure 17.

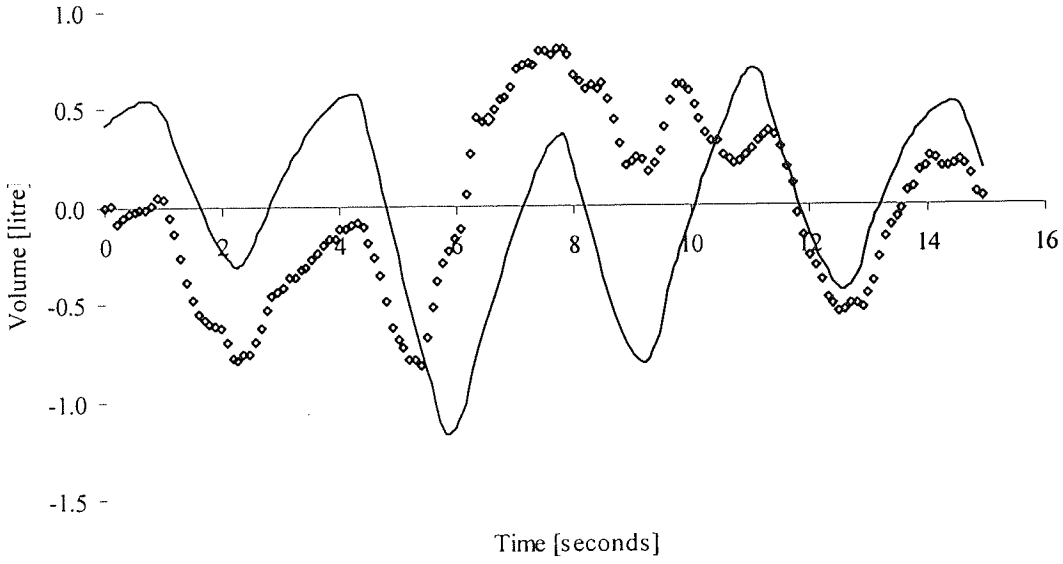

Figure 16. - Corrupted data, zero-mean instantaneous volume estimated from RLS algorithm parameters. Solid line is the volume measured at mouth, diamonds are RLS estimate.

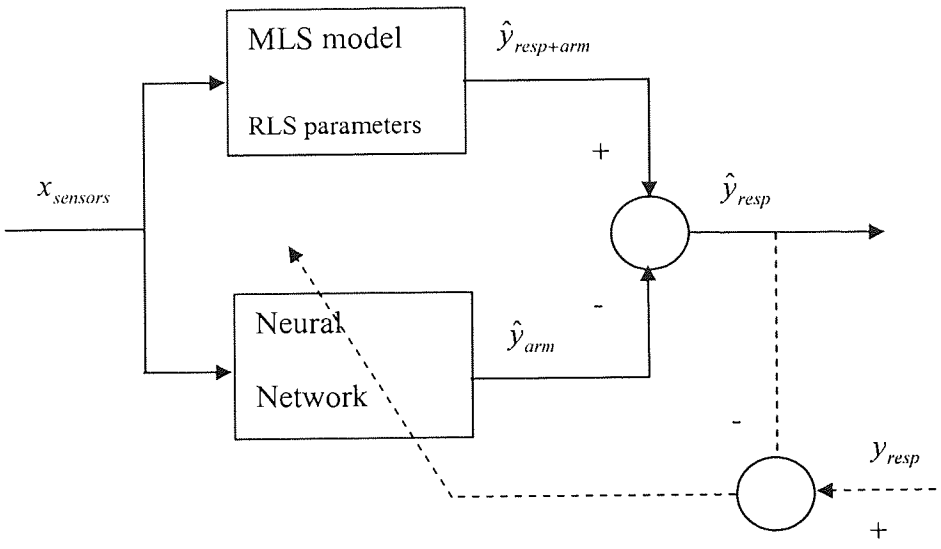

Figure 17. Data processing schematic for arm movement signal cancellation showing linear and neural network processing elements. Broken lines indicate signals flow during the training phase.

The 56-sensor element array on elastic support belts were employed once again to obtain data corrupted by body motion. Once adorned both belts cover the front of the chest and abdomen, from the 4^{th} intercostal space on the upper thorax to the lower rib margin, then extending down to the umbilicus respectively. In each experiment data was collected over a period of 15 seconds, corresponding to approximately 4 tidal periods. Simultaneous volume-flow measurements were made at the mouth with a medical profession standard orifice plate pneumotachograph. Five experiments in total were carried out and the data recorded for a healthy standing male subject. Three data sets were recorded at steady respiration frequency and at approximately constant 1,2 and 3 litre amplitudes. In each of these cases no body motion component was present in the signals. The fourth data set contains body motion. This was introduced by moving

the right arm from a vertical position above the head to a position parallel to the thigh. The remaining data set pertains to the subject breathing at a non-uniform frequency and amplitude.

A classical feed-forward network architecture was chosen for the network, with 4 linear neurones in the input layer, 4 tangent sigmoidal activation function neurones in a single hidden layer and 2 linear activation function neurones in the output layer.

Training was accomplished using the Levenberg-Marquardt gradient-descent training algorithm [Hagan and Menhaj, 1994] over 20 epochs. The training data set included both the arm motion corrupted data as well as all three constant tidal volume sets. Two neurones were employed in the output layer, one for the motion compensation signal and one trained to be zero. This second output was used during development to check the network response to new data, with any significant response indicating the networks inability to model the data reliably.

Figure 18 shows the overall processing system response to both the corrupt data and verification data of increasing amplitude of tidal breathing not presented to the network during training. The performance for the verification data was established by carefully identifying the inspiratory half of the cycle from the data and comparing the volumes breathed during these five periods. This gave a mean percentage error of 1.68% with standard deviation 10.7%. Volumetrically for this data set, a mean error of 4 ml and standard deviation of 176ml.

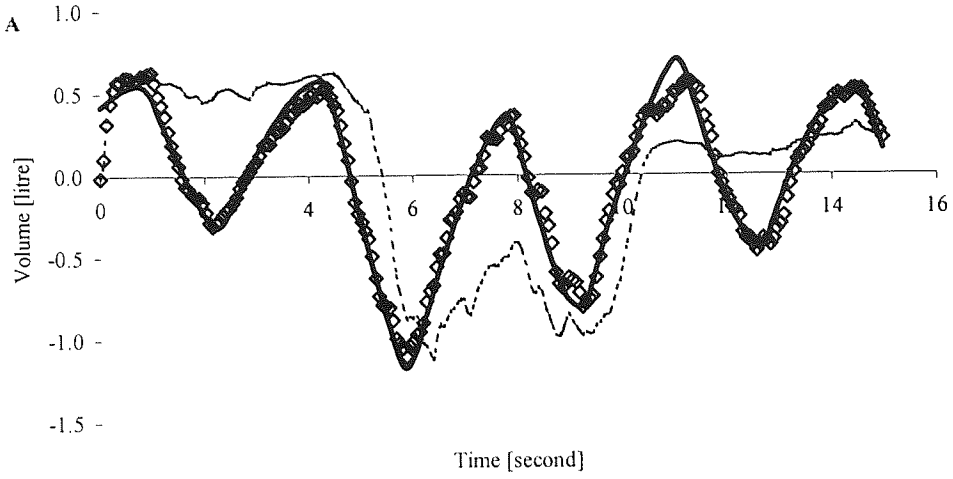

Figure 18. (A) Experimental results of signal separation for data corrupted by arm motion. Solid line is target instantaneous volume measured at the mouth. Diamond markers, the estimated tidal volume from signal processed sensor array. The broken line is the neural network signal showing the motion compensation.

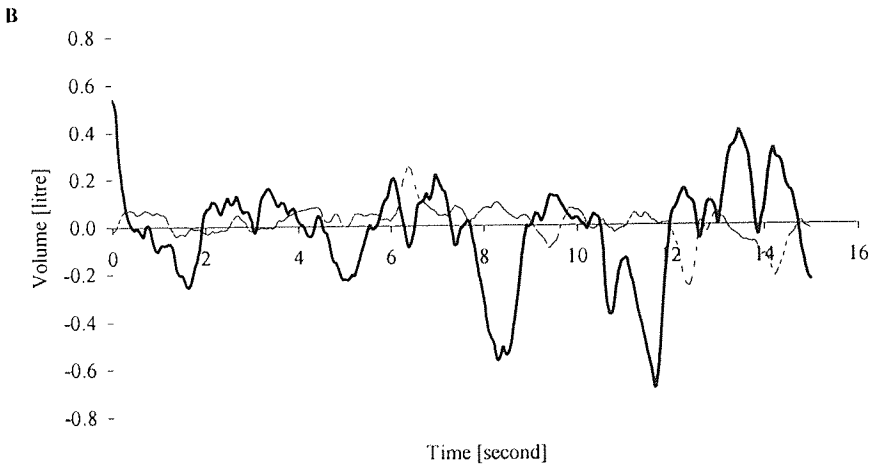

Figure 18 (B) Errors for both data are shown. Solid and broken lines indicating training and verification data respectively.

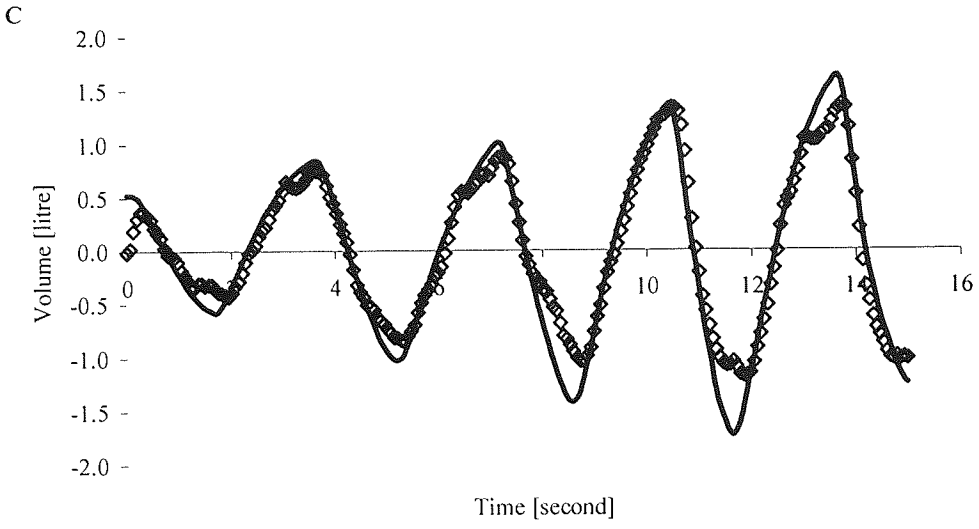

Figure 18 (C) Verification curve of non-uniform tidal breathing data set, with solid line and broken line representing training and hybrid model data respectively.

2.5 Computer based surface reconstruction

Whilst a great deal of documented work already exist in the modelling of stationary surfaces [Piegl,1991] [Woodward, 1988] little has been published concerning volumetric and regional motions at the resolution required in this application. The most prominent existing techniques include Non-Uniform Rational B-Splines (NURBS) alongside a number of alternative bi-cubic surface patch methodologies each of which are highly suitable for computer display rendering and animation. It is not clear at this point in time, which of the available range of surface modelling techniques will be best suited to this task in terms of data volume and processing performance requirements for real time surface reconstruction, however those investigated here have proved suitable for the task.

A computer animation was made using the superposition of sensing array signals from previous experiments on to wire-frame model of Figure 2 at appropriate locations.

MATLAB code for this is included in Appendix 3. This includes code for 'skinning' the wire-frame model.

2.6 Summary

Extrapolating the above results into the future to a point where reliable purpose built sensors are available, the repeatability exhibited in the results demonstrate that reconstructed raw signals from a simple sensor array give reasonable agreement with conventional spirometry. This gives confidence that multiple distributed sensors may be used as the basis of a whole chest motion monitoring system and provide an enhanced performance over measurements made with a that of 2 DOF schemes.

The results demonstrate and raw signals from a simple sensor array can be reconstructed to give reasonable agreement with conventional flow at mouth spirometry even in the presence of strong body motion artefacts.

This also indicates that the interactions between respiratory functions can be decoupled, hence provide a means by which to study components of respiration.

Enhancements in signal segmentation abilities demonstrated here have been gained purely from the increase in the number and distribution of sensing sites. It follows that this increase provides a means by which differentiation between superimposed modes of body motion on respiratory motion can more readily be accomplished.

Incorporating sensory signals into a physiological model that can be related to the physical stature and respiratory patterns for a wide variety of people with this method is a considerable task, which necessitates further investigation once a fully functioning array system has been developed.

3 Geometric surface plethymography

In this investigation the fundamental requirement is to create a highly compliant sensor with which to geometrically track selected anatomical positions on the chest and abdomen surface. Existing techniques of this type include Optical Surface Plethysmography either by optical reflectance [Cala et al, 1996][Kenyon et al, 1997] or alternatively projected light fringes [Gourlay et al, 1984][Morgan et al, 1984][Peacock et al, 1984]. It is also suggested that magnetometers can be used to track surface motions in 3 dimensions [Banzett et al, 1995][Levine et al, 1991][Goldstien & Mead, 1980][Rees et al, 1980][Robertson et al, 1980][Stagg et al, 1980]. Such approaches however require dedicated laboratory space and complex equipment to function.

This chapter investigates a possible solution to mobile respiratory function measurement based upon a curvature-sensing scheme, utilising a long period grating (LPG) fibre-optic sensors constructed in progressive three layered fibre.

Whilst fibre-optic sensors have received some attention for this application [Wehrle et al, 2001][Birch et al, 2001][Babchenko et al, 1999][Pettersson et al, 1996][Davis et al, 1999] all are either concerned with monitoring respiratory frequency or model based plethysmography as discussed in preceding chapters. One of the primary influences in this interest originates from this type of sensors construction and its transparency when used in conjunction with x-ray and magnetic imaging machines. Optical fibres also have an inherent ability to be incorporated within flexible composite structures.

3.1 Fibre optic sensors

Optical fibre is composed of a core of glass typically 10μm in diameter surrounded to an overall diameter of 125 μm by a cladding material of lower refractive index producing internal reflection. This us usually encased in a protective plastic coating. Optical power in fibres is transmitted in a set of electromagnetic waves that may travel in forwards or in reverse in relation to the longitudinal axis of the fibre. These are determined by Maxwell's equation and electromagnetic field boundary conditions at the core and cladding interface. These propagation modes are linear-polarised (LP) modes in an approximation for weakly guided transmission in standard fibre and have a finite number (Figure 19). Radiation modes exist in both the core (guided modes) as well as the cladding (non-guided modes or cladding modes). Power loss is along a fibre is influenced by external reflections at the outer cladding boundary. The strength of transmission through the core is dependent on coupling between core (Gaussian for LP modes) and cladding modes and is proportional to the overlap integral between guided and non-guided modes, illustrated in Figure 19.

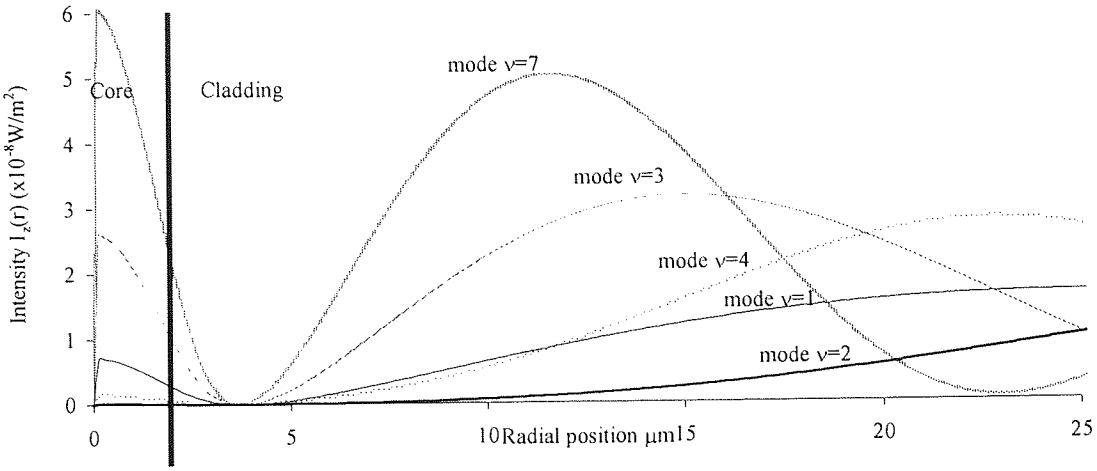

Figure 19. Plots of local electron field intensity Iz(r) as a function of optical fibre radius for various order cladding modes.

In the presence of ultraviolet (UV) light, photosensitised fibre, that is those doped with photosensitive agents such as germanium, boron, erbium etc., undergo a change in the refractive index (n), termed photo bleaching [Bhatia, 1996]. This is in the order of $\Delta\lambda \approx 3e\text{-}4$ in 3% Germanium doped single mode fibres. This can be increased by two orders of magnitude in the presence of Hydrogen and is strongly dependent on temperature and power. Thus by the precision application of high power UV light provided by laser it is possible to control the refractive index perturbation in varying portions of the fibre effecting the interactions of forward and backward propagating transmission modes within the fibre. If photo bleaching occurs at regular periodic intervals (Λ) it is possible to attenuate the transmitted radiation at specific wavelengths. These devices are termed gratings; two main types are referred to, Fibre Bragg gratings (FBG), which have a period of less than 1μm and long period gratings (LPG) with periods typically of 100μm to 600μm. The central wavelength (λ) of stop-bands is dependant on temperature and internal stress in the fibre. With LPG this also includes the surrounding refractive index. LPG have a high sensitivity to bending while in

contrast FBG is relatively insensitive, whereas the reverse is observed in axial strain [Bhatia, 1996].

3.1.1 Fibre Bragg gratings

Fibre Bragg gratings operate on phase matching between forward and backward propagation of guided modes. Phase matching tends to reflect back radiation at attenuation frequencies. Using weakly guided assumptions there is an approximately linear relationship between the coupling or Bragg wavelength (λ_B) and the grating period:

$$\lambda_B = n_{eff}\Lambda$$

Equation 6

Where n_{eff} is the effective refractive index of the fundamental mode and is strongly influenced by thermal expansion and strain and as such predominantly find application in a sensing capacity to measure these properties [Grattan & Meggit, 2000].

Fibre Bragg gratings posses a single narrow attenuation band, typically 0.2nm to 0.3nm in spectral width. The spectral profile of a typical FBG in reflectance is shown in Figure 20.

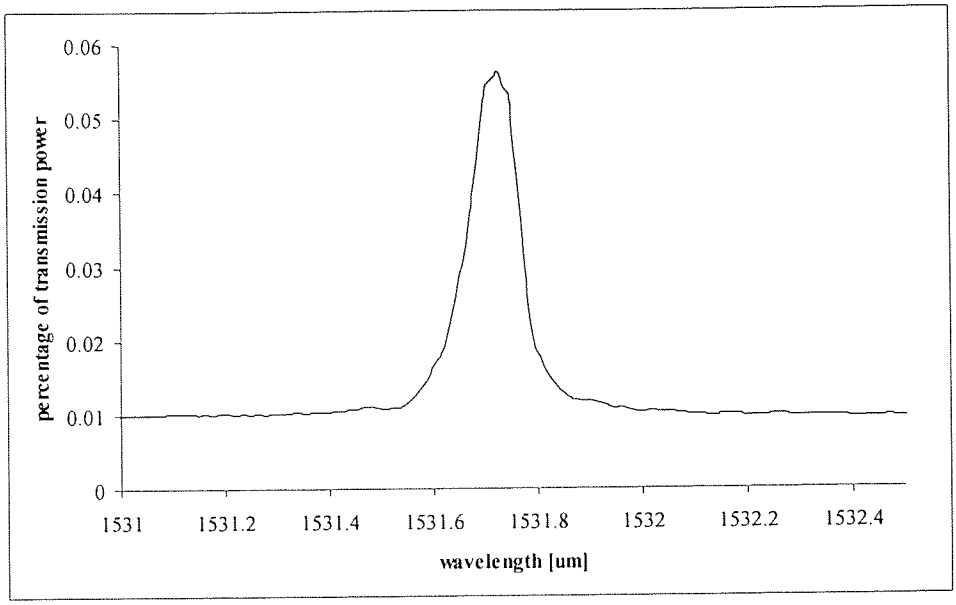

Figure 20 Spectral profile of a typical Fibre Bragg Grating

The gratings fabricated for the purposes of this study were inscribed into the fibre using a phase mask technique, in which a traversing beam of UV light is focused on the fibre through a spatial filter or amplitude mask. The period of the grating is controlled by the period of the mask however applying an axial strain to the fibre during the inscription can accommodate small changes in central wavelength.

3.1.2 Long period gratings

LPG have found numerous applications in the field of sensing through its sensitivities to strain(ε), curvature (C), temperature (T) and the refractive index of the surrounding medium (n_s) [Vengsarkar et al, 1996][Bhatia et al, 1996][Bhatia et al, 1988][Grubsky & Finberg, 2000] [Patrick, 200][Lee et al, 1998][Ye et al, 2000][Chen et al, 1999] [Allsop et al, 2001]. The physical impetus for these phenomena are considered in appendix 2.

A long period grating possesses a number of attenuation bands in the fibre's transmissivity, occurring at wavelengths where the long period grating enables phase matched coupling between guided and cladding circularly symmetrical modes.

Therefore the attenuation bands are a result of power loss into the cladding rather than a reflective process as with fibre Bragg gratings [Vasilev et al, 200]. This produces a shift in wavelength and a change in the spectral profile of the attenuation bands [Ye et al, 2000][Chen et al, 1999] according to:

$$\Delta n_{eff} \cdot \Lambda = \lambda$$

***Equation** 7*

The spectral position of the attenuation band, the magnitude of the spectral shift is dependent on the difference between the effective refractive indices at modal frequencies, which in itself is both temperature and strain sensitive [Patrick, 2000].

The spectral sensitivity of long period gratings to bending arises from the strain sensitivity as bending introduces both strain and compression to the fibre. This process is more influential than with Bragg gratings and as such long period gratings are more suitable for sensing curvature. Typical LPG attenuation bands are shown in Figure 21.

The long period gratings fabricated for the purposes of this study were inscribed into the fibre using a point by point technique, in which a continuous stream UV power is focused on the fibre through a shutter as it traverses along the fibre. Opening and closing the shutter at spatial intervals at the desired period produces the grating. This method is more flexible than the amplitude mask method (that may also be used to produce long period grating). It allows the formation of various shaped gratings, chirped etc.

The typical amount of hydrogen present in an optical fibre for grating fabrication is far in excess of that required to achieve a given change in refractive index. Therefore at the end of the inscription process there is a finite amount of unused hydrogen remaining in the core and cladding that can significantly influence the transmission spectrum.

Residual hydrogen will gradually diffuse from the fibre. This results in an overall centre wavelength in the order of 90 μm in a blue shift, i.e., towards shorter wavelength. The process has two facets, as the Hydrogen diffuses first from the core to the cladding resulting in a difference in refractive index differential that causes a red shift once a balance is reached, diffusion of residual hydrogen from the cladding results in the overall blue shift observed once equilibribrium has been reached. The initial red shift occurs over a period of hours while the slower blue shift is observed over the period of several weeks (typically 6 weeks). This process can be modified with the application of thermal energy, which speeds up the diffusion rate but also has an effect on other refractive properties in the fibre and tends to significantly weaken the strength of attenuation bands. It is therefore possible to control the width, strength and spectral location of stop-bands, however this must be achieved using empirical methods for a given type of fibre and fabrication conditions.

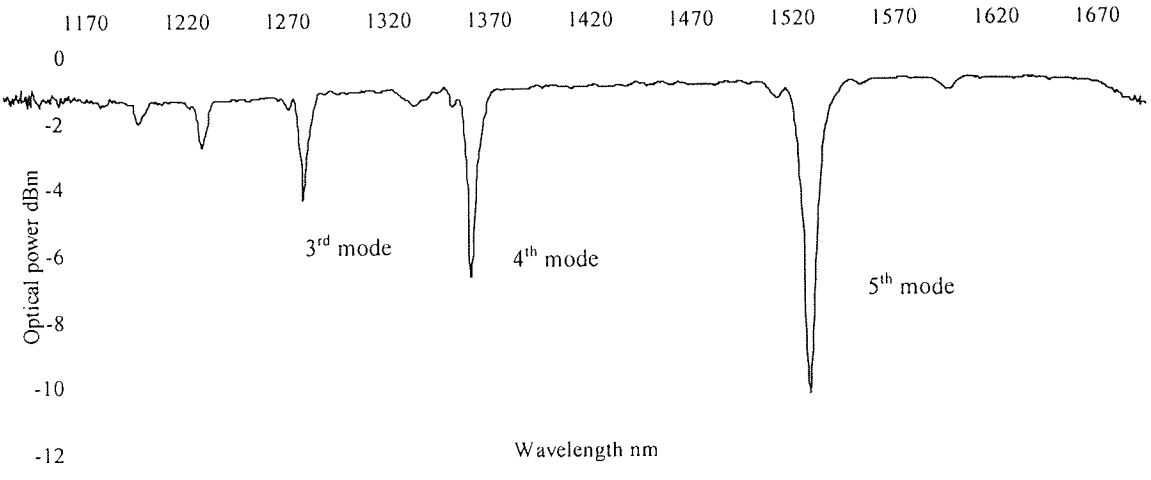

Figure 21. Core transmission spectrum of co-doped Boron/Germanium single mode optical fibre with a long period grating (Λ=325mm, length=5cm)

The long period grating as a sensing element is a prime candidate for the respiratory application but there are several disadvantages/problems to be addressed:

- The device is sensitive to the refractive index of the surrounding material.
- The device is sensitive to temperature and axial strain not produced by bending.
- Interrogating the LPG requires an expensive broadband light source and optical spectrum analyser (OSA), which is also sizeable and fragile.

Allsop et al, 2002(b), demonstrate that lower cladding modes in Progressive Three Layer (PTL) fibre are less sensitive to strain, temperature and completely insensitive to refractive index perturbations [Jang et al, 1999]. Wavelength shift sensitivity versus modal order is depicted schematically in Figure 22. This shows that both low order modes are less sensitive to perturbation but also that PTL fibre is both less sensitive in all modes but the number of insensitive lower order modes is also increased. The fibre characteristics and sensitivities are reproduced from [Allsop et al, 2002(e)] in Appendix 1. PTL fibre characteristics have been modelled and are shown in Appendix 2. Progressive three layer fibre has been adopted for the sensing scheme in later sections of this thesis. Section 3.3 considers embedding PTL fibre sensors into a composite material with reference to changes in the surrounding refractive index, temperature and compressive forces.

Thus an interrogation scheme from derivative spectroscopy [Chen et al, 1999] is adopted that requires only a laser diode source. Potentially this sensing scheme can be relatively inexpensive to implement and compact in size [Allsop et al, 2002(a) & (c)], meaning that the entire system could be portable. Such devices are expensive at present,

therefore an inexpensive interrogation scheme based on FBG are also examined. Both interrogation methodologies are discussed in section3.4 .

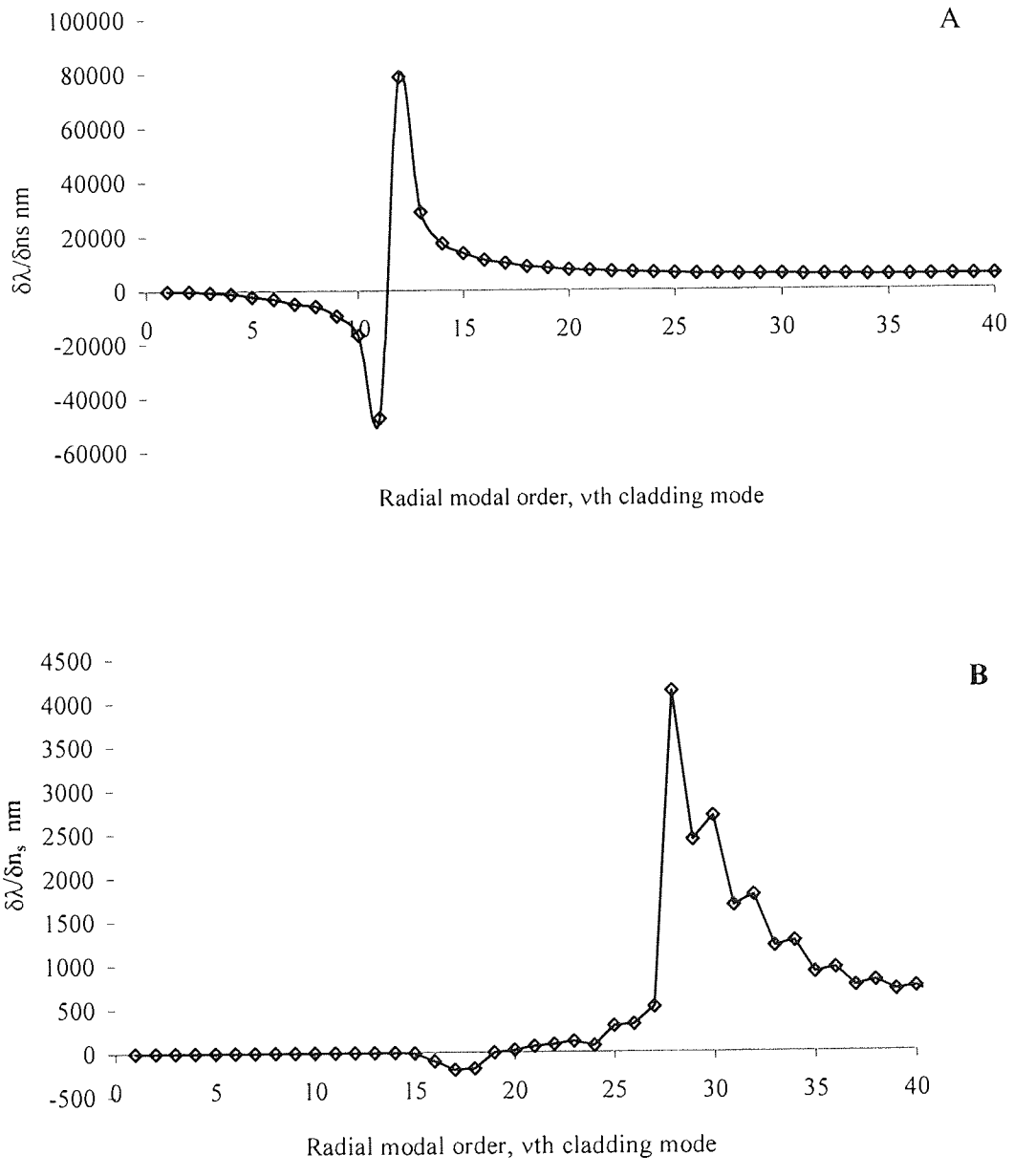

Figure 22. The maximum spectral sensitivity of the cladding modes as a function cladding mode order for (A) Standard telecom fibre and (B) Progressive three layer fibre

3.2 Long period grating bend sensor

Two LPG were formed in single mode optical fibre with periods of 240μm (total length of 8cm and a strength of ~14dB) and 480μm (total length of 10cm and a strength of ~10dB). The LPG were UV inscribed using a pulsed frequency quadrupled Yttrium Aluminum Garnet (YAG) laser and an amplitude mask in a Boron/Germanium co-doped fibre without H_2-loading. This generated an attenuation band with a centre wavelength at ~1536nm associated with the 9th cladding mode for the LPG with period of 240μm, and an attenuation band with a centre wavelength at ~1522nm associated with the 5th cladding mode for the LPG with period of 480μm. The fibre was clamped between two towers; one of the clamps was mounted on a translation stage, which was moved inwards to induce a bend in the optical fibre (Figure 23|). The fibre's bend curvature is given by [Du et al, 1998]:

$$C = \frac{2 \cdot d}{\left(d^2 + L^2\right)}$$

Equation 8

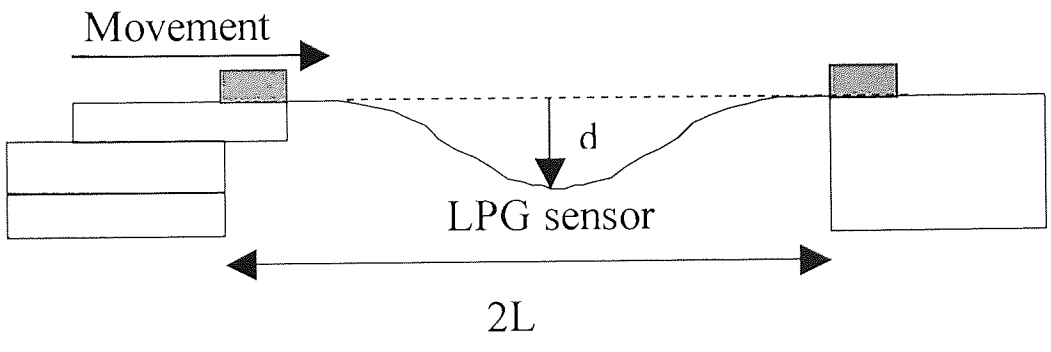

Figure 23 . Bending apparatus schematic

The spectral responses of these attenuation bands with respect to curvature were observed with an optical spectrum analyser and an example is shown in Figure 24.

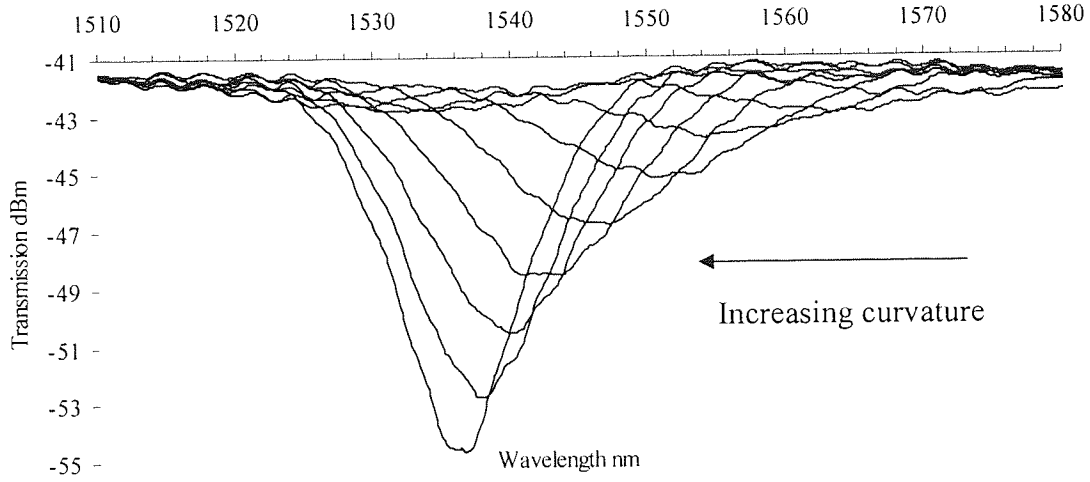

Figure 24 The effect on the optical transmission spectrum of an LPG (period=480μm) when the LPG is subjected to various curvatures.

The range of curvature over which the scheme was employed was ~$4m^{-1}$; outside this range the attenuation band splits into two. This effect is concerned with the polarisation stated of modes in birefringent fibres. Analysis shows that curvature resolution of $0.05m^{-1}$ and $0.06m^{-1}$ for LPG(Λ=240μm) and LPG(Λ=480μm) respectively. The method for this analysis is discussed in section 3.4.1 .

Relating the above findings to those that might be expected in the intended is accomplished by employing an elliptical model of the chest and abdomen cross-section to approximate the curvature. Ackerman et al [1985] employ a similar approach to estimate cross-sectional area. Here the minor elliptical axis is approximated as 2/3 that of the major. This provides a base-line curvature from the mid-tidal volume position. Deviations both above and below this level were then simulated to be indicative of respiration amplitudes on the bend sensors. A simulation was conducted for a male with a 1m chest perimeter and a 0.05m expansion. It was found from the simulation the

greatest curvature ranged from 12.0143m^{-1} to 11.4422m^{-1}, thus giving a bending motion magnitude of approximately ±0.28, whilst for the smallest curvature ranged from 3.5598m^{-1} to 3.3903m^{-1} giving a bending motion magnitude of approximately ±0.08m^{-1}. Whilst the curvatures obtained from the simulation are larger than those that were monitored using the LPG, adjusting the orientation of the LPG on the torso can accommodate this, thereby increasing or decreasing the dynamic range of curvature.

3.3 Embedding LPG sensors

Problems occur when conventional step-index single-mode fibre is recoated after the grating inscription process. The spectral position and strength of LPG attenuation bands are dependent upon the refractive index of the surrounding medium (n_s). In the process of recoating the fibre, n_s is altered, thereby changing the spectral position and profile of the stop-bands or in some cases the stop-bands disappear. This is attributed to changes in cladding refractive index, i.e., if n_{cl} becomes greater than the core waves are not guided. To overcome this LPG fabricated in multi-layered single-mode optical fibres are investigated.

Investigations include the use of air-clad fibres [Espindola et al, 1999] or depressed-cladding fibres [L. Dong et al, 1997] to desensitise the structure to changes in the refractive index of the surrounding medium. Allsop et al [2002] report that lower order cladding modes of LPG fabricated in a single mode Progressive-Three-Layered (PTL) fibre are insensitive to n_s.

3.3.1 The fabrication of and transmission spectrum of the LPG platform

PTL is a specialised optical fibre supplied by Fibercore Ltd. and was originally designed for cladding pumped erbium doped fibre lasers. The fibre is not specifically

designed to be photosensitive and so photosensitivity was increased by hydrogenation at room temperature at a pressure of 120 Bar for a period of 2 weeks. A number of LPG of various lengths and periods were fabricated in the fibre using the point-by-point inscription technique [Bhatia, 1996]. The UV beam was generated from a frequency doubled Argon ion laser and was focused to a spot size of ~10μm, the approximate diameter of the fibre core.

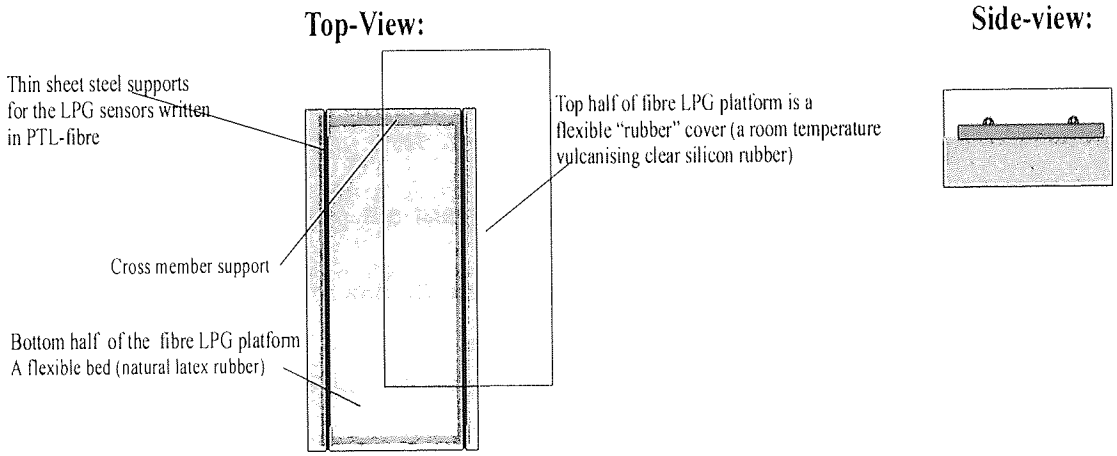

Figure 25 The long-period grating sensor platform

The periods of the LPGs were chosen between 210μm to 350μm so that the associated cladding modes of the stop-bands from the first ten modes, which are insensitive to n_s were spectrally located in the range 1400nm-1550nm.

Two LPG with periods 350μm and 240μm were embedded into a platform. The platform itself is constructed on a base pad of natural latex rubber 250mm by 120mm

and with a 2mm depth. This provides both a flexible stage as well as a thermally insulating layer to reduce the effects of body temperature. Both LPG were adhered to strips of carbon steel 200 x 12 x 0.254mm using a standard cyanoacrylate adhesive. These were then adhered using the same adhesive parallel to each other on the rubber base 75mm apart. Two additional steel strips 80mm long provide a perpendicular link between the sensors at either end. This framework lends longitudinal rigidity to the system, the steel having an elastic modulus of 210GPa. The sensors are then sealed on the sensor side of the rubber base with a room temperature vulcanising clear silicon rubber to a depth of approximately 3mm. The refractive index of the silicon encapsulation is approximately ~1.5, The platform is shown schematically in Figure 23.

The PTL-fibre with the LPG was fusion spliced at both ends to standard single mode telecom optical fibre (STO-fibre). Spectral characteristics of the attenuation bands before and after embedding were obtained by illuminating the LPG using a broadband light source and observing the transmission spectrum with an OSA, the resolution of which is ±0.04nm. Before and after spectra are shown for the 350μm sensor is depicted in Figure 26.

The two transmission spectrums in Figure 26 show that the central wavelengths of the observed attenuation bands have not changed in spectral location after being embedded. The spectral profiles have altered but not significantly.

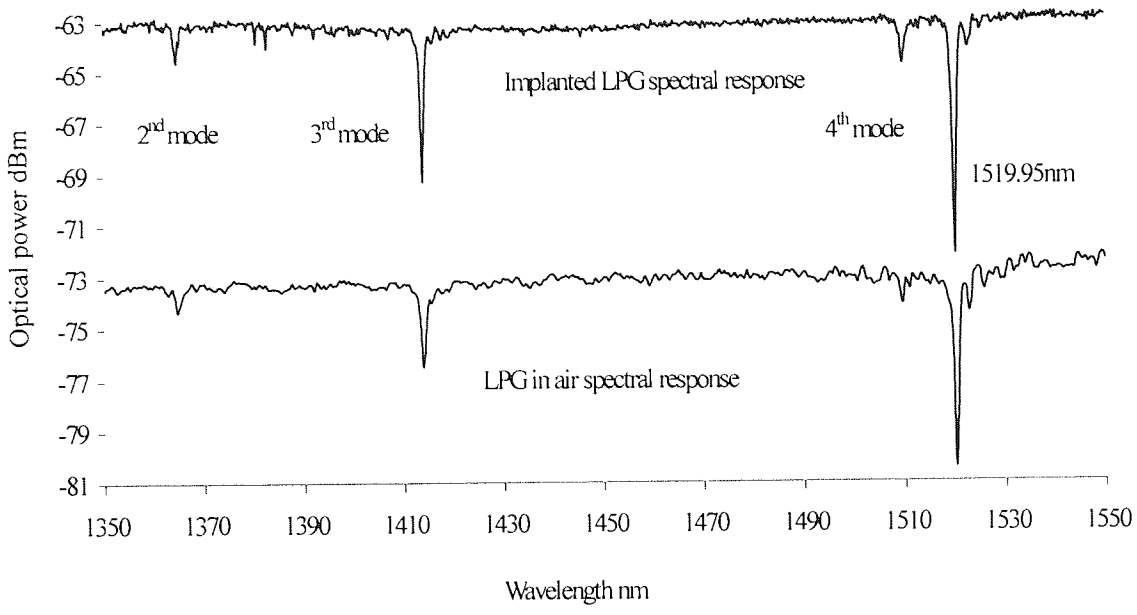

Figure 26. The transmission spectrum of a LPG (period of 350μm) written in the PTL-fibre before and after embedding, an offset as introduced for clarity.

3.3.2 Sensitivity of LPG sensor platform to perturbation

The LPG sensor platform was subjected to three perturbations, temperature, compression and bending.

3.3.2.1 Temperature sensitivity

Assuming that the skin temperature varies from ~32°C to ~35°C [Miyanaga et al, 2001]. The spectral sensitivity as a function temperature was investigated by placing the LPG platform on hotplate. The temperature measurement of the hotplate was accomplished using a platinum resistance temperature device (PRTD), which possesses an accuracy of ±0.1°C. The spectral location of the central wavelength of the stop-band associated with the 4th cladding mode versus temperature is shown in Figure 27.

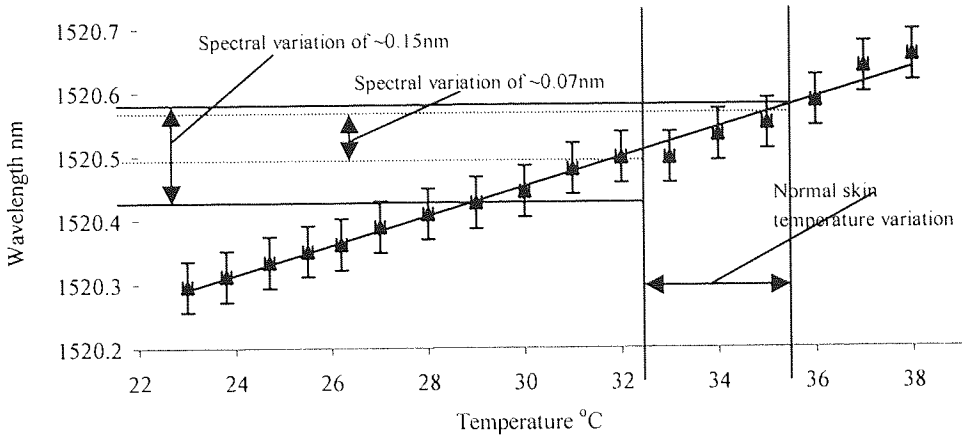

Figure 27.The spectral sensitivity of an LPG (period of 350μm) written in the PTL-fibre embedded in the platform. Error bars indicate the accuracy of the OSA (±0.04nm).

Over the range 23°C to 38°C a total wavelength shift of 0.36nm was observed which gives sensitivity of $\frac{d\lambda}{dT} \approx 2.3 \pm 0.1 \times 10^{-2}$ nm°C^{-1}. A comparison of this sensitivity to that of the same cladding mode given by [Allsop & Neal, 2002] 0.198 nm°C^{-1} with bare fibre: it is evident that the LPG sensor platform sensitivity is approximately an order of magnitude smaller than, as expected. This is accredited to the insulating properties of the platform itself and the fact that the sensor will take on the thermal properties of the Steel.

3.3.2.2 Sensitivity to external loading

The influence of external loading on the spectral sensitivity of the LPG platform was realised by placing flat weights on the top surface (the encapsulation layer) of the LPG platform. For the load applied there was no significant wavelength shift or change in the spectral profile of the LPG's attenuation band observable. Figure 28 shows the embedded LPG (period 350μm) response to loading.

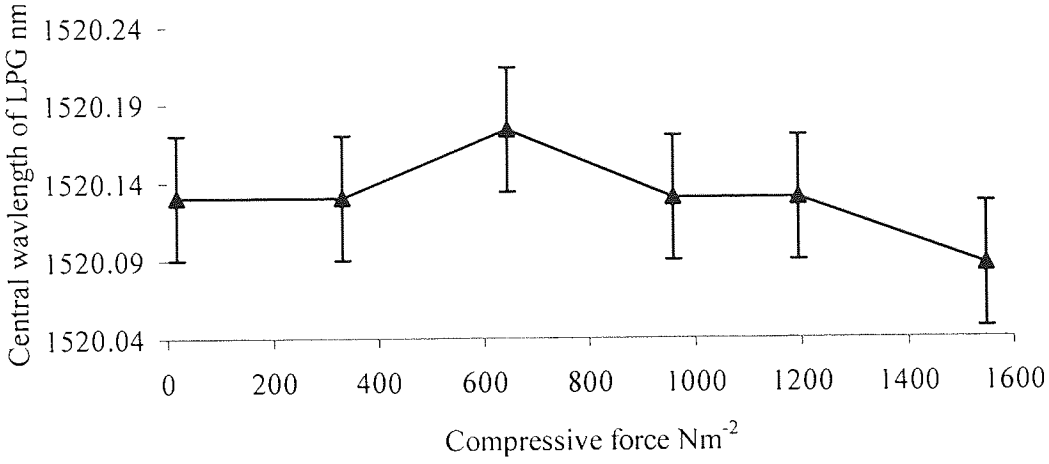

Figure 28. Spectral stability of embedded LPG (period 350μm) under compression. Error bars indicate the accuracy of the OSA used (±0.04nm).

3.3.2.3 Bend sensitivity

A third investigation to obtain the spectral sensitivity of the LPG platform as a function of bending this achieved by using the experimental rig shown in Figure 23. The procedure followed was the same as for that described in section 3.2 The experimental results for spectral sensitivity of the LPG platform as a function of curvature along with the theoretically predicted wavelength shift is shown in Figure 29. The effective refractive indices of the core and 4th cladding mode were calculated as a function of curvature using 2-D curvilinear hybrid mode eigenvalue equation, which gives effective refractive index as a function of radius of curvature [Tsao, 1992]

Using the optical constants given in Appendix 1. There appears to be reasonable agreement between the theoretical wavelength shift calculated and experimental results. The reason for the theoretical data variation is due to the precision problem of the numerical calculations to obtain δn_{eff}.

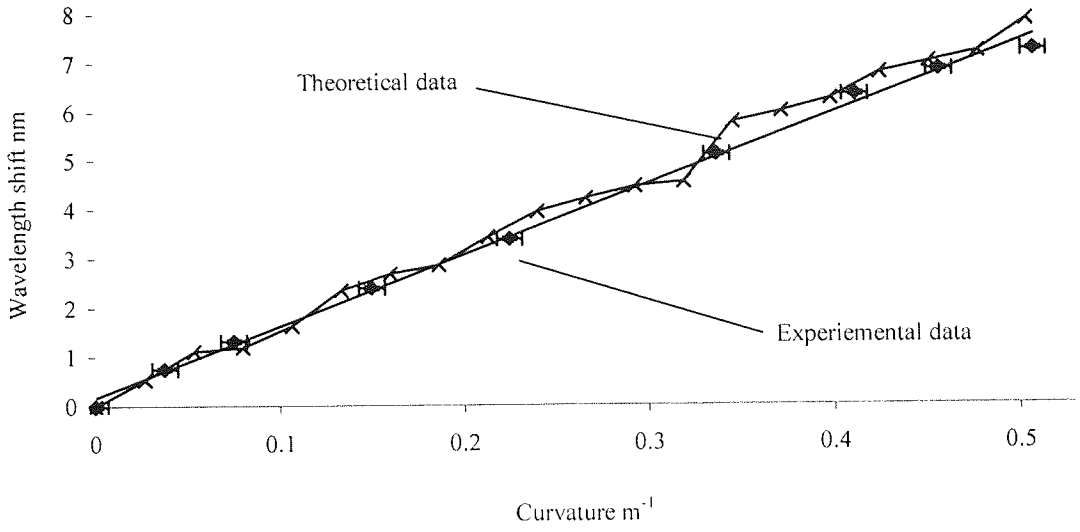

Figure 29. The central wavelength of the attenuation band (4^{th} mode) of LPG (period 350μm) embedded in the platform as a function of the curvature experienced by the platform

Over the range of curvature investigated the spectral sensitivity of the LPG platform was found to be linear with $\frac{d\lambda}{dR} \approx 14.474\,\text{nm m} \pm 8.3\times10^{-3}\,\text{nm m}$ the error was assessed from the residual analysis from the linear regression of the experimental data.

3.4 Interrogation techniques

The conventional interrogation method for LPGs adopted by researchers is to measure the wavelength shifts using an OSA. While this detection method is useful in the laboratory it is not practical for most applications because of the cost, size and lack of robustness of the OSA. Thus an interrogation scheme from derivative spectroscopy [Chen et al, 1999] is adopted which does not require an OSA and has the potential to be made compact.

The approach used was originally developed for wavelength modulation absorption spectrometry and involves applying a small sinusoidal wavelength modulation to the

optical source. This technique is mostly used for environmental monitoring and remote sensing as well as spectrochemical applications, e.g. NO_2 and CCL_4 detection. Comprehensive attention is given to this technique in [Kluczynski et al, 2001].

In this sensing system is it used to detect the changes in the spectral transmission profile of the LPG stop band induced during bending. Modulating the source wavelength at a given frequency will generate a series of harmonics at the modulating frequency in the output signal of the sensing scheme. It as been shown that the in-phase component of the n^{th} harmonic is proportional to the n^{th} derivative of the absorption profile under investigation [Allsop et al, 2002(c)]. The amplitudes of the first and second harmonics are proportional to the first and second derivatives of spectral transmission output of the sensor, and this approach relies on the ratio of the derivatives being a unique function of the position in the spectral profile as well as being independent of power level fluctuations in the system.

3.4.1 Distributed feedback laser interrogation

Employing a distributed feedback (DFB) pigtailed laser to illuminate the LPG at a mean wavelength λ_0, close to the LPG resonance and in the saturation regime, i.e., laser power is independent of wavelength. Figure 30 shows the attenuation profiles of the LPG at different curvatures along with the frequency of modulation (ω) of the DFB laser. A relationship exists between the output of the interrogation scheme ($A_{1,Amp}$, $A2_{,Amp}$ and $A_{3,Amp}$) and the level of curvature experienced by the LPG (R_1, R_2, and R_3). Using synchronous detection, the amplitudes measured at the first and second harmonics of ω are proportional to the first and second derivatives of the transmission output of the LPG with respect to wavelength.

Hence by monitoring the ratio of the first two harmonics should give the level of curvature of the LPG. Treating the DFB output as a delta function and assuming that the curvature response over the interrogated range approximates a sinus the irradiance produced at the LPG output functionally is a sine of a sine. Using Bessel identities of this trigonometric function it can be shown that the amplitudes of the 1st and 2nd harmonics are represented by $Amp^{1st} = A \cdot \sin(\xi)$ and $Amp^{2nd} = B \cdot \sin(\xi + \alpha)$, with ξ being a quantity relating degree of curvature experienced by the LPG and α the relative phase between the harmonics. Thus taking a ratio of the amplitudes of the harmonics can provide a unique ratio value for a given radius of curvature [Kluczynski et al, 2001].

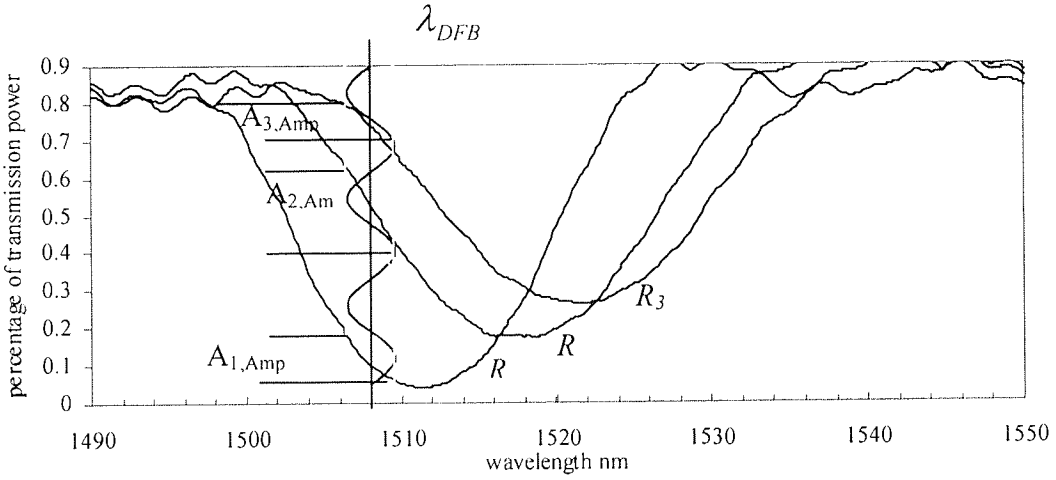

Figure 30 Transmission output of a DFB laser as a function of wavelength for different curvatures, $A_{1,Amp}(R_1)$,$A_{2,Amp}(R_2)$ and $A_{3,Amp}$ (R_3) and $\lambda_{DFB} = \lambda_0 + \Delta\lambda \cdot \sin(\omega \cdot t)$

Returning to the sensor in the experiment of section 3.2 to demonstrate this interrogation technique, one end of the fibre was connected to a thermally stabilised DFB laser, which illuminated the LPG at a wavelength of ~1532nm. The DFB laser injection current was modulated in order to produce a small sinusoidal modulation in wavelength of amplitude 0.06 nm at a frequency of 5kHz. The opposite end of the LPG

was directed to a photo-detector and the output of the detector was connected to two lock-in-amplifiers, which performed synchronous detection at a frequency of 5kHz and at 10kHz, thereby measuring the amplitudes of the first and second harmonics of the modulation frequency of the DFB laser.

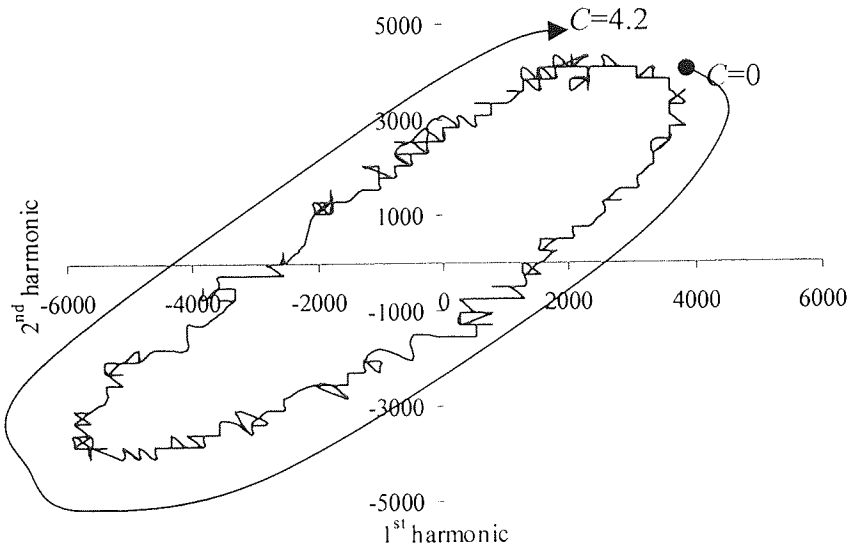

Figure 31. Experimental parametric plot of the first and second harmonic of the modulation frequency of the DFB laser (modulation amplitude of ~0.06nm), obtained using the fibre LPG with a period of 480μm.

The amplitudes of both harmonics were measured and the curvature was varied, which yielded parametric plots, an example of which is shown in Figure 31.

If over the range of perturbation the first and second harmonics are purely sine and cosine in function, which with theoretical assumptions they would be, taking the inverse tangent of the ratio of the amplitudes yields an approximately linear relationship to the LPG curvature. Figure 32 & Figure 33 show this.

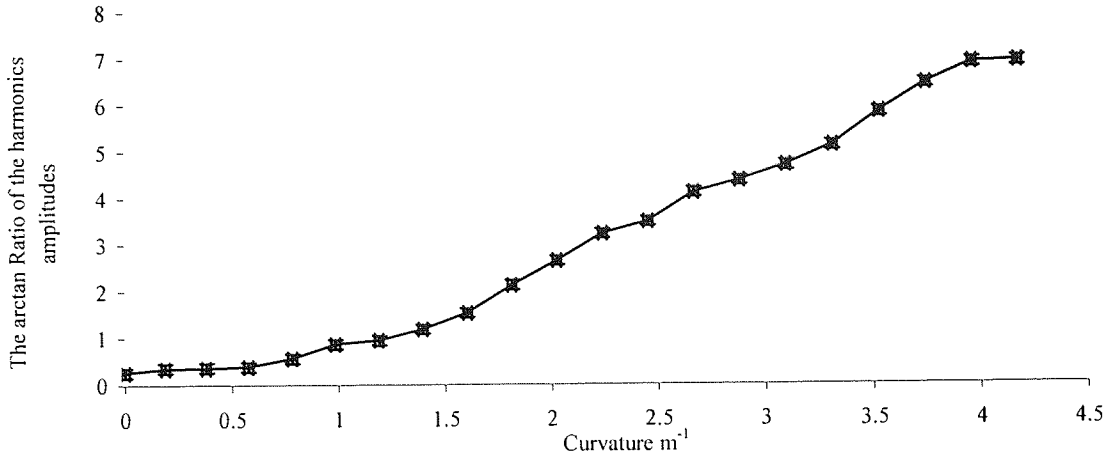

Figure 32. The approximate linear relationship generated from the bending scheme using an LPG with a period of 480μm.

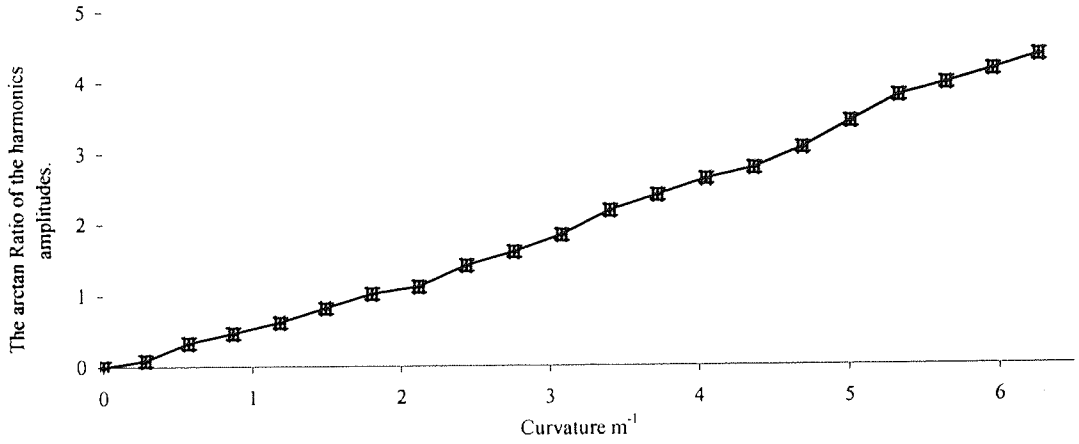

Figure 33. The approximate linear relationship generated from the bending scheme using anLPG with a period of 240μm.

The stability of the arctangent value was 0.05 for the LPG(Λ=240μm), which relates to a curvature resolution of 0.05 m^{-1} when linear regression is applied to the data and the residuals examined. For LPG(Λ=480μm) a value of 0.06 was measured, this relates to a curvature resolution of 0.06m^{-1}. In the second case however a third order polynomial was fitted to the experimental data to improve the fit. A difference is expected because the two LPG have different temperature characteristics [Jang et al, 1999]. The range of

curvature over which the scheme was employed was ~4m^{-1}, outside this range the attenuation band splits into two. This can be attributed to the overlap integral becoming stronger for different LP modes in the fibre under increased bending.

3.4.2 FBG interrogation

A similar interrogation technique as that described in the previous section based on derivative spectroscopy can also be applied to provide a more economical solution. The cost of several light sources is prohibitive using DFB lasers when there are several LPG to interrogate.

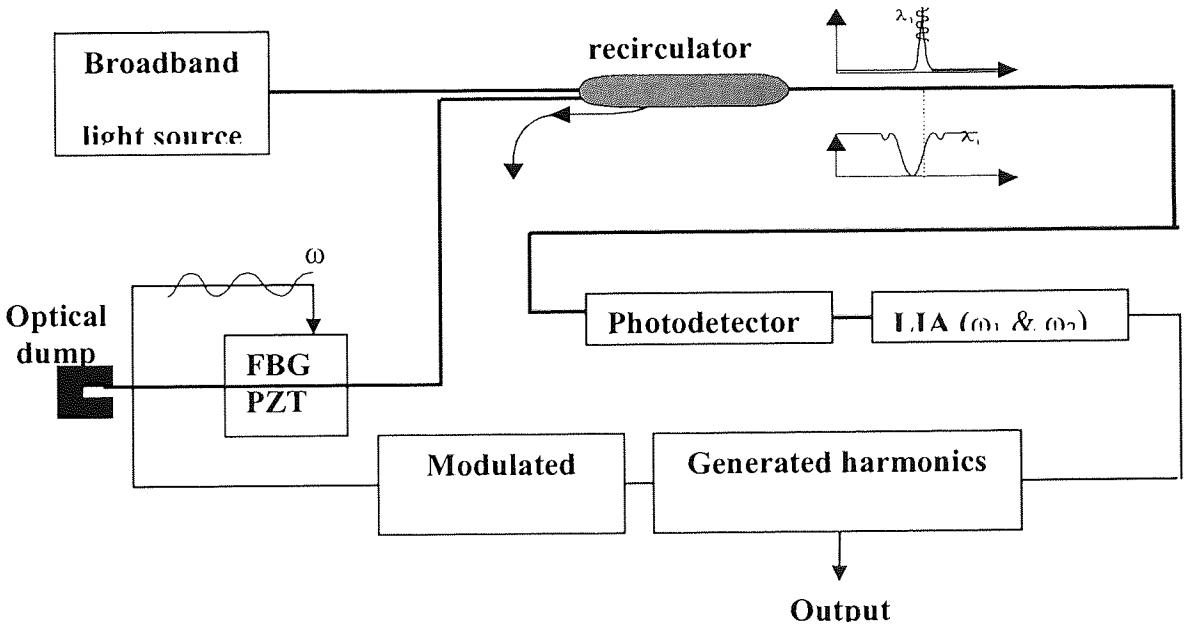

Figure 34. A schematic of FBG based interrogation scheme.

The revised scheme presented here consists of a super-luminescent diode (SLED) ~5mW light source which illuminates a FBG attached to piezoelectric (PZT) extender via a circulator. The FBG reflected spectrum with typical bandwidth of ~0.2nm is spectral matched to the sensing LPG with typical bandwidth of ~10nm. This is positioned at a slightly longer wavelength than the central wavelength of the LPG's attenuation band as the central wavelength of the LPG under bending undergoes a shift

toward the red end of the spectrum. A sinusoidal voltage is applied to the PZT extenders to induce a sinusoidal spectral variation in the reflected spectrum of the FBG. This variation gives wavelength modulating light source to the LPG that mimic the modulating DFB laser in section 3.4.1 . Figure 34 shows a schematic of the interrogation scheme.

The FBG specification used in the verification of interrogation method had a length of 4cm, a central wavelength ~1535.4nm with ~12dB side-lobe suppression and a 9dB bandwidth of ~0.28nm, which illuminated the LPG with ~2μW. The voltage supplied to the PZT extender had an amplitude ~2V and a modulation frequency of 5KHz. This induced a wavelength modulation of ~0.07nm in the FBG central wavelength.

The sensing LPG specification used had a length of 8cm period of 480μm, a central wavelength ~1522.85nm, a strength of 7dB and a 3dB bandwidth of ~7nm. The 1^{st} and 2^{nd} harmonics amplitudes were detected using lock-in-amplifiers (LIA).

Figure 35 shows an experimental parametric plot of the 1^{st} and 2^{nd} harmonics amplitudes generated from an LPG subjected to bending and inspected using a FBG.

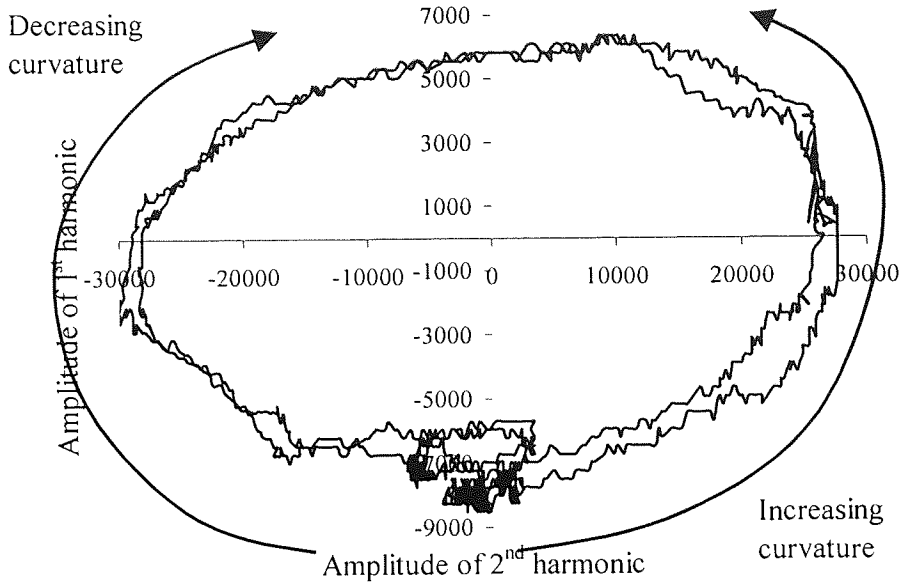

Figure 35. A parametric plot of curvature sensing using an FBG to inspect an LPG

Taking an inverse tangent function of the ratio of the amplitudes of the first and second harmonics from the experiment yields an approximately linear relationship with the curvature experienced by the sensing LPG, Figure ***36***. The reason the linearity starts at ~0.593m^{-1} is because of the spectral difference between the FBG and LPG and stops at ~1.836m^{-1} because the LPG's attenuation band has spectrally shift (red) away from the FBG central wavelength.

The spectral transmission profile of the LPG at 11 discrete curvatures was recorded with an OSA and used along with the transmission spectrum of the Bragg grating to simulate the interrogation scheme for verification. This involved convolving the FBG and LPG spectra around the FBG central wavelength of 1535.5nm. The discrete Fourier transform was then applied to 50 data points displaced sinusoidally about the centre wavelength at amplitude 0.05nm and the ratio of the 1st and 2nd harmonics used to produce the data in Figure 37.

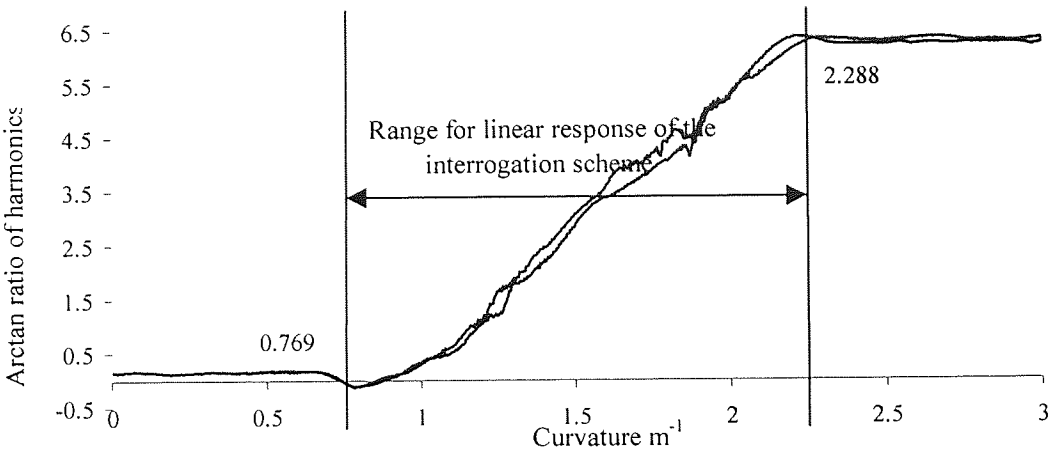

Figure 36. The quasi-linear relationship generated from the bending scheme using a sensing LPG with a length of 8cm and a period of 480μm fabricated in a step-index B/Ge codoped single mode fibre and utilising a FBG for inspection.

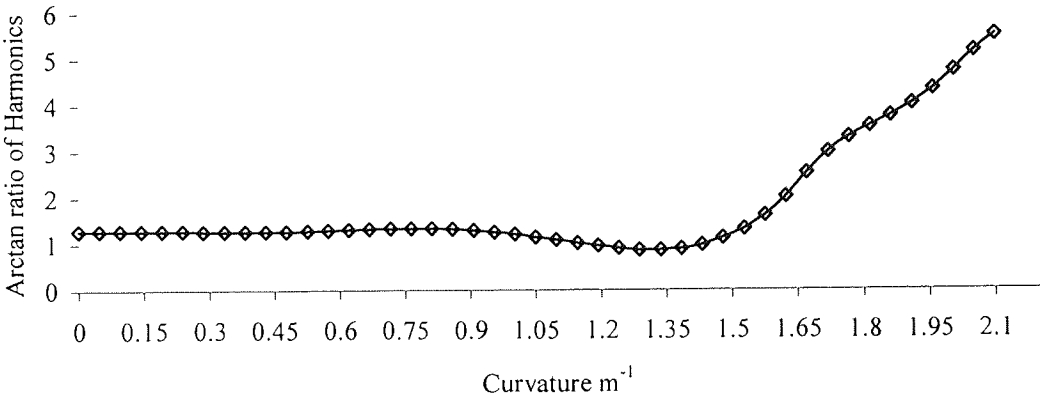

Figure 37. Simulated interrogation response for the LPG and FBG used in the experiment.

The spectral sensitivity of this sensing LPG with this interrogation scheme could be changed by altering the phase matching condition between the LIA after several tests an average sensitivity was found to be 5.537m $\pm 1\times10^{-3}$ m with a maximum of 8.305m and minimum of 4.985m. The errors were estimated after several test-runs with an average

resolution of ±0.252 which translates to an average curvature resolution of $\pm 4.4\times10^{-2}$ m^{-1} and a maximum resolution of $\pm 3.1\times10^{-2}$ m^{-1} was observed (Table 3).

Trials	*Senstivity m*	*Error in spectral radians*	*Error in curvature m^{-1}*
1	4.985	±0.222	±0.036
2	5.463	±0.221	±0.053
3	5.198	±0.272	±0.043
4	5.548	±0.247	±0.039
5	6.035	±0.271	±0.043
6	5.379	±0.285	±0.053

Table 3 Experimental results from the sensing scheme using a single LPG.

The Repeatability of the sensing scheme was investigated by applying a bend to the LPG element and then reducing the curvature repeatedly. Typical results are shown in Figure 38.

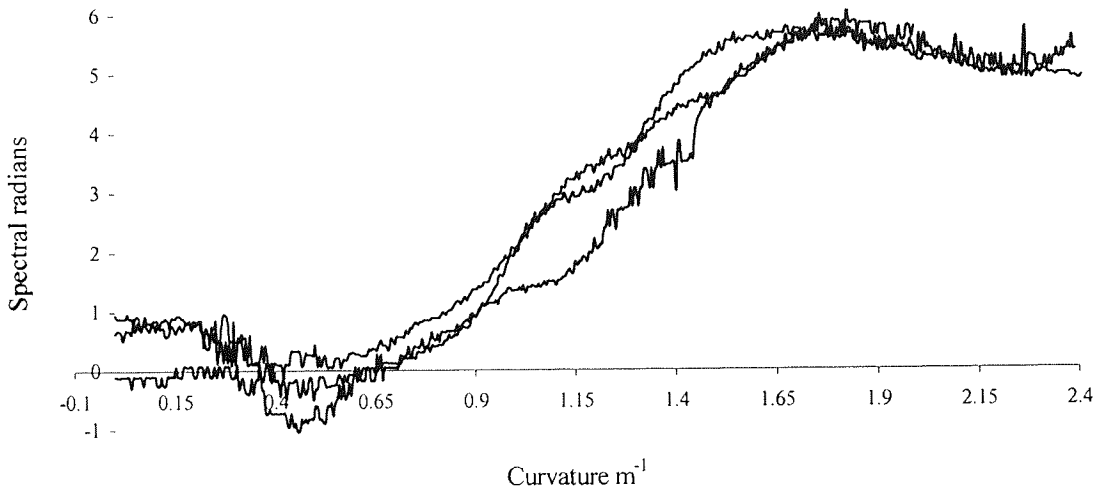

Figure 38. Showing the repeatability of the sensing scheme utilising FBG for interrogation

3.5 Sensor density

To approximate to the number of sensors that would be necessary to achieve generally accepted spirometric device efficiency standards [American Thoracic Society, 1979] was made using chest profile data obtained from a computed tomography (CT) imager. The upper chest geometry of a male subject was reconstructed using a 7^{th} order polynomial and the peripheral length of the curve evaluated symbolically. This was then compared to the same estimated numerically using simple trapezoidal integration at lower spatial resolutions in order to obtain an estimate of the error with respect to number of sensing locations. Assuming that identical longitudinal and lateral resolution is required the total number of points over the torso versus surface area error is depicted in Figure 39. This error may be further reduced with the application of 4-point cubic-spline interpolation. This indicates that relatively few (~20) sensing elements may be required to provide an accurate volumetric representation of respiration. In both cases the performance benefits reduces significantly with increase in the number of elements above approximately 20. This has been chosen to represent the ideal number of elements as at this level robust surface reconstruction will give way as redundancy is introduced.

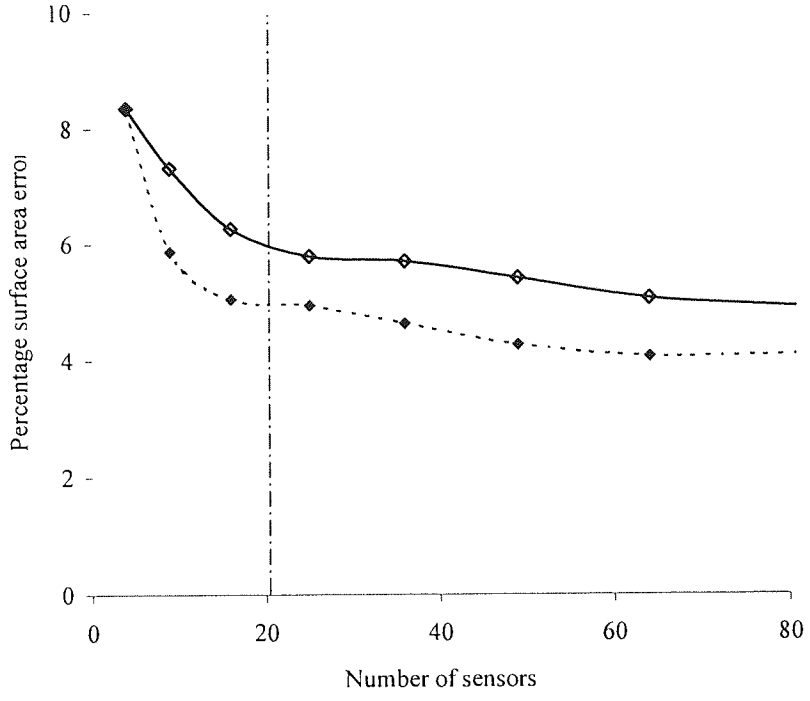

Figure 39. Density of sensing positions versus surface error for reconstructed CT scan chest profile data. Solid and broken curves represent point and interpolated error respectively. Dash-dot line shows the approximate position of the ideal number of sensors for this application.

3.6 System demonstration

3.6.1 Respiratory monitoring Application of LPG platform

In order to validate this approach a commercially made manikin used as resuscitation training aid has been employed. This comprises a rigid under-frame over which is stretched a polymer skin. An air bag placed between the frame and skin, when inflated or deflated, is then used to simulate expansion and contraction of the surface of the torso in similar volumetric proportions to that of breathing. While this does not truly reflect the changes in chest and abdomen geometry during human respiration it provides a test platform of similar dimensions and variation to those that are expected.

The response of the sensor platform was recorded at various states of inflation at five different orientations on the manikin. Each location is represented by a set of dimensions as indicated on Figure 40 and Table 4. The shift in central wavelength is also recorded with reference to the peripheral expansion of the dummy's skin in Figure 41 and Figure 42. The variation in response apparent between the upper and lower chest regions mimic that which might be expected in a real subject as the expansion of the rib cage has a more significant contribution at higher levels of ventilation [Wilson et al, 1987]. In this case however this phenomena can be attributed to the profile and position of the internal airbag.

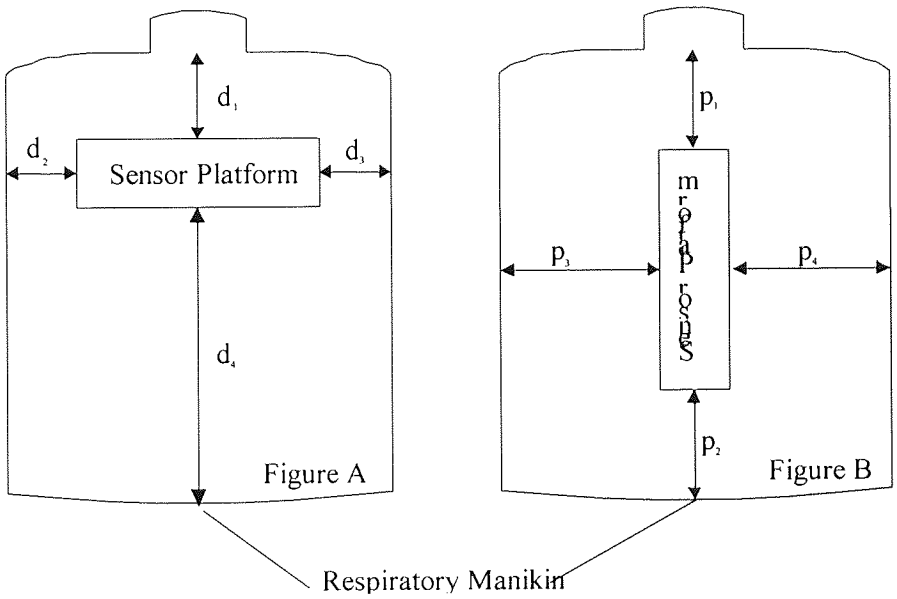

Figure 40. The positioning of the LPG sensor platform on the manikin.

Position on Dummy *Figure 40(A)*	d_1 *(mm)*	d_2 *(mm)*	d_3 *(mm)*	d_4 *(mm)*	*Maximum detected wavelength shift (nm)*
1	90	50	50	250	~1.05
2	185	50	50	185	~3.18
3	287	50	50	75	~0.95
Position on Dummy *Figure 40 (B)*	p_1 *(mm)*	p_2 *(mm)*	p_3 *(mm)*	p_4 *(mm)*	*Maximum detected wavelength shift (nm)*
4	205	25	165	165	~1.98
5	100	128	165	165	~1.70

Table 4. The measured central wavelength shift of the LPG sensor at various positions on the manikin

Assuming that the skin temperature varies from ~32°C to ~35°C [Miyanaga et al, 2001] this would generate a maximum spectral error of ~±0.075nm for this detection method (due to the accuracy of OSA) which can be improve to ~±0.035nm. Using the Maximum detected wavelength shift presented in Table 4 this gives maximum relative error of ~±5% for position 3 and minimum relative error of ~±1% for position 2.

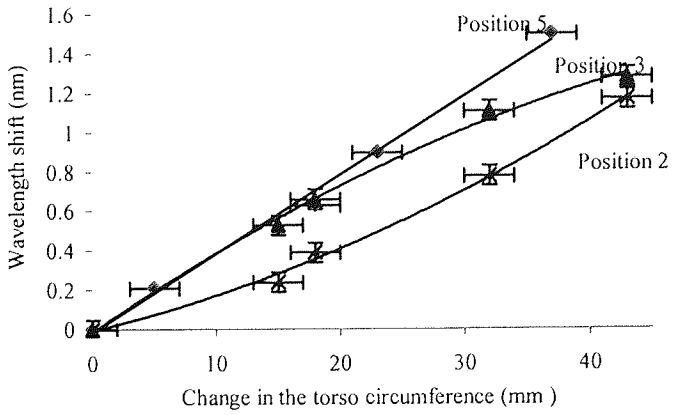

Figure 41. Spectral functionality of the LPG positioned on the lower chest sensor

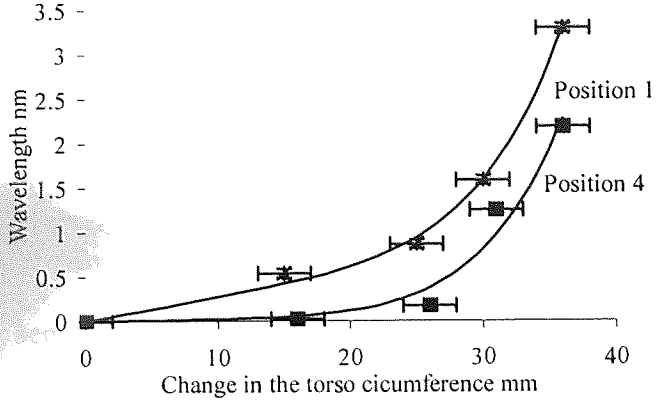

Figure 42. Spectral functionality of the LPG sensor positioned on the upper chest

Inspecting Figure 41 and Figure 42 shows that the spectral response of the LPG sensor platform as a function of peripheral expansion of the manikin's skin varies from position to position. The errors in these figures occur due to the spectral accuracy of the OSA (±0.04nm) and a circumferential error of ±1cm. The error is an estimate of the variation of manikins skin deformation from each set of results. Using polynomial regression technique on the experimental results illustrated in Figure 41, and Figure 42, the spectral functionality of the sensor as function of peripheral expansion at positions 1 and 4 were given by 8^{th} and 6^{th} order polynomials compared to quadratic expressions for positions 2 and 3 which indicates different movement during inflation of the manikin.

3.7 Multiplexing

Solutions to the problem of de-multiplexing an array of such sensors is being pursued at the present. It is envisaged that a tree architecture for the sensors and detectors would be adopted. Power loss within the array is not a major problem because the illuminating light source for the sensor is a DFB pigtailed laser which delivers ~2mW of power which can service several sensors/detectors at once. The proposed configuration is depicted in Figure 43.

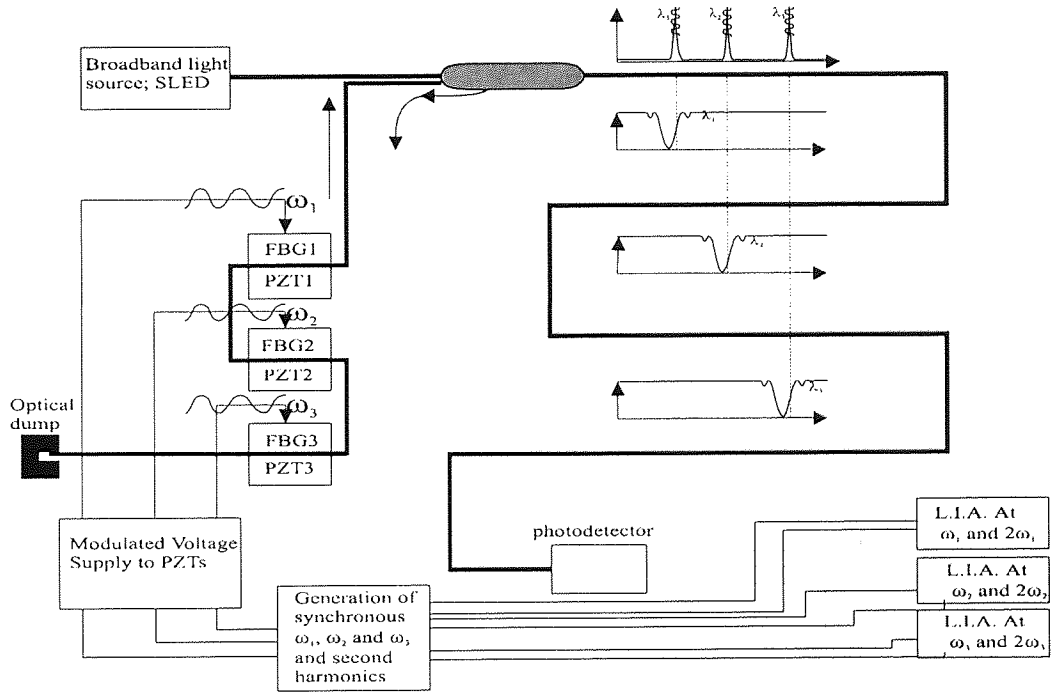

Figure 43 Schematic for multiplexed interrogation scheme

Summary

This chapter investigated a possible solution to mobile respiratory function measurement based upon a curvature-sensing array scheme, utilising a long period grating fibre-optic bend sensors constructed in optical fibre. The primary motivations for this approach are the sensors construction and their ability to be incorporated within flexible composite structures and transparency when used in conjunction with x-ray and magnetic imaging machines.

The sensors transduce the localised curvature on the thoracoabdominal surface by virtue of a change in central wavelength and profile of a selected attenuation band in the UV spectrum introduced into the fibre. The curvature spectral sensitivity of the sensing elements is shown to be within the range expected for geometric change in adult respiration.

The LPG sensors have been fabricated in a PTL-fibre, which lends itself to being incorporated into composite structures as this type of fibre has been found to be insensitive to perturbation by the refractive index of its surrounding medium, as is observed with standard step-index fibre.

Investigation proved that embedded LPG sensors are also de-sensitised to temperature at an order of magnitude lower than for bare fibre. This too can be attributed to its encapsulation in an insulating medium.

Axial strain for this sensor was assumed to be negligible due to the fact that the sensors are adhered to a steel supports.

The sensor platform has also been used to distinguish between the geometry at different locations on a dummy torso during respiratory like movement.

It is estimated that approximately 20 sensors arranged in an array can be calibrated and used to generate a geometrical profile of the chest and abdomen in three dimensions with a volumetric fidelity comparable to existing systems and standards.

A derivative spectroscopy interrogation technique has been employed to detect changes in curvature of the fibre LPG over an acceptable range. The experimental results are repeatable and are within the dynamic curvature range expected during respiratory motion.

The peripheral electronics and optics can be made very small and portable. The entire system could ultimately be attached to the patient who is wearing a garment in which the sensors are incorporated.

Two variations of the derivative spectroscopy interrogation scheme have been identified. The simplest is to use DFB lasers to illuminate the optical system. This requires a number of laser light sources to be employed, which is prohibitively expensive. A more economical approach is to the back reflection from fibre Bragg gratings from a single broadband light source to interrogate a number of sensors in series. Both approaches have been shown to work acceptably well.

The fabrication process by which to obtain matching FBG and LPG remains a problematic process and should be the subject of further investigation to obtain empirical rules with which to judge the final location of LPG wavelength in particular. This will entail characterising the degree of Hydrogenation of the fibre, optical power used during inscription, speed of inscription against the initial location of attenuation bands and period.

Future work in this application area is also required to complete the multiplexing interrogation electronics, and incorporate a full array of sensing elements into a garment structure. At this point a fully functioning prototype device will be available for evaluation.

4 Discussion and future work identified

As described previously respiration is a complex activity. If the relationship between all neurological and skeletomuscular interactions was perfectly understood, an accurate dynamic model of the respiratory system could be developed and the interaction between different inputs and outputs could be investigated in a fairly straightforward fashion. Unfortunately, this is not the case and does not appear to be viable at this time. In addition, the provision of appropriate sensor signals for such a model would be a considerable invasive task. Whist devices that measure the flow of gases at the mouth can be used to diagnose a variety of respiratory conditions they are less than ideal for continuous respiratory monitoring and are limited in the sense that they provide only a general appreciation of the performance of the respiratory system as a whole and contributions from different parts of the respiratory system are not measured.

During chapter 1 it has been identified that useful quantitative information with respect to respiratory performance can be gained from non-invasive monitoring of chest and abdomen motion. Thus, there is potential to enhance the diagnostic capabilities of at mouth measurement systems by increasing the depth of information.

Currently available devices based on this principle are not well suited for application for spirometric measurement for ambulatory monitoring. 2 degree of freedom devices, such as RIP are sensitive to changes in posture, movement and are subject to frequent calibration, as such they generally find application as monitors for recumbent patients, for example monitoring of sleep and postoperative apnoeas. In either case in actual use the measurements provided are essentially qualitative rather than quantitative. It is

suggested here that if this is the case then this must also apply to some extent to other instrumentation identified that measure ventilation as two independent compartments.

Three-dimensional systems exhibit a higher fidelity, however at the cost of added complexity of equipment and operational methods as too with the loss of portability available with existing products. They provide many of the desired attributes that enhance the performance and functionality of existing clinical tools. They are not however suited to ambulatory monitoring because they must be used with a specific clinical environment and are limited in data throughput at present. The ELITE system in particularly, remains at the cutting edge of surface plethysmography investigation and physiological studies using this device are published regularly to this date.

It is evident that none of the existing surface plethysmography devices fit the specific requirements for the purposes of this investigation, however an examination of the desirable attributes of those methodologies on offer leads to the conclusion that a solution may be formed from one of two approaches. These are; model based respiratory surface plethysmography, examined in chapter 2 and geometrically based surface plethysmography investigated in chapter 3.

Each method is thus investigated in the body of the text in relation to the fundamental requirements established by examining both the strengths and weaknesses of the existing techniques. Irrespective of whether a physiological model base or a geometrical approach is employed a number of considerations must be contended with:

- **Non-respiratory motion artefacts** - Signals are strongly influenced by perturbations resulting from the measured subjects posture (walking, arm movements etc.) this has an influence on both the pattern of breathing as well as the shape of the thoraco-abdominal volume. As a consequence the system must

provide a sophisticated adaptive process that can either identify or filter out signal elements, which are not part of respiration.

- **Breathing patterns** - Different individuals exhibit different breathing patterns and this needs to be investigated to decide to what extent this is taken into account by the calibration system and the overall medical implications on the measurements made. The recognition of speech and how this alters the pattern of breathing is also required.

- **Factors governing respiratory performance** - The system provides the facilities to observe the regional contributions made by the different muscle actions of the chest. Again each action will contribute towards the total volumetric flow developed within the respiratory system. The extent of which these actions can (or should) be related need to be investigated and defined. This requires the creation of a data library to include a full range of subjects and respiratory conditions, particularly with a respiratory model based approach.

- **Validation** - The sensor signal outputs need to be related to those generated by conventional spirometric devices and standards, which provide information in terms of volume and flow rate. However with no such equivalent mechanism being available for the comparison of regional contributions an objective method of verification needs to be resolved. In order to diagnose accurately various respiratory conditions from readily available sensor readings, an alternative solution must be developed that will concur with the established standards associated with existing spirometric devices and be robust to a wide range of operational conditions.

- **Application specific calibration** - If the combined use of the sensor outputs and the dynamic 3D image of the chest are considered in relation to the clinical requirements and it is clear that the system has to be calibrated relative to an individual. The calibration will depend upon the purpose to which the system is being used, for example, if the system is used for direct diagnostic assessment of lung function then the regional actions around the surface model need to be related to volumetric output of the lung system. On the other hand, if the system is being used for corrective treatment then rules for examining the relationship between effort and the resulting actions need to be established. This applied principally to model based surface plethysmography.

The model-based approach to respiratory plethysmography investigated in the text is based on a development of two degree of freedom plethysmography techniques. Essentially the idea has been to augment simple RIP type techniques by increasing the degree of freedom by the addition of more sensors. This is accomplished by increasing the density of sensing sites on the chest and abdomen in an array configuration. The experimental approach to this has been documented in chapter 2. The thrust of the investigation has been to approach the interpretation of arbitrarily constructed tactile sensor signals in two ways. Firstly by establishing the performance of the sensing array with statistical models to reconstruct volume flow measure synchronously and secondly by considering a physiological model with which to superimpose sensor signals and interpret 3 dimensional volume variations of the chest surface and abdomen.

The selecting of and optimal array configuration for this application necessitates the development of application specific sensors, as no suitable sensing elements are available commercially. This leads to the conclusion that purpose built sensors needed

to be constructed. With many possible sensor constructions on hand (section 1.4) and due to the limited fabrication facilities available a generic sensing approach was adopted.

The sensors initially chosen in this investigation were chosen to provide an inexpensive solution with which to validate the model-based approach. In characteristics they performed poorly in terms of repeatability and linearity (section 2.1), however in an array configuration were able to demonstrate performance gains over a lower degree of freedom system (section 2.2). Extrapolating experimental results from the investigation into model base plethysmography in chapter 2 to the future to a point where reliable purpose built sensors are available, the repeatability exhibited demonstrates that reconstructed raw signals from a simple sensor array give reasonable agreement with conventional spirometry even in the presence of strong body motion artefacts. This gives some confidence that multiple distributed sensors may be used as the basis of a whole chest motion monitoring system with future development.

Enhancements in signal segmentation abilities demonstrated in (section 2.3) have been gained purely form the increase in number distribution of sensing sites. It follows that this increase provides a means by which differentiation between superimposed modes of body motion on respiratory motion can more readily be accomplished.

It is known that for a single sensing site respiratory surface motion follows a near-linear trajectory regardless of the pattern of breathing and that if the relative thoracic and abdominal contributions remain steady for a given time period then any signal component caused by other than respiratory movement will not match the pattern either spatially, temporally or both. This is the key idea for the application of sensing arrays to this problem. However this application might not be a special case. Essentially what we

are trying to do is infer a three-dimensional relationship with a number of single dimension measurements spatially separated. This would not be tractable in a general sense, however in this example the underlying physiology permits a solution, which can be applied over finite and distinct operational range. This must be the case too when the underlying physical constraints to a surface motion problem is understood, even at least partially.

There is a wide scope for the selection of a signal processing scheme and the choice will be influenced by the complexity of interactions, which have yet to be found. This may be the subject of future work together with the refinement of sensing techniques and array configuration expressly for the purpose of respiratory measurement. Incorporating sensory signals into a physiological model that can be related to the physical stature and respiratory patterns for a wide variety of people with this method is a considerable task, which necessitates further investigation once a fully functioning array system has been developed.

A key factor in achieving success will be that of signal processing and will require the development of more complex algorithms than those presented here. There is a wide scope for the selection of a processing scheme, for instance, either a generic model of respiration is used to which parameters are fitted or whether the application of 'black box' approach Neural Network or statistical models are identified from data. The problem may be tackled as a whole or alternatively be composed smaller functional interactive components. For example, modules for posture, breathing patterns, etc. There is also the option to sense posture and limb movement externally from the sensor array and use this information for adaptive parameter tuning. The choice will be influenced by the complexity of interactions found in what is an undetermined

operational envelope for this approach. This as well as the refinement of sensing techniques and array configuration will be the subject of future work.

This kind of compliant sensor array may be used as the basis of a whole chest motion monitoring system and provide an enhanced performance and functionality over measurements made with 2 degree of freedom devices. Whilst providing a solution a solution which can be applied as an off the shelf clinical tool as opposed to measurements made with an off-body reference.

Validating the model-based approach to volumetric reconstruction has not been challenged at this time. This is primarily because of suitable published data from 3D plethysmography schemes and because investigations into geometric surface plethysmography sensing offered a less complex task in terms of surface reconstruction and signal processing.

With the nature of inferring three-dimensional relationships with a collection of signals of lower dimension, the most challenging aspect to contract is concerned with the architecture and parameter identification of a suitable model with which to condition the signals. Of principle concern is the ability of a solution to be insensitive in respect of respiration signal to changes in posture of the subject and other contributory motion signal during motion. A variety of modes of ventilation are also to be expected and to which the solution must be insensitive.

In these respects 3D systems such as ELITE have the advantage that postural and motion information are accounted as part of the fundamental measurement. As respiratory monitoring tools existing 3-D approaches posses practical limitations. The system structure outlined in chapter 3 provides similar benefits over 2DOF

measurement systems and is one, which will facilitate continuous and ambulatory monitoring. Existing geometric plethysmography techniques do not provide this facility.

The primary differences between existing approaches and the one detailed here is that it does not rely on an off body reference point for the measurement. Therefore its operation is not confined to a specific environment.

Chapter 3 investigated a possible solution to mobile respiratory function measurement based upon a curvature-sensing array scheme, utilising a long period grating fibre-optic bend sensors constructed in optical fibre. The primary motivations for this approach are the sensors construction and their ability to be incorporated within flexible composite structures and transparency when used in conjunction with x-ray and magnetic imaging machines.

The sensors transduce the localised curvature on the thoracoabdominal surface by virtue of a change in central wavelength and profile of a selected attenuation band in the UV spectrum introduced into the fibre. The curvature spectral sensitivity of the sensing elements is shown to be within the range expected for geometric change in adult respiration.

The LPG sensors have been fabricated in a PTL-fibre, which lends itself to being incorporated into composite structures as this type of fibre has been found to be insensitive to perturbation by the refractive index of its surrounding medium, as is observed with standard step-index fibre.

Investigation proved that embedded LPG sensors are also de-sensitised to temperature at an order of magnitude lower than for bare fibre. This too can be attributed to its encapsulation in an insulating medium.

Axial strain for this sensor was assumed to be negligible due to the fact that the sensors are adhered to a steel supports.

The sensor platform has also been used to distinguish between the geometry at different locations on a dummy torso during respiratory like movement.

It is estimated that approximately 20 sensors arranged in an array can be calibrated and used to generate a geometrical profile of the chest and abdomen in three dimensions.

A derivative spectroscopy interrogation technique has been employed to detect changes in curvature of the fibre LPG over an acceptable range. The experimental results are repeatable and are within the dynamic curvature range expected during respiratory motion.

One major advantage of this detection system is that the peripheral electronics and optics can be made very small and portable. The entire system could ultimately be attached to the patient who is wearing a garment in which the sensors are incorporated.

Two variations of the derivative spectroscopy interrogation scheme have been identified. The simplest is to use DFB lasers to illuminate the optical system. This requires a number of laser light sources to be employed, which is prohibitively expensive. A more economical approach is to the back reflection from fibre Bragg gratings from a single broadband light source to interrogate a number of sensors in series. Both approaches have been shown to work acceptably well.

The fabrication process by which to obtain matching FBG and LPG remains a problematic process and should be the subject of further investigation to obtain empirical rules with which to judge the final location of LPG wavelength in particular. This will entail characterising the degree of Hydrogenation of the fibre, optical power

used during inscription, speed of inscription against the initial location of attenuation bands and period.

Future work in this application area is also required to complete the multiplexing interrogation electronics, and incorporate a full array of sensing elements into a garment structure. At this point a fully functioning prototype device will be available for evaluation.

There may also be a requirement for adding further degrees of freedom to the bend measurement. That would be the case if it proves necessary to differentiate between convex and concave profiles on the torso. This might be accomplished by introducing so asymmetry into the fibre sensors cross-section. Although a number of types fibre with either asymmetric core position or cross section are available it is unclear whether PTL fibre with such properties, as such manufacture of specialised fibre would need to be investigated.

The sensing methods created as part of this study are directly applicable in a number of alternative technological areas. These include many applications concerned with dynamic ergonomics (such as automotive crash analysis) or indeed a wide variety of industrial application in which, the dynamic motion of surfaces are of interest. The potential for scalability for the surface reconstruction algorithms lends itself to such applications including: large and small scale fluid boundary dynamics, remote monitoring and surface digitisation. These are alongside numerous medical and micro surgical devices and implants.

This work has produced a new measuring tool. Its advantages over existing methods are:

- It is fully mobile; this will facilitate ambulatory monitoring and may be employed outside of the laboratory.
- It provides continuous transient measurement of respiratory motion within an acceptable accuracy.
- It provides distributed transient information on respiration with which to study physiology.
- It provides a means by which to isolate coupled physiological functions and thus allows individual contributions to be analysed separately.

The consequences are that measurements of the unconstrained human subject can lead to accurate performance evaluation; this is now possible for the first time. This will lead to more accurate diagnosis to improve performance and to recognise different pathologies. These near possibilities need to be investigated fully and need to be evaluated.

In future the potential of a full simulation model of the system needs to be explored. In the first instance such a model could be used to identify how to optimise its own configuration in respect to normal variations of the population. Secondly by reforming those principles revealed and converting them, an inverse model scheme can be used to form the basis of an automated advisory system.

5 Conclusions

The specific achievements of the work in relation to the objectives are:

- Having investigated various methods of non-invasive methods of respiratory function methods two methodologies have been identified for further exploration. These correspond to model and geometrical based surface plethysmography techniques. Each has been examined in detail and experimental results show that either may be applied to provide a working solution for this application.

  A model-based array sensing approach has been shown to provide an increase in volumetric performance when compared to existing surface plethysmography methods and devices. It has been demonstrated that a system based on this methodology can measure volumetric flow within an accepted standard accuracy of 5%, even in the presence of perturbation from limb movement.

- Because of potential difficulties in representing a wide variety of human physiques in a volumetric model of the chest and abdomen a geometrical approach has been favoured in the absence of representative data. In the geometrical measurement approach such problems are negated when it comes to surface reconstruction. This has been subject to the development of highly compliant shape transducer.

  Fibre optical bend sensors have been investigated and developed as part of the study. These are based on long period grating written in progressive three layer

fibre that develop a high sensitivity to bending and a lower sensitivity to strain and temperature than other sensors of the same ilk. PTL fibre has been adopted because of it inherent ability to retain its spectral properties when embedded in a composite structure. This is because it is insensitive to the refractive index of its surrounding medium unlike LPG fabricated in twin-layered fibre.

The detectable range of curvature is $\sim\pm 4m^{-1}$. This is shown to be compatible with the requirements for surface-motion sensing the measurement of human respiratory function.

- A low cost and novel detection scheme to detect the degree of curvature experienced by long period gratings has been demonstrated, which has the potential to be made portable. The interrogation technique is based upon derivative spectroscopy, which utilises the change in transmission spectral profile of the attenuation band of the LPG induced by bending. The interrogation scheme also has the ability to be applied in parallel to service an array of sensors.

- These combined provide the basis for the basis for a three-dimensional surface contour sensing system that is suitable for respiratory function monitoring and has the prospect with future development to be incorporated into a garment based clinical tool. At which time the system could be validated against flow at mouth spirometry for volumetric performance and against known surface profiles for geometric conformity.

The sensor technology developed has been demonstrated to be consistent with the level of performance required for incorporation into a respiratory measurement garment. This would facilitate ambulatory monitoring and would allow a number of medical conditions to be measured, e.g., for asthma management, etc. Such a device would also be applicable for use in treatment and rehabilitation in speech therapy as well as other treatment and diagnosis applications for which there is no available clinical measurement and / or visualisation tool.

It provides continuous transient measurement of respiratory motion within an acceptable accuracy using approximately 20 sensing elements. Because of the potential size and complexity of the system it is possible to deploy it as a fully mobile ambulatory monitoring device, which may be used outside of the laboratory.

It provides a means by which to isolate coupled physiological functions and thus allows individual contributions to be analysed separately. Thus facilitating greater understanding of respiratory physiology and diagnostic capabilities.

The consequences are that measurements of the unconstrained human subject can lead to accurate performance evaluation; this is now possible for the first time. This will lead to more accurate diagnosis to improve performance and to recognise different pathologies. Therefore the scheme described may in future form the basis of an automatic diagnostic tool for clinicians. These near possibilities need to be investigated fully and need to be evaluated.

6 References

Abramowitz,1977 **Abramowitz M.**, *Handbook of mathematical Functions*, Dover Publications, 1977

Ackerman et al, 1984 **Ackerman MJ and Clarke JR.** *An automated method for measuring chest-wall motion during high frequency oscillation.* Proceedings of the Annual Symposium on Computer Applications in Medical Care. 1984:722-726

Allsop et al, 2002(a) **Allsop T, Chisholm K, Bennion I, Malvern A & Neal R.** *A strain sensing system using a novel optical fibre Bragg grating sensor and a synthetic heterodyne interrogation technique*, Meas. Sci. Technol. 2002(a); 13: 731-740

Allsop et al, 2002(b) **Allsop T, Earthrowl-Gould T, Webb DJ, Bennion I.** *Embedded Progressive-Three-Layered fibre long-period gratings for respiratory monitoring.* to be published,2002(b)

Allsop et al, 2002(c) **Allsop T, Earthrowl-Gould T, Webb DJ, Bennion I.** *Low cost and novel bend sensing scheme with a long-period grating for respiratory function monitoring.* to be published, 2002(c)

Allsop et al, 2002(d) **Allsop T, Reeves R, Neal R & Bennion I.** *A high accuracy/sensitive refractive index sensing system based upon a long period grating Mach-Zehnder interferometer with a heterodyne detection technique*, to be published ,2002(d)

Allsop et al, 2002(e) **Allsop T, Webb DJ & Bennion I.** *Investigations of the spectral sensitivity of Long Period Gratings fabricated in 3-layered optical fiber,* to be published, 2002(e)

Allsop et al, 1996 **Allsop T. et al,** *High resolution optical-fibre strain gauge for bio-engineering applications*, Conf. Proc. Bio-Sensors, Vienna, Austria, 1996.

Allsop,1999 **Allsop T.,** *A fibre optical strain sensor*, PhD. thesis, University of Plymouth, U.K., Sept. 1999.

Allsop et al, 2001 **Allsop T., Zhang L. & Bennion I.** Opt. Commun., Vol 191, pp. 181, 2001

American Thoracic Society, 1979 **American Thoracic Society** *ATS Statement - Snowbird Workshop on Standardization of Spirometry*, Am Rev Respir Dis, 1979; 119: 831-838

Balfour et al, 1981 **Balfour, N.S., Hamilton, L.H.** *Respiratory physiology* 4th ed., St. Louis, London, Mosby, 1981

Banzett et al,1995 **Banzett, R.B., Mahan, S.T., Garner, D.M., Brughera, A. & Loring, S.H.** *A simple reliable method to calibrate magnetometers and respitrace.* Jnl. Appl. Physiol. 1995;79(6):2169-2176.

Bennion et al, 1996 **Bennion I. et al,** *UV written in fibre Bragg grating*, Opt. and Quant. Elect., vol 28, pp93, 1996 .

Bhatia et al, 1996(a) **Bhatia V & Vengsarkar.** *Optical fibre long-period sensors.* Otics Letters; 1996(a); 21(9)

Bhatia, 1999 **Bhatia V**, *Applications of long-period gratings to single and multi-parameter sensing*, Opt. Express., 1999, vol. 4, no. 11, pp.457-466

Bhatia et al, 1997 **Bhatia V, D'Alberto T. et al**, *Temperature-insensitive and strain-insensitive long-period gratings sensor for smart structures*, Opt. Eng., Vol.36, pp1872, 1997.

Bhatia, 1996(b) **Bhatia V.** *Properties and applications of long period gratings.* PhD Thesis, Virginia Polytechnic. 1996(b).

Birch et al,2001 **Birch M, MacLeod D & Levine M.** *An analogue instrument for the measurement of repiratory impedence using the forced oscillation technique.* Physiol. Meas. 2001; 22: 323-339

Blanchard et al, 1998 **Blanchard PM, Greenaway AH, Burnett j & Harrison P.** *Two-dimensional bend sensing with a single multiple-core optical fibre.* Proc. SPIE 1998; 3483: 54-58

Block et al, 1995 **Block KE, Barandun J. & Sackner MA.** *Effect of Mouthpiece Breathing on Cardiorespiratory Response to Intense Exercise,* Am J Respir Crit Care Med, 1995; 151:1087-92

Brimacombe, 1993 **Brimacombe J.** *Noninvasive monitoring of tidal volumewith an extensometer: Laboratory and clinical studies.* Anaesth. Intens Care 1993; 21:62-66

Buck,1995 **Buck JA.** *Fundementals of optical fibres,* 1995; Wiley-Interscience Publication.

Butter et al, 1978 **Butter CD and Hocker GB**, *Fibre optics strain gauge*, Appl. Opt., vol 17, no18,

pp2867, 1978 .

Cala et al, 1996 **Cala SJ, Kenyon CM, Ferigno G, Carnevali P, Aliverti A, Maklem PT & Rochester DF.** (1996) *Chest wall and lung volume estimation by optical reflectance motion analysis.* J. Appl. Physiol. 1996; 81(6): 2680-2689.

Cantineau et al, 1992 **Cantineau JP, Escourrou P, Sartene R, Gaultier C & Goldman M.** *Accuracy or respiratory inductance plethysmography during wakefulness and sleep in patients with obstructive sleep apnoea.* CHEST 1992; 102(4): 1145-1151

Chadha et al, 1982 **Chadha, T.S., Watson, H., Birch, S., Jenouri, G.A., Schneider, A.W.,Cohn, M.A. & Sackner, M.A.** *Validation of inductive plethysmography using different calibration procedures.* Am. Rev. Respir. Dis. 1982; 125:644-649

Chen et al , 1999 **Chen Z, Chiang KS, Ng MN, Chan YM & Ke H.** *Bent long - period fibre gratings for sensor applications.* Proc SPIE 1999; 3897: 94-103

Dai et al, 2000 **Dai C, Yang D,Tao X & Tam H-Y.** *Effects of pure bending on the sensing characteristics of fibre Bragg gratings.* Proc. SPIE. 2000; 4077: 9296

Davis et al, 1999 **Davis C, Mazzolini A, Mills J & Dargaville P.** *A new sensor for monitoring the chest wall motion during high-frequency oscillatory ventilation.* Med. Eng. & Physic. 1999; 21: 619-623

De Groote et al, 2000 **De Groote A, Verbandt Y, Pavia M and Mathys P.** *Measurement of thoracoabdominal asynchrony: importance of sensor sensitivity to cross section deformations.* **Jnl. Appl. Physiol. 2000; 88: 1295-1302.**

De Groote et al, 1997 **De Groote A, Wantier M, Cheron G, Estenne M & Pavia M.** *Chest wall motion during tidal breathing.* Jnl. Appl. Physiol 1997; 83(5): 1531-1537.

Delgado et al, 1982 **Delgado HR, Braun SR, Skatrud JB, Reddan WG & Pegelow DF.** *Chest wall and abdominal motion during exercise in patients with chronic obstructive pulmonary disease.* AM. Rev. of Repir. Dis. 1982; 126: 200-205.

Dong et al, 1997 **Dong L. et al,** *Long period gratings formed in depressed cladding fibres*, Electron. Letts., vol.33, no. 22, pp. 1897-1898, 1997.

Drummond et al, 1996 **Drummond GB, Nimmo AF & Elton RA.** *Thoracic impedance used for measuring chest wall movement in postoperative patients.* British Jnl. Of Anaesthesia 1996; 77:327-332.

Du et al, 1998 **Du W, Tam H-Y, Liu MS & Tao X.** *Long-period grating bending sensor in laminated composite structures.* Proc SPIE 1998; 3330: 284-292

Earthrowl-Gould et al, 2001 **Earthrowl-Gould T, Jones B & Miller MR.** *Chest and abdominal surface motion measurement for continuous monitoring of respiratory function.* Proceedings of ImechE, Part H, Engineering in medicine. 2001; 215(5): 515-520

Earthrowl-Gould et al, 2000 **Earthrowl-Gould, T., Jones, B.,Miller, M. R.and Jeffs J.P.,** *Non-invasive chest and abdominal surface motion sensing to evaluate respiratory function*, Conference presentation, IEE MEDSIP2000, Bristol Sept. 2000

Erdogan, 1997 **Erdogan T,** *Cladding mode resonances in short- and long- period fibre gratings.* J. Opt. Soc. Am. 1997:14(8);17601773.

Espindola et al, 1999 **Espindola RP et al,** *External refractive index insensitive air-clad long period fibre grating*, Electron. Lett., vol.35, no.4, pp.327-328, 1999.

Gander et al, 1998 **Gander MJ, Macrae D, Galliot EAC, McBride R & Jones JDC.** *Measurement of bending in two dimensions using multicore optical fibre.* Proc. SPIE. 1998; 3483: 6468

Ganzalez et al, 2001 **Ganzalez DA, Arce-Diego JL, Cobo A & Lopez-Higuera.** *Spectral modelling of curved long period fibre gratings.* Meas. Sci. Technol. 2001; 12:786-792

Gauthier et al, 1997 **Gauthier RC & Ross C.** *Theoretical and experimental considerations for a single-mode fibre-optic bend-type sensor.* Applied Optics 1997; 36(25): 6264-6273

Goldman et al, 1986 **Goldman JM, Rose LS, Morgan MDL & Denison DM.** *Measurement of abdominal wall compliance in normal subjects and tetraplegic patients*. Thorax 1986; 41: 513-518.

Goldman et al, 1988 **Goldman JM, Williams SJ & Denison DM.** *The rib cage and abdominal components of respiratory system compliance in tetraplegic patients*. Eur Respir. Jnl. 1988; 1: 242-247.

Goldstein et al, 1980 **Goldstein D & Mead J.** *Use of magnetometers to volume-reference flow-volume curves.* Jnl. Appl. Physiol. 1980; 48(4): 731-736.

Gourlay et al, 1984 **Gourlay AR, Kaye G, Dennison DM, Peacock AJ & Morgan MDL.** *Analysis of an optical mapping technique for lung function studies.* Comput. Biol. Med. 1984;14(1):47-58.

Grattan et al, 2000 **Grattan KTV and Meggit BT. (Editors),** ***Optical*** *Fiber Sensor Technology: Advanced Applications-Bragg Gratings and Distributed Sensor,* 2000; Kluwer Academic Publishers

Grimby et al, 1968 **Grimby G, Bunn J & Mead J.** *Relative contribution of rib cage and abdomen to ventilation during exercise.* Jnl. Appl. Physiol 1968; 24(2): 159-166.

Grubsky et al, 2000 **Grubsky V. & Feinberg J.** *Long-period gratings with variable coupling for real-time sensing applications*, Opt. Lett., vol.25, no.4, pp.203-205, 2000.

Hagan et al, 1994 **Hagan MT and Menhaj M,** *"Training feed-forward networks with the Marquardt algorithm,"* IEEE Transactions on Neural Networks, 1994: 5(6); 989-993.

Hecht, 1998 **Hecht E.**, *Optics*, Addison-Wesley, Reading, MA, 1998

Hill et al, 1978 **Hill KO. et al**, *Photosensitivity in optical fibre waveguides. Application to reflection filter fabrication*, Appl. Phys. Lett., vol. 32, pp647, 1978

Hocker, 1979 **Hocker GB**, *Fibre optic sensing of pressure and temperature*, Appl. Opt., vol 18, no 9, pp1445, 1979.

Huang et al, 1995 **Huang S. et al**, *Bragg intragrating structural sensing*, Appl. Opt., vol 34, no22, pp5003, 1995 .

Hudgel et al, 1984 **Hudgel DW, Capehart M, Johnson B, Hill P & Robertson D.** *Accuracy of tidal volume, lung volume and flow measurements by inductance vest in COPD patients.* Jnl. Appl. Physiol. 1984; 56(6): 1659-1665.

Jang et al, 1999 **Jang J et al,** *Temperature insensitive long-period fibre gratings*, Electron. Letts., vol.35, no. 24, pp. 2134-2136, 1999

Kenyon et al, 1997 **Kenyon CM, Cala SJ, Yan S, Aliverti A, Scano G, Duranti R, Pedotti A & Macklem PT.** *Rib cage mechanics during quiet breathing and exercise in humans.* Jnl. Appl. Physiol. 1997; 83(4): 1242-1255.

Kluczynski et al, 2001 **Kluczynski P, Gustafsson J, Lindberg AM & Axner O.** *Wavelength modulation absorbtionspectrometry - an extensivescrutiny of the generation of signals.* Spetrochimica Acta Pt. B 2001; 56: 1277-1354

Konno and Mead, 1967 **Konno K & Mead J.;** *Measurement of the separate volume changes of the rib cage and abdomen during breathing.* J. Appl. Physiol. 1967; 22(3): 407-422

Lafortuna et al, 1995 **Lafortuna CL, & Passerini L.** *A new instrument for the measurement of rib cage and abdomen circumference variation in respiration at rest and during exercise.* Eur J Appl. Physiol 1995; 71:259-265

Lee et al, 1998(a) **Lee BH & Nishill J.** *Cladding-surrounded interface insensitive long-period grating.* Elect. Lett. 1998(a); 34(11)

Lee et al, 1998(b) **Lee BH & Nishill J.** *I Bending sensitivity of in-series long-period fibre gratings.* Optics Letters. 1998(b); 23(20)

Lee et al, 1989 **Lee C.E. et al.** *Optical fibre Fabry Perot embedded sensor*, Opt. Lett. vol. 4, no21 , pp832 , 1989.

Lee et al, 1992 **Lee C.E. et al.** *Optical fibre Fabry Perot sensors for smart structures*, SPIE Conf. Proc. Active Materials and Adaptive structures, session 34, Blacksburg, VA, U.S.A., pp657, 1992.

Levine et al, 1991 **Levine S, Silage D, Henson D, Wang J, Kreig J, LaManca J & Levy S.** *Use of triaxial magnetometer for respiratory measurements.* Jnl. Appl. Physiol. 1991; 70(5): 2311-2321.

Liu et al, 2000 **Liu Y, Zhang L, Williams JAR & Bennion I.** *Optical bend sensor based on measurement of resonance mode splitting of long-period grating.* IEEE Photonics Technol. Lett. 2000; 12(5)

Liu et al, 1999 **Liu Y., Williams J., Zhang L. & Bennion I.** Opt. Commun., Vol 164, pp. 27, 1999

Loveridge et al, 1983 **Loveridge, B., West, P., Anthonisen, N.R. & Kryger, M.H.** *Single-position calibration of the respiratory inductance plethysmograph.* Jnl. Appl. Physiol. 1983; 55(3): 1031-1034

Ma et al, 1996 **Ma J. et al,** *Optical-fibre sensor for simultaneous measurement of pressure and temperature: analysis of cross sensitivity,* App. Optics, 1996, vol.35, no.25, pp. 5206-5210.

McCool et al, 1986 **McCool, D., Kelly, K.B., Loring, S.H., Greaves, I.A. and Mead, J.** *Estimates of ventilation from body surface measurements in unrestrained subjects.* Jnl. Appl. Physiol. 1986; 61(3): 1114-1119.

Mead et al, 1967 **Mead J, Peterson N, Grimby *G & Mead J.*** *Pulmonary Ventilation Measured from Body Surface Movements.* Science 1967; 156:1383-1384

Measures et al, 1992 **Measures R.M. et al**, *Wavelength demodulation Bragg grating fibre optic sensing systems for addressing smart structure critical issues*, Smart .Mater.Struct., vol. 1, pp36, 1992 .

Measures, 1989 **Measures R.M.**, *Fibre optic sensor - The key to smart structures*, SPIE,vol. 1120 ,Fibre Optic's 89, pp161, 1989.

Melle et al, 1993 **Melle S.M. et al**, *Practical fibre optic Bragg grating strain gauge system*, Appl. Opt., vol 32, no 19, pp3601, 1993.

Metz et al, 1989 **Metz G. et al**, *Formation of Bragg gratings in optical fibres by transverse holographic method*, Opt. Lett. vol. 14, pp823, 1989.

Miller et al, 2000 **Miller MR, Jones B, Xu Y, Pedersen OF, Quanjer PhH.** *Peak expiratory flow profiles delivered by pump systems: limitations due to wave action*. Am. J. Respir. Crit. Care Med. 2000 161: 1887-1896.

Miyanaga et al, 2001 **Miyanaga T. et al**, *Simplified human body-model for evaluating thermal radiant environment in a radiant cooled space*,2001, Building and Environment, vol.36, no.7, pp. 801-808.

Morel et al, 1983 **Morel, D.R., Forster, A. & Suter, P.** *Non-invasive ventilatory monitoring with bellows pneumographs in supine subjects*. Jnl. Appl. Physiol. 1983;55(2):598-606.

Morey et al, 1991 **Morey W.W.et al**. *Multiplexing fibre Bragg grating sensors*, Proc. Soc. Photo- opt. Instrum. - Distributed and multplexed fibre optic sensors, Boston, U.S.A., SPIE, vol. 1586, pp216, 1991.

Morgan et al, 1984 **Morgan MDL, Gourlay S & Dennison DM.** *An optical method of studying the shape and movement of the chest wall in recumbent patients.* Thorax 1984; 39:101-106.

Murphy et al, 1991 **Murphy K.A. et al.** *Quadrature phase-shifted, extrinsic Fabry Perot optical fibre sensors*, Opt Lett, vol 16, no 4, pp273, 1991

Nakesch et al, 1994 **Nakesch H & Pfüzner H.** *Magnorestrictive amorphous sensor for the detection of human respiration.* Jnl of Magnetism and Magnetic Materials 1994; 133:634-636

Paek et al, 1992 **Paek D & McCool D.** *Breathing patterns during varied activities.* Jnl. Appl. Physiol. 1992; 73(3): 887-893.

Patrick et al, 1998(a) **Patrick HJ, Chang CC & Vohra ST.** *Long-period fibre gratings for structural bend sensing.* Elec. Lett. 1998(a); 34(18)

Patrick et al, 1998(b) **Patrick HJ, Kersey AD & Bucholtz F.** *Analysis of the response of long period fiber gratings to external index of refraction*, J. Lightwave Technol., vol.16, no.9 pp.1606-1612, 1998(b).

Patrick et al, 1998(c) **Patrick HJ, Vohra ST.** *Fibre Bragg grating with long period grating superstructure for simultaneous strain and temperature measurement.* Proc. SPIE. 1998(c), 3483: 264-267

Patrick, 2000 **Patrick HJ.** *Self-aligning, bipolarbend transducer based on long period grating written in eccentric core fibre.* Elect. Lett. 2000; 36(21)

Patterson et al, 1996 **Patterson H, Stenow END, Cai H & Oberg PA.** *Optical aspects of a fibre-optic sensor for respiratory rate monitoring.* Med. & Biol. Eng. & Comput. 1996; 34: 448-452

Peacock et al, 1984 **Peacock AJ, Morgan MDL, Gourlay S & Dennison DM.** *Optical mapping of the thoacoabdominal wall.* Thorax 1984; 39:93-100.

Piegl,1991 **Piegl, l.,** *On Nurbs: A Survey.* IEEE Computer graphics & applications, Jan 1991, 55-71

Promayon et al, 1997 **Promayon E, Baconnier P, Puech C.** *Physically based model for simulating the human trunk respiration movements.* Lecture notes in Computer Science 1997; 1205: 379-388. Springer Verlag.

Rao et al, 2000 **Rao Y.R. et al,** *Absolute strain measurement using an in-fibre-Bragg-grating-based Fabry-Perot sensor*, Electron. Lett., vol 36, no8, pp231, 2000.

Rao, 1997 **Rao Y-J.,** *In-fibre Bragg grating sensors*, Meas. Sci. Tech., vol. 8, pp355, 1997.

Rees et al, 1980 **Rees PJ, Higenbottam TW & Clark TJH.** *Use of single pair of magnetometer coils to monitor breathing patterns in an intensive care unit.* Thorax 1980; 35:384-388

Robbertson et al, 1980 **Robbertson CH, Bradley ME & Homer LD.** *Comparison of two- and four-magnetometer methods of measuring ventilation.* Jnl. Appl. Physiol. 1980; 49(3): 355-362

Roberts et al, 1998 **Roberts D. and Foote P.** *Carbon spars for superyachts and smart technology*, Conf. Proc. The Modern Yacht , Portsmouth , U.K. , paper No 13 , 1998 .

Ruan et al, 1999 **Ruan Y. et al**, *The Design and Simulation of Cascade Long-period Fiber Gratings for flattening EDFA's Gain*, in Proc. SPIE conf. Photorefractive Fiber and Crystal devices: Mateials, Optical Properties and Applications V (Denver Col), July 1999, vol.3801, pp240-245, 1999.

Sackner et al, 1989 **Sackner, M.A., Watson, H., Belsito, A.S., Feinerman, D., Suarez, M., Gonzalez, G., Bizousky, F. & Krieger, B.** *Calibration of inductive plethysmograph during natural breathing.* Jnl. Appl. Physiol. 1989; 66(1): 410-420

Sanna et al, 1999 **Sanna A, Bertoli F, Misuri G, Gigliotti F, Iandelli I, Mancini M, Duranti R, Ambrosino N & Scano G.** *Chest wall kinematics and respiratory muscle action in walking healthy humans.* Jnl. Appl. Physiol. 1999; 97(3): 938-946.

Sergio et al, 1994 **Sergio F, Almeida M & Salvador JF.** *Novel strain-bend sensor using two mode optical fibre.* Proc. SPIE. 1994; 2072: 257-261

Sharp et al, 1975 **Sharp JT, Goldberg NB, Druz WS & Danon J.** *Relative contributions of rib cage and abdomen to breathing in normal subjects.* Jnl. Appl. Physiol. 1975; 39(4): 608-618.

Sirkis et al, 1993 **Sirkis J.S. et al.** *In-line fibre etalon for strain measurement.*, Opt. Lett. , vol. 18 , no. 22 , pp1973 , 1993.

Stagg et al, 1978 **Stagg D, Goldman M & Newsom Davis J.** *Computer aided measurement of breath volume and time components using magnetometers*. Jnl. Appl. Physiol. 1978; 44(4): 623-633.

Tabachnik et al, 1981 **Tabachnik E, Muller N, Toye B & Levinson H.** *Measurement of ventilation in children using the respiratory inductive plethysmograph*. Jnl. Of Pediatrics 1981; 99(6): 895-899.

Tian et al, 2000 **Tian X & Tao T.** *Torsion measurement by FBG sensors* Proc. SPIE, 2000; 4077: 154-164

Tobin et al, 1983 **Tobin MJ, Jenouri G, Lind, B, Watson H, Schneider A & Sackner MA.** *Validation of respiratory inductive plethysmography in patients with pulmonary disease*. CHEST 1983;83(4):615-620

Todd et al, 1999 **Todd M.D. et al,** *Passive, light intensity-independent interferometric method for fibre Bragg grating interrogation,* Electron. Lett., vol 35, no22, pp362, 1999.

Tsao et al, 1992 **Tsao C.** *Optical Fibre Waveguide Analysis*. New York: Oxford, 1992

Tutton et al, 1993 **Tutton P.A. et al,** *Structural health monitoring using embedded fibre optic sensors,* AGARD Conf . Proc. ,Smart struct aircraft and spacecraft, Lindau, Germany, pp 531, 1993 .

Vasilev et al, 2000 **Vasilev S. et al,** *Long-period refractive index fiber gratings: properties, applications and fabrication techniques*, Proc. SPIE 4083, pp212-223, 2000

Vengsarkar et al, 1996 **Vengsarkar A. et al**, *Long-Period Gratings as Band-Rejection Filters*, J. Lightwave Technol., vol.14, no.1, pp.58-64, 1996

Warren et al, 1997 **Warren RH, Horan SM & Robertson PK.** *Chest wall motion in pre-term infants using respiratory inductive plethysmography.* Eur Respir. Jnl. 1997; 10: 1195-2300.

Warren et al, 1988 **Warren, R.H., Fewell, J.E. & Alderson, S.H.** *Calibration of the respiratory inductive plethysmograph with single position graphical technique, Accuracy in different behaviour states in lambs.* CHEST 1988; 94(2): 325-328

Watson, 1980 **Watson H.** *The technology of respiratory inductance plethysmography.* In ISAM 1979. Proceedings of the third international symposium on ambulatory monitoring. ED. Scott, FD. Rafferty, EB. & Goulding, L., PUB. London: Academic, 1980 pp537

Wherle et al, 2000 **Wherle G & Kalinowski HJ.** *Fibre optic Bragg grating strain sensor used to monitor the respiratory spectrum.* Proc. SPIE 2000; 2895; 310-313

Wherle et al, 2001 **Wherle G, Nahama P, et al.** *A fibre Bragg grating strain sensor for monitoring ventilatory movements.* Meas. Sci. Technol. 2001; 12: 805-809

Wilkes et al, 1987 **Wilkes DL, Revow M, Bryan MH & England SJ.** *Evaluation of respiratory inductive plethysmography in infants weighing lass than 1,500 grams.* AM. Rev. of Repir. Dis. 1987; 136: 416-418

Williams et al, 1998 **Williams, E.M., Madgwick, R.G., Morris, M.J.** *Tidal expired airflow patterns in adults with airway obstruction.* Eur Respir J 1998; 12: 1118-1123.

Wilson et al, 1987 **Wilson TA, Rehder K, Krayer S, Hoffman EA, Whitney CG & Rodarte JR** *Geometry and displacement of human ribs.* Jnl. Appl. Physiol. 1987; 62(5): 1872-1877.

Woodward, 1988 **Woodward, C.D.,** *Skinning techniques for interactive B-spline surface interpolation.* Computer-aided design. 1988; 20: 441451

Xu et al, 1994 **Xu MG, Archambault J-L, Reekie I & Dakin JP.** *Structural bending sensor using fibre grating.* Proc. SPIE 1994; 2292: 407-413

Ye et al, 2000(a) **Ye CC, James SW & Tatam RP.** *Long-period fibre gratings for simultaneous temperature and bend sensing.* Proc SPIE 2000; 4047: 305-312

Ye et al, 2000(b) **Ye CC, Wei C et al.** *Bend sensing in structures using long-period optical fibre gratings.* Proc. SPIE 2000; 4073: 311-315

7 Glossary of Acronyms

CT	Computed Tomography
DFB	Distributed feedback laser
DIL	Duel in line
DOF	Degree of freedom
DVRT	Differential variable reluctance transducer
FBG	Fibre Bragg gratings
IC	Integrated circuit
LIA	Lock in amplifier
LP	Linear polarised
LPG	Long period gratings
MSE	Mean square error
NURBS	Non-uniform rational B-splines
OSA	Optical spectrum analyser
PTL	Progressive three layer
RIP	Respiratory inductance plethysmography
UV	Ultra violet
YAG	Yttrium Aluminium Garnet

Appendix 1 Properties of progressive three layered fibre

Reproduced from: Allsop T. Webb DJ. Bennion I. *Investigations of the spectral sensitivity of Long Period Gratings fabricated in 3-layered optical fiber*, (to be published).

PTL f

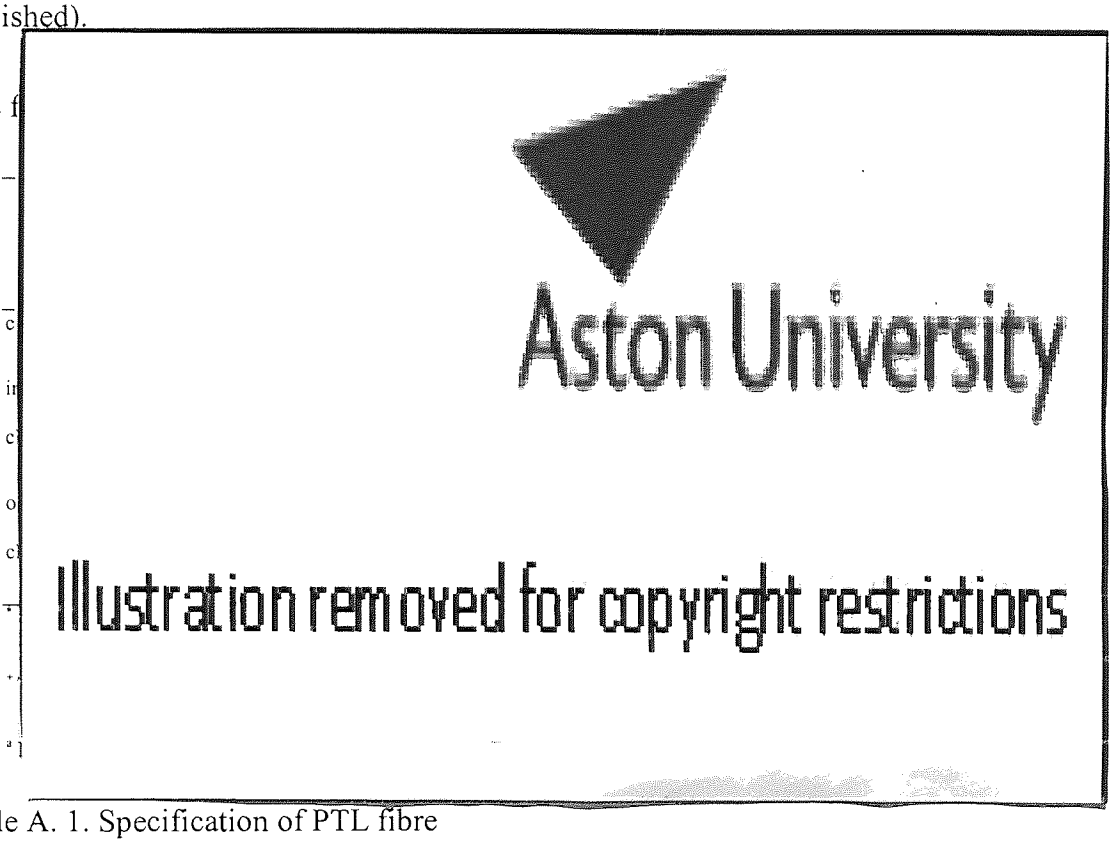

Table A. 1. Specification of PTL fibre

Appendix 2 Theoretical analysis

The characteristics of coupling between guided and cladding modes and the centre wavelength λ_ν of an attenuation band is specified by the phase-matching condition:

$$\delta n_{eff\,\nu} \Lambda = \lambda_\nu$$

Equation A. 1

where Λ is the period of the LPG and δn_{eff_ν} is the differential effective refractive index of the ν^{th} radial cladding mode given by:

$$\delta n_{eff_\nu} = \left[n_{eff} - n_{cl}^{(\nu)} \right]$$

Equation A. 2

here n_{eff} is the effective index of the core mode, and $n_{cl}^{(\nu)}$ the effective index of the ν^{th} radial cladding mode. Both indices are dependent on the core refractive index n_1, the inner cladding refractive index n_2 as well as temperature and strain state of the grating. $n_{cl}^{(\nu)}$ is also dependent on the refractive indices of the outer cladding layer, n_3, and the surrounding medium, n_s.

Differentiating Equation A. 1 with respect to wavelength gives:

$$\frac{d\Lambda}{d\lambda} = \frac{\delta n_{eff} - \lambda\left(\frac{d(dn_{eff})}{d\lambda}\right)}{(\delta n_{eff})^2}$$

Equation A. 3

Defining the group refractive indices of both core (n_g) and cladding ($n_{g,cl}$) modes as:

$$n_g = n_{eff} - \lambda \frac{dn_{eff}}{d\lambda}$$

Equation A. 4

$$n_{g,cl} = n_{cl} - \lambda \frac{dn_{cl}}{d\lambda}$$

Equation A. 5

Equation A. 3 is rewritten as:

$$\frac{d\lambda}{d\Lambda} = \frac{(\delta n_{eff})^2}{\delta n_g}$$

Equation A. 6

Where n_g is the group differential effective index:

$$\delta n_g = n_g - n_{g,cl}$$

Equation A. 7

The number and the spectral properties of cladding modes are determined by the fibre structure. Fibre properties can be estimated form Sellmeier equations (Equation A. 3, Table A.1)[Buck, 1995] are essentially empirical fits to the actual refractive index of a particular material and doping concentrations. Generally the first three parameters provide an accuracy od 10^{-5}. These equations are a useful way of providing data on the refractive index of a material vs. wavelength, without the need for extensive tables.

$$n^2(\lambda) = 1 + \sum_{i=1}^{M} \frac{A_1 \lambda^2}{\lambda^2 - \lambda_i^2}$$

Equation A. 8

Composition	A_1	$\lambda_1(\mu m)$	A_2	$\lambda_2(\mu m)$	A_3	$\lambda_3(\mu m)$
SiO_2	0.6961663	0.0684043	0.4079426	0.1162414	0.8974794	9.896161
$GeO_2(13\%):SiO_2$	0.711040	0.064270	0.451885	0.129404	0.704048	9.425478

Table A.1 Sellmeier parameters for glass samples of different compositions

The spectral position of the attenuation band, the magnitude of the spectral shift is dependent on two factors: the difference between the effective refractive indices and the difference between the group effective refractive indices of the two modes [Patrick, 2000]. The two quantities δn_{eff} and δn_g have a strong influence on the slope of the coupling wavelength versus period and are both dependent on physical propertied of the fibre.

For three layered fibres expressions that describe electric field are considered next. Propagation modes in core and are approximated [Erdogan, 1997]:

$$E_r^{co} \cong iE_{01}^{co} J_0(V\sqrt{1-br/a_1})\exp(i\phi)\exp[i(\beta z-\varpi t)] \qquad (r \le a_1)$$

Equation A. 9

$$E_\phi^{co} \cong -E_{01}^{co} J_0(V\sqrt{1-br/a_1})\exp(i\phi)\exp[i(\beta z-\varpi t)] \qquad (r \le a_1)$$

Equation A. 10

Given;

$b = \dfrac{(n_{eff}^2 - n_2^2)}{(n_1^2 - n_2^2)}$ is the normalised refractive index,

$V =_1 \dfrac{2\pi}{\lambda} a_1 \sqrt{n_1^2 - n_2^2}$, the normalised frequency parameter,

$\beta = \frac{2\pi}{\lambda} n_{eff}$, the mode propagation constant in direction z

$J_0(.)$ is a zero order Bessel function of the first kind.

E_{01}^{co} is a normalisation constant of the fundamental core mode based on a total power of 1 Watt carried by the mode:

$$E_{01}^{co} \cong \sqrt{\frac{b\sqrt{\mu_0/\varepsilon_0}}{2\pi \cdot n_2 \sqrt{1+2b\left(\frac{n_1-n_2}{n_1}\right)}}} \frac{1}{a_1 J_1(V\sqrt{1-b})}$$

Equation A. 11

The subscript 01 denotes the fundamental core mode LP_{01}. ϕ and r represent radius and azithmuth, $n_{1...3}$ the refractive index if successive layers and a_1 and a_2 the radii of interfaces with $a_3 \to \infty$. For the cladding mode μ_0, ε_0 are the impedence of free space and permittivity of free space respectively.

The dispersion relationships for the cladding mode of azimuthal number l:

$$\zeta_0 = \frac{1}{\sigma_2} \frac{u_2\left(JK + \frac{\sigma_1\sigma_2 u_{21}u_{32}}{n_2^2 a_1 a_2}\right)P_l(a_2) - Kq_l(a_2) + Jr_l(a_2) - \frac{1}{u_2}s_l(a_2)}{-u_2\left(\frac{u_{32}}{n_2^2 a_2}J - \frac{u_{21}}{n_2^2 a_1}K\right)p_l(a_2) + \frac{u_{32}}{n_1^2 a_2}q_l(a_2) + \frac{u_{21}}{n_1^2 a_1}r_l(a_2)}$$

Equation A. 12

with,

$$\sigma_1 \equiv \frac{il \cdot n_{eff}}{\sqrt{\mu_0 \varepsilon_0}}$$

Equation A. 13

$$\sigma_2 \equiv il \cdot n_{eff} \sqrt{\mu_0 \varepsilon_0}$$

Equation A. 14

$$u_{21} \equiv \frac{1}{u_2^2} - \frac{1}{u_1^2}$$

Equation A. 15

$$u_{32} \equiv \frac{1}{\varpi_3^2} - \frac{1}{u_2^2}$$

Equation A. 16

$$u_j^2 \equiv \left(\frac{2\pi}{\lambda}\right)^2 \left(n_j^2 - n_{eff}^2\right)$$

Equation A. 17

$$\varpi_3^2 \equiv \left(\frac{2\pi}{\lambda}\right)^2 \left(n_{eff}^2 - n_3^2\right)$$

Equation A. 18

$$J \equiv \frac{J_l'(u_1 a_1)}{u_1 J_l(u_1 a_1)}$$

Equation A. 19

$$K \equiv \frac{K_l'(\varpi_3 a_2)}{u_1 J_l(\varpi_3 a_2)}$$

Equation A. 20

$$p_l(r) \equiv J_l(u_2 r) N_l(u_2 a_1) - J_l(u_2 a_1) N_l(u_2 r)$$

Equation A. 21

$$q_l(r) \equiv J_l(u_2 r) N_l'(u_2 a_1) - J_l'(u_2 a_1) N_l(u_2 r)$$

Equation A. 22

$$r_l(r) \equiv J_l'(u_2 r) N_l(u_2 a_1) - J_l(u_2 a_1) N_l'(u_2 r)$$

Equation A. 23

$$s_l(r) \equiv J_l'(u_2 r) N_l'(u_2 a_1) - J_l'(u_2 a_1) N_l'(u_2 r)$$

Equation A. 24

$$\beta \equiv \frac{2\pi}{\lambda}$$

Equation A. 25

The prime notation undicated differentiation with respect to the total argument. N is a Bessel function of the second kind. Using this identity to define the cladding mode field:

$$E_r^{cl} = iE_{1\nu}^{cl} \frac{u_1}{2} \left\{ J_2(u_1 r) + J_0(u_1 r) - \frac{\sigma_2 \zeta_0}{n_1^2} \left[J_2(u_1 r) - J_0(u_1 r) \right] \right\} \exp(i\phi) \exp\left[i(\beta z - \varpi t) \right]$$

$$(r \le a_1)$$

Equation A. 26

$$E_{\phi}^{cl} = iE_{1\nu}^{cl}\frac{u_1}{2}\left\{J_2(u_1 r) - J_0(u_1 r) + \frac{\sigma_2\zeta_0}{n_1^2}\left[J_2(u_1 r) - J_0(u_1 r)\right]\right\}\exp(i\phi)\exp[i(\beta z - \varpi t)]$$

$$(r \le a_1)$$

Equation A. 27

$$E_z^{cl} = iE_{1\nu}^{cl}\frac{{u_1}^2\sigma_2\zeta_0}{n_1^1\beta}J_2(u_1 r)\exp(i\phi)\exp[i(\beta z - \varpi t)] \qquad (r \le a_1)$$

Equation A. 28

Where $E_{1\nu}^{cl}$ is the normalization constant for the field. For the magnetic fields:

$$H_r^{cl} = E_{1\nu}^{cl}\frac{u_1}{2}\{i\sigma J_1\left[J_2(u_1 r) - J_0(u_1 r)\right] - i\zeta_0\left[J_2(u_1 r) + J_0(u_1 r)\right]\}\exp(i\phi)\exp[i(\beta z - \varpi t)]$$

$$(r \le a_1)$$

Equation A. 29

$$H_{\phi}^{cl} = -iE_{1\nu}^{cl}\frac{u_1}{2}\{i\sigma J_1\left[J_2(u_1 r) + J_0(u_1 r)\right] + i\zeta_0\left[J_2(u_1 r) - J_0(u_1 r)\right]\}\exp(i\phi)\exp[i(\beta z - \varpi t)]$$

$$(r \le a_1)$$

Equation A. 30

$$H_z^{cl} = -iE_{1\nu}^{cl}\frac{{u_1}^2 i\sigma_{10}}{\beta}J_1(u_1 r)\exp(i\phi)\exp[i(\beta z - \varpi t)] \qquad (r \le a_1)$$

Equation A. 31

To visualize the transverse distribution of light propagating in the z direction for mode l = 1 cladding mode intensity I is defined as:

$$I_z(r) = \frac{1}{2}\mathrm{Re}\left(E_r^{cl}H_{\phi}^{cl*} - H_r^{cl*}E_{\phi}^{cl}\right)$$

Equation A. 32

The overlap integral can be evaluated from these equations.

$$\Delta\lambda = \left[\frac{\Lambda\lambda}{\left(\delta n_{eff} - \delta n_g\right)} \cdot \frac{d\delta n_{eff}}{dR} + \frac{\left(\delta n_{eff}\right)^3}{\delta n_g} \frac{d\Lambda}{dR} \right] \cdot \Delta R$$

Equation A. 33

The theoretical wavelength shift due to Temperature []

$$\left(\frac{d\lambda}{dT}\right)_\nu = \left(\frac{\lambda}{\left(\delta n_{eff_\nu} - \delta n_{g_\nu}\right)} \right) \cdot \left(\frac{dn_{CO}}{dT} - \frac{dn_{cl}{}^\nu}{dT} \right) + \frac{\left(\delta n_{eff_\nu}\right)^2}{\delta n_{g_\nu}} \cdot \frac{\Lambda}{L} \cdot \frac{dL}{dT}$$

Equation A. 34

where $\frac{dn_{CO}}{dT}$ is the thermo-optic coefficient of the core mode, which can be calculated from the thermo-optic coefficient of the core material [21] and $\frac{dn_{cl}{}^\nu}{dT}$ is the thermo-optic coefficient of the ν^{th} cladding mode, which in turn can be calculated approximately from the thermo-optic coefficient of the cladding layer material containing the majority of the energy of the ν^{th} cladding mode, and $\frac{1}{L}\frac{dL}{dT}$ is the thermal expansion coefficient of the core.

The theoretical wavelength shift due to bending []

$$\Delta\lambda = \left[\frac{\Lambda\lambda}{\left(\delta n_{eff} - \delta n_g\right)} \cdot \frac{d\delta n_{eff}}{dR} + \frac{\left(\delta n_{eff}\right)^3}{\delta n_g} \frac{d\Lambda}{dR} \right] \cdot \Delta R$$

Equation A. 35

The cross sensitivity between bending and temperature []

$$\lambda = \delta n_{eff_V} \Lambda + \frac{\partial \lambda}{\partial T} \cdot \Delta T + \frac{\partial \lambda}{\partial R} \cdot \Delta R + \frac{\partial^2 \lambda}{\partial R \partial T} \cdot \Delta T \Delta R$$

Equation A. 36

Using the expression given in reference [Bhatia, 1999] for $\left(\frac{d\lambda}{dT}\right)$ and differentiating with respect to curvature; R, yields the following expression for spectral cross sensitivity of this LPG sensor

$$\frac{\partial^2 \lambda}{\partial T \partial R} = \frac{-\Delta\xi \cdot \lambda}{\left(\delta n_{eff} - \delta n_g\right)^2} \cdot \left[\frac{\partial \delta n_{eff}}{\partial R} - \frac{\partial \delta n_g}{\partial R}\right] +$$

$$\Lambda\alpha \cdot \left[2\frac{\delta n_{eff}}{\delta n_g} \cdot \frac{\partial \delta n_{eff}}{\partial R} - \left(\frac{\delta n_{eff}}{\delta n_g}\right)^2 \cdot \frac{\partial \delta n_g}{\partial R}\right] + \alpha \cdot \frac{\left(\delta n_{eff}\right)^2}{\delta n_g} \cdot \frac{\partial \Lambda}{\partial R}$$

Equation A. 37

Some the terms in the above expression are already defined, the others are α the thermal expansion coefficient of the core and $\Delta\xi_V$ the differential thermo-optic coefficient between the core and the inner-cladding material, which are given in REF 13. Using the condition that the amount of birefringence induced in a typical single mode fibre is negligibly small for curvatures of less than 2 m^{-1}, (no splitting of the attenuation bend). Using the results obtained from the eigenvalue equation [15] the spectral cross-sensitivity temperature/curvature was calculated to be 1×10^{-3}nm $m^{o}C^{-1}$. This figure is

small and over the experimental measurement range gives a relative cross sensitivity error of 0.01%.

Appendix 3 Wire frame modelling and animation code

```
%%%%%%%%%%%%%%%%%%%%%%%%%%%%%%%%%%%%%%%%%%%%%%%%%%%%%%%

%for the thorax

%%%%%%%%%%%%%%%%%%%%%%%%%%%%%%%%%%%%%%%%%%%%%%%%%%%%%%%

load txsurf

look=1

neck_centre=[0.5 8.5 1487];

dummyXslices=ones(24,2)*neck_centre(1);%dummy points for
closure

dummyYslices=ones(24,2)*neck_centre(2);

dummyZslices=ones(24,2)*neck_centre(3);

xs=[txXsurf ;txXsurf(2:4,:)]; %preiodic on slices

ys=[txYsurf ;txYsurf(2:4,:)];

zs=[txZsurf ;txZsurf(2:4,:)];

points=[];

points(:,1,:)=[xs(:,1) xs dummyXslices];%augment

points(:,2,:)=[ys(:,1) ys dummyYslices];

points(:,3,:)=[zs(:,1) zs dummyZslices];


[m,n,o]=size(points);

%assume for now (need to make this in the call later)

% s goes with slices t with ordinates

numt=4;nums=4;

dt=1/numt;ds=1/nums;

newspln=[];%zeros(m*3-3,n,o*3-3);

x=[];y=[];z=[];
```

```
for slice=1:o-3 %slice
   stx=[];sty=[];stz=[];
   for coord=1:m-3 %x,y
      %extract data from array
      Gz=squeeze(points(coord:coord+3,3,slice:slice+3));
      Gy=squeeze(points(coord:coord+3,2,slice:slice+3));
      Gx=squeeze(points(coord:coord+3,1,slice:slice+3));
      %over surface patch Q(s,t)
      for tt=0:numt-1
         t=tt*dt;
         T=[t^3 t^2 t 1]';
         ssx=[];ssy=[];ssz=[];
         for ss=0:nums-1
            s=ss*ds;
            S=[s^3 s^2 s 1]';
            Ns=[(1-s)^3,3*s^3-6*s^2+4,-
3*s^3+3*s^2+3*s+1,s^3]/6;
            Nt=[(1-t)^3,3*t^3-6*t^2+4,-
3*t^3+3*t^2+3*t+1,t^3]/6;
            Ptx=Nt*Gx*Ns';
            Pty=Nt*Gy*Ns';
            Ptz=Nt*Gz*Ns';
            if (look==1)
               if (slice==1)
                  clf
                  hold on
               end
               plot3(Ptx,Pty,Ptz,'o')%,col(slice,:))
```

```
            end %if
            ssx=[ssx;Ptx];ssy=[ssy;Pty];ssz=[ssz;Ptz];
         end  %ss
         stx=[stx ssx];sty=[sty ssy];stz=[stz ssz];
      end %tt
   end  %coord
   x=[x ;stx];y=[y;sty];z=[z;stz];
end %slice
%display
clf

thxXdata=x;
thxYdata=y;
thxZdata=z;
surf(thxXdata,thxYdata,thxZdata)


%%%%%%%%%%%%%%%%%%%%%%%%%%%%%%%%%%%%%%%%%%%%%%%%%%%%%%
%do it all again for the abdomen
%%%%%%%%%%%%%%%%%%%%%%%%%%%%%%%%%%%%%%%%%%%%%%%%%%%%%%
load absurf
xs=[abXsurf(end-3:end,:); abXsurf]; %preiodic on slices
ys=[abYsurf(end-3:end,:);abYsurf ];
zs=[abZsurf(end-3:end,:);abZsurf ];
points=[];
points(:,1,:)=[xs(:,1) xs xs(:,end-1:end)];%augment
points(:,2,:)=[ys(:,1) ys ys(:,end-1:end)];
```

```
points(:,3,:)=[zs(:,1) zs zs(:,end-1:end)];


[m,n,o]=size(points);
%assume for now (need to make this in the call later)
% s goes with slices t with ordinates
numt=4;nums=4;
dt=1/numt;ds=1/nums;
newspln=[];%zeros(m*3-3,n,o*3-3);
x=[];y=[];z=[];
for slice=1:o-3 %slice
   stx=[];sty=[];stz=[];
   for coord=1:m-3 %x,y
      %extract data from array
      Gz=squeeze(points(coord:coord+3,3,slice:slice+3));
      Gy=squeeze(points(coord:coord+3,2,slice:slice+3));
      Gx=squeeze(points(coord:coord+3,1,slice:slice+3));
      %over surface patch Q(s,t)
      for tt=0:numt-1
         t=tt*dt;
         T=[t^3 t^2 t 1]';
         ssx=[];ssy=[];ssz=[];
         for ss=0:nums-1
            s=ss*ds;
            S=[s^3 s^2 s 1]';
            Ns=[(1-s)^3,3*s^3-6*s^2+4,-
3*s^3+3*s^2+3*s+1,s^3]/6;
            Nt=[(1-t)^3,3*t^3-6*t^2+4,-
3*t^3+3*t^2+3*t+1,t^3]/6;
```

```
                Ptx=Nt*Gx*Ns';
                Pty=Nt*Gy*Ns';
                Ptz=Nt*Gz*Ns';
                if (look==1)
                   if (slice==1)
                      clf
                      hold on
                   end
                   plot3(Ptx,Pty,Ptz,'o')%,col(slice,:))
                end %if
                ssx=[ssx;Ptx];ssy=[ssy;Pty];ssz=[ssz;Ptz];
             end  %ss
             stx=[stx ssx];sty=[sty ssy];stz=[stz ssz];
          end %tt
       end  %coord
       x=[x ;stx];y=[y;sty];z=[z;stz];
end %slice
%display
clf

abdXdata=x;
abdYdata=y;
abdZdata=z;
surf(abdXdata,abdYdata,abdZdata)
```

```
%%%%%%%%%%%%%%%%%%%%%%%%%%%%%%%%%%%%%%%%%%%%%%%%%%%%%%
% display other bits
%%%%%%%%%%%%%%%%%%%%%%%%%%%%%%%%%%%%%%%%%%%%%%%%%%%%%%
clf
hold on
surf(abdXdata,abdYdata,abdZdata)
surf(thxXdata,thxYdata,thxZdata-50)
load head_arms
headnarms=data;
[m,n]=size(data);

for i=1:4:m-3
   x=data(i:i+3,1);
   y=data(i:i+3,2);
   z=data(i:i+3,3)-50;
   patch(x,y,z,32*ones(1,length(z)))
end

axis equal
axis off
save fullmodel abdXdata abdYdata abdZdata thxXdata thxYdata
thxZdata headnarms
```

Appendix 4

CHEST AND ABDOMINAL SURFACE MOTION MEASUREMENT FOR CONTINUOUS MONITORING OF RESPIRATORY FUNCTION

Proceedings of ImechE, Part H, Engineering in medicine. 2001; 215(5): 515-520

T. Earthrowl-Gould*, B. Jones* and M. R. Miller#

Aston University

Content has been removed for copyright reasons

LOW COST AND NOVEL BEND SENSING SCHEME WITH A LONG-PERIOD GRATING FOR RESPIRATORY FUNCTION MONITORING

T. Allsop, T. Earthrowl-Gould, D.J. Webb, I. Bennion

Aston University

Content has been removed for copyright reasons

EMBEDDED PROGRESSIVE-THREE-LAYERED FIBRE LONG-PERIOD GRATINGS FOR RESPIRATORY MONITORING

T. Allsop[a], T. Earthrowl-Gould, D.J. Webb, I. Bennion
Photonics Research Group, Aston University, Aston Triangle, Birmingham, B4 7ET, United Kingdom.

Aston University

Content has been removed for copyright reasons